TECHNISCHE
UNIVERSITÄT
WIEN

INSTITUT FÜR
MECHANIK UND
MECHATRONIK
Mechanics & Mechatronics

Predictive and Lyapunov-Based Control Strategies for Traction Battery Impedance Emulation

DIPLOMA THESIS

Conducted in partial fulfillment of the requirements for the degree of a
Diplom-Ingenieur (Dipl.-Ing.)

supervised by

Univ.Prof. Dr. Stefan Jakubek
Institute of Mechanics and Mechatronics
Department for Control and Process Automation

submitted at the

TU Wien
Faculty of Electrical Engineering and Information Technology

by

Wolfgang Falmbigl
Matriculation number 1026047
Charasgasse 3/35
1030 Wien

Vienna, 10th June, 2017

Die approbierte gedruckte Originalversion dieser Diplomarbeit ist an der TU Wien Bibliothek verfügbar.
The approved original version of this thesis is available in print at TU Wien Bibliothek.
TU WIEN Bibliothek Your knowledge hub

Danksagung

Die vorliegende Diplomarbeit entstand in der Arbeitsgruppe Regelungstechnik und Prozessautomatisierung am Institut für Mechanink und Mechatronik der Technischen Universität Wien. An erster Stelle möchte ich mich herzlich bei meinem Betreuer Univ. Prof. Dr. Stefan Jakubek bedanken, der mich wie selbstverständlich in seine Gruppe aufgenommen hat und mir es somit ermöglicht hat, diese Arbeit zu verfassen und dabei an einem hochspannenden Forschungsfeld mitzuwirken. Weiters möchte ich mich bei allen Mitarbeitern des Instituts bedanken, insbesondere Eva Schirmbrand, die stets für einen reibungslosen Ablauf sorgte. Mein Dank gilt außerdem den Mitarbeitern der AVL List GmbH in Graz, insbesondere Oliver König, Alexander Eder und Günther Prochart.

Weiters möchte ich Herrn Univ. Prof. Dr. Andreas Kugi vom Institut für Automatisierungs- und Regelungstechnik danken, der mit seinen engagierten Vorträgen auch in mir die Begeisterung für die Regelungstechnik geweckt hat. Zudem möchte ich Frau Dietlinde Egger meinen Dank aussprechen, die während meines gesamten Studiums in allen organisatorischen Belangen eine große Hilfe war.

Meinen Eltern danke ich ganz besonders für ihre jahrelange Unterstützung und Geduld, erst sie haben mir den Abschluss dieses Studiums ermöglicht.

Zu guter Letzt möchte ich mich bei meinen Studienkollegen Daniel Duller, Tobias Wolfmayr, Ulrich Knechtelsdorfer, Jakob Maderthaner, Christoph Zech, David Gruber, Hannes Dillinger, David Brunner und Romana Wiesinger bedanken. Der gemeinsame Weg hat uns nicht nur zusammengeschweißt, sondern währenddessen sind auch gute Freundschaften entstanden.

Die approbierte gedruckte Originalversion dieser Diplomarbeit ist an der TU Wien Bibliothek verfügbar.
The approved original version of this thesis is available in print at TU Wien Bibliothek.

Kurzfassung

Die Emulation von Traktionsbatterien ermöglicht das Testen von elektrischen und hybriden Antriebssträngen unter exakt reproduzierbaren Bedingungen. Dabei dient ein Batteriemodell zur Vorgabe eines Sollverhaltens anhand einer Strom-Spannungskennlinie, welches durch einen synchronen mehrphasigen Tiefsetzsteller nachzubilden ist. Dieses Konzept wird als Impedanzregelung bezeichnet und stellt hohe Anforderungen an Genauigkeit, Führungsverhalten und Störgrößenunterdrückung. Die vorliegende Arbeit beschäftigt sich daher mit dem Entwurf hierfür geeigneter Regelungsstrategien.

Typischerweise kommen dabei Regelungsmethoden auf Basis von Pulsweitenmodulation (PWM) zum Einsatz. Diese erzielen für stationäre Betriebspunkte hohe Genauigkeit, sind in ihrem dynamischen Verhalten allerdings Finite Control-Set-modellprädiktiven Reglern (FCS-MPC) unterlegen. Die geringe Zeitauflösung von FCS-MPC hingegen schränkt die Genauigkeit dieser Methode ein und erfordert sehr hohe Abtastraten.

Um beide Vorteile zu kombinieren, wird Predictive Pulse Pattern Control (PPPC) vorgestellt. Dabei wird zunächst ein geeignetes Pulsmuster ausgewählt, dessen Schaltzeitpunkte durch Minimieren eines Kostenfunktionals gewählt werden. Auf diese Art und Weise wird sowohl für stationäre als auch transiente Bedingungen eine hohe Regelgüte erzielt. Das zugehörige beschränkte quadratische Problem lässt sich mittels state-of-the-art Methoden effizient lösen. Nichtsdestrotz stellt der Rechenaufwand des PPPC-Verfahrens je nach verfügbarer Rechenkapaziät eine Einschränkung dar. Aus diesem Grund wird darüberhinaus ein PWM-basierter Command Filtered Backstepping (CFBS) Ansatz vorgeschlagen. Dieser erlaubt es, mit geringem Rechenaufwand unter Berücksichtigung von Eingangs- und Zustandsbeschränkungen den geschlossenen Kreis asymptotisch im Sinne von Lyapunov zu stabilisieren.

Die hohe Güte der vorgestellten Verfahren wird anhand von Simulationsergbnissen nachgewiesen. Die CFBS-Methode wird darüber hinaus durch experimentelle Versuche an einem Testsystem validiert.

Die approbierte gedruckte Originalversion dieser Diplomarbeit ist an der TU Wien Bibliothek verfügbar.
The approved original version of this thesis is available in print at TU Wien Bibliothek.

Abstract

Traction battery emulation enables repeatable conditions for testing of electric and hybrid electric vehicle powertrains. Thereby the current-voltage characteristics is extracted from a virtual battery model and is provided as a setpoint to a synchronous multiphase buck converter (SMPB). This concept is called impedance control and goes along with high requirements on accuracy, tracking performance and disturbance rejection. This thesis deals with the design of suitable control strategies to this purpose.

Typically, carrier-based pulse width modulation (PWM) approaches are used that achieve good steady-state performance but are inferior to Finite Control-Set model predictive control (FCS-MPC) in transient response. However, the steady-state performance of FCS-MPC is usually poor as the time resolution is limited by the sampling rate.

In order to combine both advantages, the Predictive Pulse Pattern Control (PPPC) method is presented. A minimal switching effort pulse pattern is selected whose switching instants are obtained by minimizing an objective function, resulting in high accuracy and fast dynamic response. The associated constrained quadratic program can be solved efficiently with state-of-the-art methods. Nevertheless, the computational cost can be a restriction for platforms with limited computational power. For this reason, the PWM-based Command Filtered Backstepping (CFBS) approach is proposed as alternative with little computational cost that incorporates input and state constraints and inherently guarantees asymptotic stability in the sense of Lyapunov.

Simulation results demonstrate the high performance of the suggested control strategies. Beyond that, the CFBS method is also validated experimentally on a hardware test bed.

Die approbierte gedruckte Originalversion dieser Diplomarbeit ist an der TU Wien Bibliothek verfügbar.
The approved original version of this thesis is available in print at TU Wien Bibliothek.
TU WIEN Bibliothek Your knowledge hub

Contents

1 Introduction 1
1.1 Organization . . . 2

2 System description and model 3
2.1 Nonlinear power source emulation . . . 3
2.2 Battery Emulation . . . 4
2.3 DC-DC converter model . . . 5
2.4 UUT model . . . 6
2.5 Coupled linearized model . . . 8
2.6 Reduced order model . . . 9
2.7 Virtual input reduced order model . . . 9
2.8 Battery Emulator Test Bed . . . 10

3 Control Design 11
3.1 Related literature . . . 11
  3.1.1 Model predictive control . . . 11
  3.1.2 Backstepping Control . . . 13
3.2 Cascade control . . . 14
  3.2.1 Outer loop - voltage control . . . 14
  3.2.2 Inner loop - current control . . . 17
3.3 Finite Control-Set MPC . . . 18
  3.3.1 Total switching problem . . . 18
  3.3.2 Current balancing problem . . . 22
3.4 Predictive Pulse Pattern Control . . . 23
3.5 Backstepping control . . . 27
3.6 Command Filtered Backstepping . . . 32
3.7 Inner Loop Command Filtered Backstepping . . . 36
3.8 Observer Design . . . 38

Die approbierte gedruckte Originalversion dieser Diplomarbeit ist an der TU Wien Bibliothek verfügbar.
The approved original version of this thesis is available in print at TU Wien Bibliothek.
TU WIEN Bibliothek Your knowledge hub

4 Optimization Techniques 40
4.1 Overview . . . 40
4.2 Integer quadratic programming . . . 41
4.2.1 Exhaustive search . . . 41
4.2.2 Sphere Decoding Algorithm . . . 41
4.3 Quadratic programming with continuous variables . . . 42
4.4 Backstepping-based dynamic pruning . . . 44

5 Results 45
5.1 Simulation results . . . 45
5.1.1 Steady-state performance . . . 45
5.1.2 Comparing FCS-MPC with PPPC . . . 46
5.1.3 Comparing CBS with PPPC . . . 50
5.1.4 Comparing CBS with CFBS . . . 53
5.1.5 Outer Loop Variants . . . 55
5.1.6 Load estimation . . . 56
5.2 Computational Effort . . . 56
5.2.1 FCS-MPC . . . 57
5.2.2 PPPC . . . 61
5.2.3 Backstepping-based control . . . 61
5.3 Experimental results . . . 64

6 Conclusion 66
6.1 Outlook . . . 66

A Pulse Pattern Prediction Matrices 68

B System Parameter 77

C Controller Parameters 78

D Listing of MATLAB Setup 82

Bibliography 83

Die approbierte gedruckte Originalversion dieser Diplomarbeit ist an der TU Wien Bibliothek verfügbar.
The approved original version of this thesis is available in print at TU Wien Bibliothek.

Die approbierte gedruckte Originalversion dieser Diplomarbeit ist an der TU Wien Bibliothek verfügbar.
The approved original version of this thesis is available in print at TU Wien Bibliothek.
TU WIEN Bibliothek Your knowledge hub

List of Figures

2.1 Nonlinear power source emulation based on a reference model providing a setpoint v_2^* for the control unit. 4
2.2 Interacting components of a traction battery emulation system. 4
2.3 Battery emulator comprising a synchronous multiphase buck converter including cable and UUT model. 5
2.4 Constant power load (CPL) model. 7
2.5 Battery emulator laboratory setup. 10

3.1 Principle of model predictive control for the SISO-case. The input sequence $\boldsymbol{u}_k$ is chosen such that the output tracking error $\|\boldsymbol{y}_k^* - \boldsymbol{y}_k\|^2$ is minimized over the prediction horizon N_p. Beyond the control horizon N_c the input is held constant with u_{k+N_c-1}. Out of $\boldsymbol{u}_k$ only the first element u_k is applied and the procedure is repeated at $k+1$, following the receding horizon policy. 12
3.2 Cascade control structure with outer voltage control loop and inner current loop. 14
3.3 Different time scales of the inner and outer control loop. 15
3.4 Two step current tracking approach. 19
3.5 Example of a switching scheme for pulse pattern A. 24
3.6 Current prediction at time instant k based on decision variables $t_1 - t_7$ for different pulse pattern switching sequences that differ in number of simultaneously active phases. 25
3.7 Backstepping control structure for the single control law case as defined in (3.75). The virtual control signals α_i and its time derivatives have to be calculated explicitly for the next stage. 32

3.8 Command filtered backstepping structure. The virtual control signals $\tilde{\alpha}_i$ are computed as defined in (3.81), (3.86), (3.91) and (3.96) use the tracking errors $\tilde{z}_i$ and the time derivative of the filtered previous virtual control signal. The command filters (CF) allow imposing magnitude and rate constraints and provide the reference and its derivation for the next stage. 35
3.9 Command filter structure for $i = 2, 3, 4$. For an implementation on a digital control unit, the discrete-time state-space representation of (3.99) has to be used. 36

5.1 FCS-MPC steady-state performance for varying prediction horizon lengths N. 46
5.2 Setpoint step from $v_2 = 0\,\mathrm{V}$ to $v_2 = 350\,\mathrm{V}$. 47
5.3 (a) and (c): Setpoint step from $v_2 = 0\,\mathrm{V}$ to $v_2 = 350\,\mathrm{V}$. (b) and (d): Load disturbance rejection when enabling a constant power load with 125 kW. 48
5.4 Steady-state performance at $v_2 = 350\,\mathrm{V}$ without load. 49
5.5 (a) and (c): Setpoint step from $v_2 = 0\,\mathrm{V}$ to $v_2 = 350\,\mathrm{V}$. (b) and (d): Load disturbance rejection when enabling a constant power load with 125 kW. 51
5.6 Steady-state performance at $v_2 = 350\,\mathrm{V}$ with load $i_\mathrm{L} = 350\,\mathrm{A}$ and transient performance for a setpoint step from $v_2 = 0\,\mathrm{V}$ to $v_2 = 350\,\mathrm{V}$. . . . 52
5.7 Comparison of CBS and CFBS. (a) and (c): Setpoint step from $v_2 = 0\,\mathrm{V}$ to $v_2 = 350\,\mathrm{V}$. (b) and (d): Load disturbance rejection when enabling a constant power load with 125 kW. 53
5.8 Steady-state performance at $v_2 = 350\,\mathrm{V}$ with load $i_\mathrm{L} = 350\,\mathrm{A}$. 54
5.9 Outer loop variants with PPPC in the inner loop. (a): MPC, (b): LQR, (c): CFBS. 55
5.10 Output voltage v_2 and sum phase current i_1 load recovery with MPC in the outer and the PPPC in the inner loop and the corresponding load disturbance estimation for a constant disturbance. 56
5.11 The SDA requires significantly more iterations to find the optimal solution during transients which increases the turnaround time t_t. 57
5.12 Maximum required iterations for transient operating condition on a logarithmic scale. 58
5.13 FCS-MPC computational cost for varying prediction horizons N with and without dynamic pruning (DP). 59
5.14 Turnaround time for FCS-MPC. 60
5.15 Computational demand for PPPC. 62

Die approbierte gedruckte Originalversion dieser Diplomarbeit ist an der TU Wien Bibliothek verfügbar.
The approved original version of this thesis is available in print at TU Wien Bibliothek.

5.16 Computational demand for backstepping-based control. 63
5.17 Setpoint change and load step on test bed. 65

Die approbierte gedruckte Originalversion dieser Diplomarbeit ist an der TU Wien Bibliothek verfügbar.
The approved original version of this thesis is available in print at TU Wien Bibliothek.
TU WIEN Bibliothek Your knowledge hub

List of Tables

3.1 The switching combinations grow exponentionally with the prediction horizon. 18
3.2 Switching sequences for the set of pulse patterns. 23

5.1 Required iterations for varying prediction horizon. 58

B.1 Parameters of the BE. 77

C.1 LQR with i_1 as virtual control input. 78
C.2 FCS-MPC. 78
C.3 PPPC. 79
C.4 CFBS (1 phase, simulation setup). 79
C.5 CFBS (1 phase, experimental setup). 80
C.6 Kalman Filter design (reduced order). 81
C.7 Kalman Filter design (full order). 81

Die approbierte gedruckte Originalversion dieser Diplomarbeit ist an der TU Wien Bibliothek verfügbar.
The approved original version of this thesis is available in print at TU Wien Bibliothek.

Die approbierte gedruckte Originalversion dieser Diplomarbeit ist an der TU Wien Bibliothek verfügbar.
The approved original version of this thesis is available in print at TU Wien Bibliothek.

Chapter 1

Introduction

Electric drives will more and more assist and replace combustion engines in the automotive sector. Reasons are numerous: high efficiency, small size and weight, energy recuperation and possibly zero-emissions, to name a few. This trend poses new challenges on powertrain validation not only involving mechanical but also electric test environments including the traction battery. However, using real traction batteries to achieve defined operating conditions is a costly and time consuming task which also involves safety hazards [1]. For these reasons, traction battery emulators are used instead to emulate the electric characteristics under repeatable conditions based on a battery model considering state of charge, state of health, temperature, aging effects, etc. Due to high power levels up to hundreds of kilowatts an efficient switched mode power supply is preferred to a linear power supply which would suffer from extensive conversion losses. The switching converter structure does not only significantly complicate the control problem but also causes voltage and current ripples that do not normally occur in batteries and hence, have to be kept at a minimum. Therefore, a powerful control strategy needs to be elaborated, that allows fast output voltage tracking with high accuracy and load current rejection to achieve robust battery impedance emulation.

Finite control-set model predictive control (FCS-MPC) is a promising candidate for this purpose with high dynamic performance compared to carrier-based pulse width modulation (PWM) approaches while avoiding unnecessarily high switching frequencies that would increase switching losses [2]. However, the limited time resolution often leads to poor steady-state performance and can only be overcome with higher sampling rates that dramatically increase the computational burden [3]. The aim of this master thesis is to resolve the limitations of the conventional FCS-MPC method by

1. improving the time resolution to achieve high accuracy, and
2. formulating efficient algorithms that can be implemented in real-time on an embedded platform with limited computational power.

To this end, two different control strategies are presented. Firstly, a tailored approach called predictive pulse pattern control (PPPC) that achieves high performance for transient and steady-state operating conditions with feasible computational demand is proposed. At each time step, a pulse pattern with minimal switching effort is selected whose switching instants are chosen such that an objective function is minimized, yielding in high tracking accuracy.
Secondly, the Command Filtered Backstepping (CFBS) [4] control framework is adapted and suggested as a PWM-based computational efficient alternative that includes input and state constraints and achieves asymptotic stability in the sense of Lyapunov. Finally, it is shown how the search space of a FCS-MPC formulation can be dramatically reduced by Backstepping-based dynamic pruning, enabling longer prediction horizons and thus, higher time resolution. The control strategies are compared and the high performance is demonstrated by simulation and experimental results.

1.1 Organization

The remainder of this work is organized as follows. In chapter 2 the battery emulator system is described and a mathematical model is derived. Consequently, the requirements for the control loop are formulated. The control design is treated in detail in chapter 2. The FCS-MPC framework is introduced before the PPPC and CFBS control strategies are presented as viable concepts to overcome the limitations of FCS-MPC. Suitable optimization techniques are discussed in chapter 4. Moreover, a Backstepping-based method to dynamically prune the search space of an integer quadratic program is proposed. Simulation and experimental results are presented in chapter 5. The suggested control strategies are compared in transient and steady-state performance as well as in the associated computational effort. Chapter 6 closes with a conclusion and remaining open challenges.

Die approbierte gedruckte Originalversion dieser Diplomarbeit ist an der TU Wien Bibliothek verfügbar.
The approved original version of this thesis is available in print at TU Wien Bibliothek.

Die approbierte gedruckte Originalversion dieser Diplomarbeit ist an der TU Wien Bibliothek verfügbar.
The approved original version of this thesis is available in print at TU Wien Bibliothek.
TU Bibliothek WIEN Your knowledge hub

Chapter 2

System description and model

This chapter describes the concept of nonlinear power source emulation in general and the specific characteristics and architecture of a traction battery emulator. A mathematical model of the DC-DC converter and the unit under test is derived to serve for the control design.

2.1 Nonlinear power source emulation

Recently, there has been growing interest in using nonlinear power source emulators instead of real power sources such as batteries, photovoltaic arrays, fuel cells or thermoelectric generators for testing and development purposes [5]. This is due to several advantages they provide over real power sources:

- reduced cost
- reduced time effort
- repeatable conditions
- improved safety .

A detailed review of existing implementations is given in [5]. Common to all nonlinear power source emulators is that the electric characteristics of the power source of interest is given by a reference model and shall be tracked as fast and accurate as possible by regulating a DC-DC converter. The load current is measured and fed to the reference model that provides the setpoint for the control unit which in turn adds a feedback loop that has to be considered as it modifies resulting closed loop dynamics [6]. A voltage source model as depicted in fig. 2.1 with open circuit voltage v_{oc} and complex impedance Z can serve as basis for the electric impedance emulation. A suitable reference model is crucial therefore. In [7] a data-driven approach to find a generic battery model using

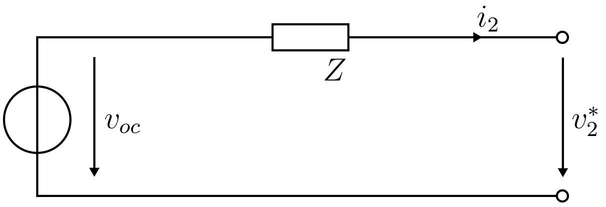

Figure 2.1: Nonlinear power source emulation based on a reference model providing a setpoint v_2^* for the control unit.

local model networks is suggested which is extended in [6] to achieve battery impedance emulation. A different application of mechanical impedance emulation of a panthograph current collectors is presented in [8].
This thesis focuses on the related output voltage tracking problem only.

2.2 Battery Emulation

A schematic illustration of an electric or hybrid electric vehicle is shown in fig. 2.2a. The internal combustion engine (ICE) is omitted in the former case. The engine control unit (ECU) controls the ICE and the voltage source inverter (VSI) which handles the power flow between the electric motor and traction battery. Fig. 2.2b shows the test bed of an electric or hybrid electric powertrain including the traction battery emulator, also described in [1]. The electric drive is flanged to a dynamometer to emulate the

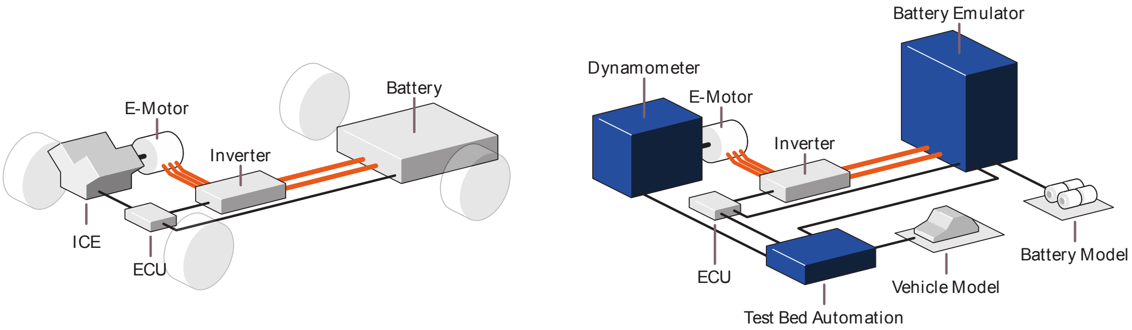

(a) Electric or hybrid electric vehicle powertrain. (b) Electric powertrain test bed.

Figure 2.2: Interacting components of a traction battery emulation system.

mechanical load based on a vehicle model. The battery response on the other hand is extracted from a battery model and emulated by a battery emulator (BE). The BE is essentially a buck-type DC-DC converter and its associated control problem is the

Die approbierte gedruckte Originalversion dieser Diplomarbeit ist an der TU Wien Bibliothek verfügbar.
The approved original version of this thesis is available in print at TU Wien Bibliothek.

main focus of this thesis. The VSI and electric drive on the other hand refer to the unit under test (UUT) in this setup.

2.3 DC-DC converter model

The DC-DC conversion in a BE is achieved with a synchronous multiphase buck converter (SMPB) topology as depicted in fig. 2.3. The rectifier dynamics are neglected, hence, DC-link capacitance C_0 is considered to be high enough to assume constant DC-voltage link voltage V_0. The insulated-gate bipolar transistors (IGBT) semiconductor switches $T_1 - T_8$ are driven by the control unit with binary, complementary signals $S_a - S_d \in \boldsymbol{u} = \{0, 1\}$. The resistances of phase inductors $L_{1_a} - L_{1_d}$ are modeled with $R_{1_a} - R_{1_d}$ respectively. The filter capacitance is denoted by C_1, L_2 and R_2 can model a cable impedance or an additional output filter together with C_2. The generic UUT model consists of C_2 and R_L. Define the state vector as

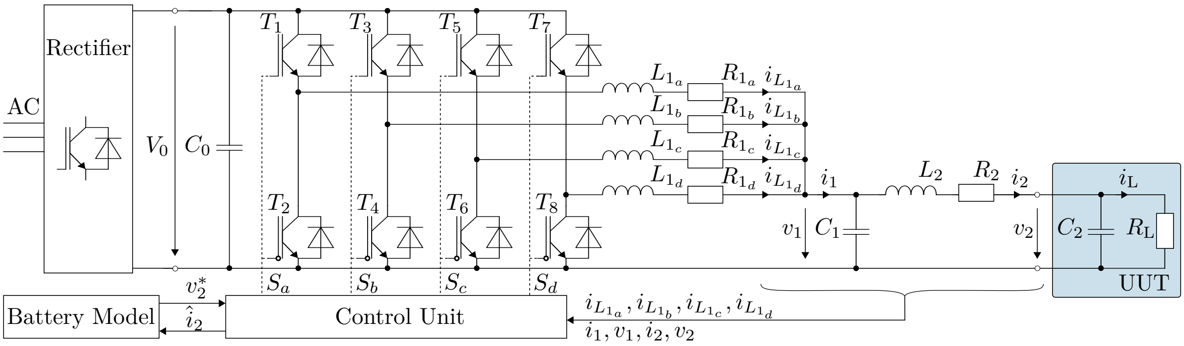

Figure 2.3: Battery emulator comprising a synchronous multiphase buck converter including cable and UUT model.

$\boldsymbol{x} = \begin{bmatrix} i_{L_{1_a}} & i_{L_{1_b}} & i_{L_{1_c}} & i_{L_{1_d}} & v_1 & i_2 & v_2 \end{bmatrix}^\mathrm{T}$, the input vector as $\boldsymbol{u} = \begin{bmatrix} S_a & S_b & S_c & S_d \end{bmatrix}^\mathrm{T}$ and let the ohmic share of the load current be the disturbance input $d = i_\mathrm{L}$. The

Die approbierte gedruckte Originalversion dieser Diplomarbeit ist an der TU Wien Bibliothek verfügbar.
The approved original version of this thesis is available in print at TU Wien Bibliothek.

system dynamics can then be written as

$$
\begin{aligned}
\dot{\boldsymbol{x}} = &\begin{bmatrix}
-\frac{R_{1_a}}{L_{1_a}} & 0 & 0 & 0 & -\frac{1}{L_{1_a}} & 0 & 0 \\
0 & -\frac{R_{1_b}}{L_{1_b}} & 0 & 0 & -\frac{1}{L_{1_b}} & 0 & 0 \\
0 & & -\frac{R_{1_c}}{L_{1_c}} & 0 & -\frac{1}{L_{1_c}} & 0 & 0 \\
0 & 0 & 0 & -\frac{R_{1_d}}{L_{1_d}} & -\frac{1}{L_{1_d}} & 0 & 0 \\
\frac{1}{C_1} & \frac{1}{C_1} & \frac{1}{C_1} & \frac{1}{C_1} & 0 & -\frac{1}{C_1} & 0 \\
0 & 0 & 0 & 0 & \frac{1}{L_2} & -\frac{R_2}{L_2} & -\frac{1}{L_2} \\
0 & 0 & 0 & 0 & 0 & \frac{1}{C_2} & 0
\end{bmatrix} \boldsymbol{x} \\
&+ \begin{bmatrix}
\frac{V_0}{L_{1_a}} & 0 & 0 & 0 \\
0 & \frac{V_0}{L_{1_b}} & 0 & 0 \\
0 & & \frac{V_0}{L_{1_c}} & 0 \\
0 & 0 & 0 & \frac{V_0}{L_{1_d}} \\
0 & 0 & 0 & 0 \\
0 & 0 & 0 & 0 \\
0 & 0 & 0 & 0
\end{bmatrix} \boldsymbol{u} + \begin{bmatrix}
0 \\ 0 \\ 0 \\ 0 \\ 0 \\ 0 \\ -\frac{1}{C_2}
\end{bmatrix} d,
\end{aligned}
\tag{2.1}
$$

with $i_1 = i_{L_{1_a}} + i_{L_{1_b}} + i_{L_{1_c}} + i_{L_{1_d}}$.

2.4 UUT model

As depicted in fig. 2.3, the UUT is modelled as an ohmic load R_L with input capacitance C_2. In general, R_L is time-variant and unknown. The related current i_{L} cannot be measured directly.

Voltage source inverters (VSI) that power electric drives are a major challenge when tightly speed regulated, as they keep the output power constant regardless of input voltage variations [9]. This behaviour is known as constant power load (CPL) and can cause negative impedance instability [9, 10]. The voltage-current characteristics and nonlinear model is depicted in fig. 2.4a and 2.4b. The nonlinear relation is given by

$$
i_{\mathrm{L}} = \frac{P}{v_2}, \tag{2.2}
$$

with constant power P. Apparently, validity of this model is restricted to a minimum voltage that results in a feasible current. Depending on the control approach discussed

Die approbierte gedruckte Originalversion dieser Diplomarbeit ist an der TU Wien Bibliothek verfügbar.
The approved original version of this thesis is available in print at TU Wien Bibliothek.
TU WIEN Bibliothek Your knowledge hub

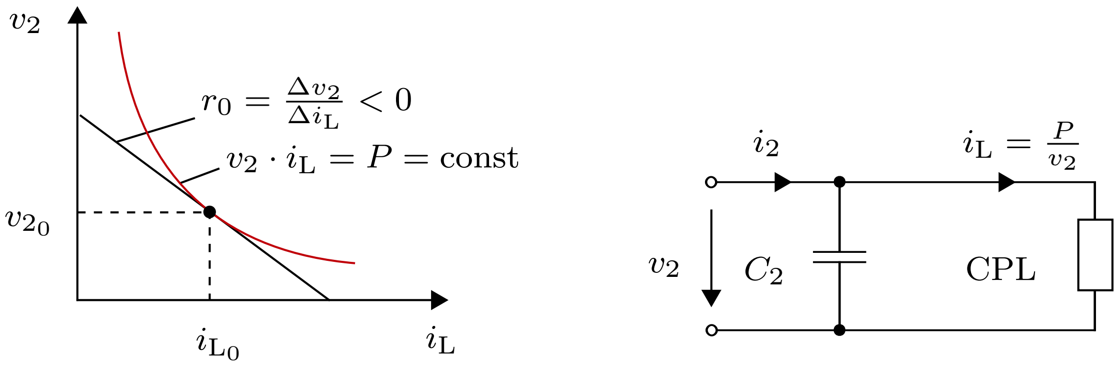
v_2
$r_0 = \frac{\Delta v_2}{\Delta i_L} < 0$
$v_2 \cdot i_L = P = \text{const}$
v_{2_0}
i_{L_0}
i_L
i_2
$i_L = \frac{P}{v_2}$
v_2
C_2
CPL

(a) Voltage-current characteristics.

(b) Nonlinear CPL model.

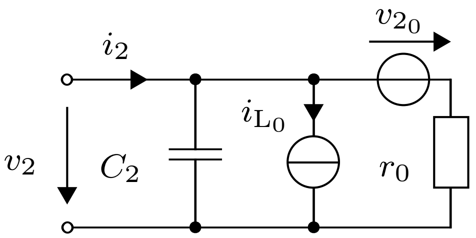

(c) Small-signal model linearized around (v_{2_0}, i_{L_0}).

Figure 2.4: Constant power load (CPL) model.

in detail in chapter 3, the CPL nonlinearity can directly be handled or has to be linearized at first. Linearizing (2.2) around an operating point (v_{2_0}, i_{L_0}) gives

$$i_L \approx i_{L_0} + \frac{\partial}{\partial v_2} \frac{P}{v_2}\bigg|_{v_{2_0}, i_{L_0}} (v_2 - v_{2_0}) = i_{L_0} - \frac{P}{v_{2_0}^2}(v_2 - v_{2_0}), \tag{2.3}$$

which simplifies with $P = v_{2_0} i_{L_0}$ to

$$i_L \approx 2 i_{L_0} - \frac{i_{L_0}}{v_{2_0}} v_2. \tag{2.4}$$

This leads by introducing the equivalent resistance $r_0 = -\frac{v_{2_0}}{i_{L_0}}$ to the small-signal model depicted in fig. 2.4c, similarly to [9, 11].

Die approbierte gedruckte Originalversion dieser Diplomarbeit ist an der TU Wien Bibliothek verfügbar.
The approved original version of this thesis is available in print at TU Wien Bibliothek.

2.5 Coupled linearized model

Combining the DC-DC converter model (2.1) with small-signal model of the UUT (2.4) results in the coupled dynamics

$$
\begin{aligned}
\dot{\boldsymbol{x}} = &\underbrace{\begin{bmatrix}
-\frac{R_{1_a}}{L_{1_a}} & 0 & 0 & 0 & -\frac{1}{L_{1_a}} & 0 & 0 \\
0 & -\frac{R_{1_b}}{L_{1_b}} & 0 & 0 & -\frac{1}{L_{1_b}} & 0 & 0 \\
0 & & -\frac{R_{1_c}}{L_{1_c}} & 0 & -\frac{1}{L_{1_c}} & 0 & 0 \\
0 & 0 & 0 & -\frac{R_{1_d}}{L_{1_d}} & -\frac{1}{L_{1_d}} & 0 & 0 \\
\frac{1}{C_1} & \frac{1}{C_1} & \frac{1}{C_1} & \frac{1}{C_1} & 0 & -\frac{1}{C_1} & 0 \\
0 & 0 & 0 & 0 & \frac{1}{L_2} & -\frac{R_2}{L_2} & -\frac{1}{L_2} \\
0 & 0 & 0 & 0 & 0 & \frac{1}{C_2} & -\frac{1}{C_2 r_0}
\end{bmatrix}}_{\boldsymbol{A}} \boldsymbol{x} \\
&+ \underbrace{\begin{bmatrix}
\frac{V_0}{L_{1_a}} & 0 & 0 & 0 \\
0 & \frac{V_0}{L_{1_b}} & 0 & 0 \\
0 & & \frac{V_0}{L_{1_c}} & 0 \\
0 & 0 & 0 & \frac{V_0}{L_{1_d}} \\
0 & 0 & 0 & 0 \\
0 & 0 & 0 & 0 \\
0 & 0 & 0 & 0
\end{bmatrix}}_{\boldsymbol{B}} \boldsymbol{u} + \underbrace{\begin{bmatrix}
0 \\ 0 \\ 0 \\ 0 \\ 0 \\ 0 \\ -\frac{2}{C_2}
\end{bmatrix}}_{\boldsymbol{e}} z,
\end{aligned}
\tag{2.5}
$$

with $z = i_{\mathrm{L}_0}$.
The discrete-time dynamics of (2.5) has the form

$$\boldsymbol{x}_{k+1} = \boldsymbol{\Phi}\boldsymbol{c}_k + \boldsymbol{\Gamma}\boldsymbol{u}_k + \boldsymbol{g}z, \qquad \boldsymbol{x}(0) = \boldsymbol{x}_0 \tag{2.6a}$$

$$y_k = \boldsymbol{c}^{\mathrm{T}}\boldsymbol{x}_k, \tag{2.6b}$$

with the output v_2, hence, $\boldsymbol{c}^{\mathrm{T}} = \begin{bmatrix}0 & 0 & 0 & 0 & 0 & 0 & 1\end{bmatrix}$. The dynamic matrix $\boldsymbol{\Phi}$, input matrix $\boldsymbol{\Gamma}$ and disturbance vector $\boldsymbol{g}$ are given by

$$\boldsymbol{\Phi} = \exp\left(\boldsymbol{A}T_s\right), \tag{2.7a}$$

$$\boldsymbol{\Gamma} = \int_0^{T_s} \exp\left(\boldsymbol{A}\tau\right) \mathrm{d}\tau \boldsymbol{B}, \tag{2.7b}$$

$$\boldsymbol{g} = \int_0^{T_s} \exp\left(\boldsymbol{A}\tau\right) \mathrm{d}\tau \boldsymbol{e}, \tag{2.7c}$$

where T_s denotes the sampling time.

Die approbierte gedruckte Originalversion dieser Diplomarbeit ist an der TU Wien Bibliothek verfügbar.
The approved original version of this thesis is available in print at TU Wien Bibliothek.
TU WIEN Bibliothek Your knowledge hub

2.6 Reduced order model

As discussed in [12], for identical phases, hence,

$$L_{1_a} = L_{1_b} = L_{1_c} = L_{1_d} \quad \text{and} \tag{2.8}$$

$$R_{1_a} = R_{1_b} = R_{1_c} = R_{1_d}, \tag{2.9}$$

the full order model (2.5) can be simplified by lumping phase inductors and corresponding resistances to one common inductance $L_1 = \frac{1}{4}L_{1_a}$ and resistance $R_1 = \frac{1}{4}R_{1_a}$ to the reduced form

$$\dot{\boldsymbol{x}}_r = \underbrace{\begin{bmatrix} -\frac{R_1}{L_1} & -\frac{1}{L_1} & 0 & 0 \\ \frac{1}{C_1} & 0 & -\frac{1}{C_1} & 0 \\ 0 & \frac{1}{L_2} & -\frac{R_2}{L_2} & -\frac{1}{L_2} \\ 0 & 0 & \frac{1}{C_2} & -\frac{1}{C_2 r_0} \end{bmatrix}}_{\boldsymbol{A}_r} \boldsymbol{x}_r + \underbrace{\begin{bmatrix} \frac{V_{0,r}}{L_1} \\ 0 \\ 0 \\ 0 \end{bmatrix}}_{\boldsymbol{B}_r} u_r + \underbrace{\begin{bmatrix} 0 \\ 0 \\ 0 \\ -\frac{2}{C_2} \end{bmatrix}}_{\boldsymbol{e}_r} z \tag{2.10a}$$

$$y = \boldsymbol{c}_r^{\mathrm{T}} \boldsymbol{x}_r, \tag{2.10b}$$

with $\boldsymbol{x}_r = \begin{bmatrix} i_1 & v_1 & i_2 & v_2 \end{bmatrix}^{\mathrm{T}}$, $\boldsymbol{c}_r^{\mathrm{T}} = \begin{bmatrix} 0 & 0 & 0 & 1 \end{bmatrix}$, $u_r = S$ and $V_{0,r} = \frac{V_0}{4}$. Thereby $S \in \{0, 1, 2, 3, 4\}$ refers to the number of active phases, thus, $S = \sum_{j \in \mathcal{P}} S_j$, with the set of phases $\mathcal{P} = \{a, b, c, d\}$.

2.7 Virtual input reduced order model

A different reduced order model than in section 2.6 is stated here that considers i_1 instead of switching states as virtual control input. Hence, $\boldsymbol{x}_v = \begin{bmatrix} v_1 & i_2 & v_2 \end{bmatrix}^{\mathrm{T}}$ and $u_v = i_1$. Consequently, model (2.10) yields

$$\dot{\boldsymbol{x}}_v = \underbrace{\begin{bmatrix} 0 & -\frac{1}{C_1} & 0 \\ \frac{1}{L_2} & -\frac{R_2}{L_2} & -\frac{1}{L_2} \\ 0 & \frac{1}{C_2} & -\frac{1}{C_2 r_0} \end{bmatrix}}_{\boldsymbol{A}_v} \boldsymbol{x}_v + \underbrace{\begin{bmatrix} \frac{1}{C_1} \\ 0 \\ 0 \end{bmatrix}}_{\boldsymbol{B}_v} u_v + \underbrace{\begin{bmatrix} 0 \\ 0 \\ -\frac{2}{C_2} \end{bmatrix}}_{\boldsymbol{e}_v} z \tag{2.11a}$$

$$y = \boldsymbol{c}_v^{\mathrm{T}} \boldsymbol{x}_v, \tag{2.11b}$$

where $\boldsymbol{c}_v^{\mathrm{T}} = \begin{bmatrix} 0 & 0 & 1 \end{bmatrix}$. This lumped model with virtual current control input as well as the lumped model of section 2.6 are used for control and observer design in the next chapter. Both discrete-time dynamics have the form as (2.6), with $\boldsymbol{\Phi}_r$, $\boldsymbol{\Gamma}_r$, $\boldsymbol{g}_r$, $\boldsymbol{\Phi}_v$, $\boldsymbol{\Gamma}_v$ and $\boldsymbol{g}_v$ of appropriate dimensions. They are calculated as (2.7) in section 2.5.

Die approbierte gedruckte Originalversion dieser Diplomarbeit ist an der TU Wien Bibliothek verfügbar.
The approved original version of this thesis is available in print at TU Wien Bibliothek.

2.8 Battery Emulator Test Bed

The BE laboratory setup is depicted in fig. 2.5.

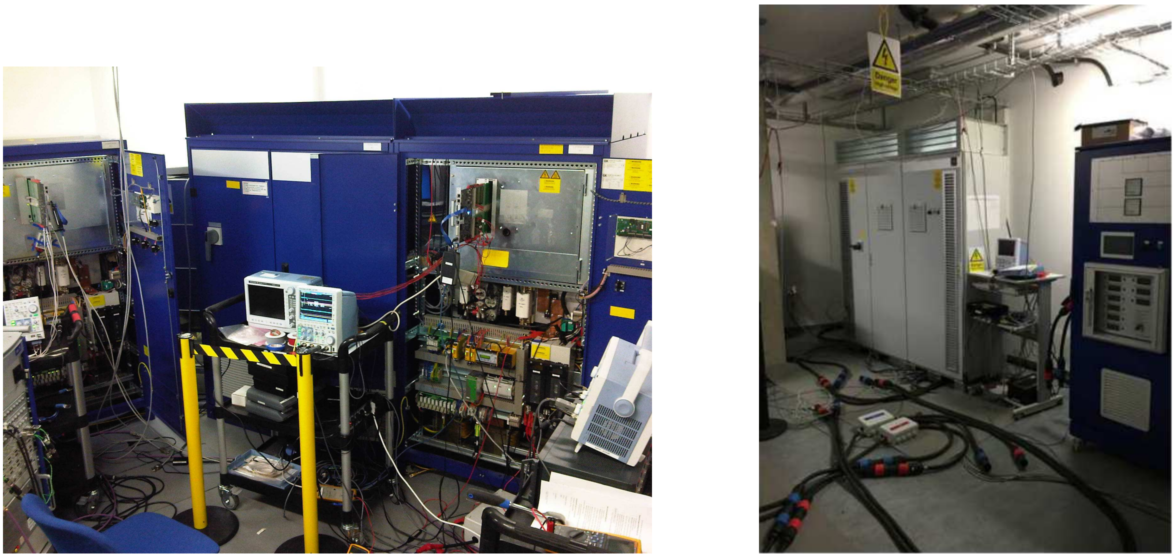

Figure 2.5: Battery emulator laboratory setup.

Die approbierte gedruckte Originalversion dieser Diplomarbeit ist an der TU Wien Bibliothek verfügbar.
The approved original version of this thesis is available in print at TU Wien Bibliothek.

Die approbierte gedruckte Originalversion dieser Diplomarbeit ist an der TU Wien Bibliothek verfügbar.
The approved original version of this thesis is available in print at TU Wien Bibliothek.
TU Bibliothek WIEN Your knowledge hub

Chapter 3

Control Design

A BE has to achieve fast and accurate output voltage tracking of a reference extracted from a battery model. The control design of the BE is crucial for tight coupling between the physical test bed and the battery model. Moreover, the current needs to be equally balanced among the phases while respecting safe operating condition limits. The switching input structure poses further challenges on the control design. Finally, stability has to be guaranteed for the entire operating range with a high degree of uncertainty towards UUT including negative impedance instability [9].
For these reasons, this chapter elaborates two different control frameworks, namely model predictive control (MPC) and backstepping (BS) control, and discusses suitability and limitations to achieve the above mentioned goals.

3.1 Related literature

This section reviews the MPC and BS frameworks and gives an overview of the concepts.

3.1.1 Model predictive control

Model predictive control (MPC) has become an attractive and well-established control strategy for power electronic converters and drives [2]. One of the major advantages over traditional control approaches is that it allows intuitively incorporating constraints and nonlinearities [13] as well as requirements such as switching losses [14]. The basic idea is to use a system model to predict the state and output evolution over a prediction horizon N_p when applying an input sequence of control horizon length N_c. Usually N_c is chosen shorter than N_p, in this case the input is held constant for time steps beyond N_c. The input sequence is chosen to minimize a cost function while respecting constraints on states and inputs by solving an optimization problem. Only the first element of the optimal input sequence is actually applied and the procedure is repeated at the next time step to close the loop in a receding horizon policy [15]. The principle of model predictive control (MPC) is illustrated in fig. 3.1.

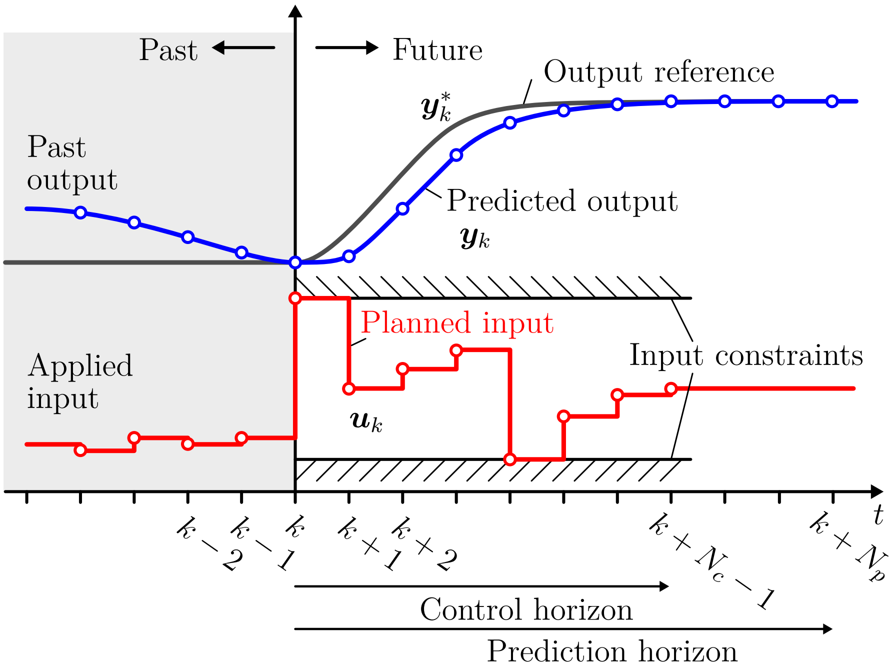

Figure 3.1: Principle of model predictive control for the SISO-case. The input sequence $\boldsymbol{u}_k$ is chosen such that the output tracking error $\|\boldsymbol{y}_k^* - \boldsymbol{y}_k\|^2$ is minimized over the prediction horizon N_p. Beyond the control horizon N_c the input is held constant with u_{k+N_c-1}. Out of $\boldsymbol{u}_k$ only the first element u_k is applied and the procedure is repeated at $k+1$, following the receding horizon policy.

The MPC framework can be classified based on the associated type of optimization problem, i.e., whether it is an integer optimization problem or not [3]. Classical MPC on the one hand is based on state-space averaging [16] and consequently uses a continuous control input, the duty cycle, and pulse width modulation (PWM) which yields in a fixed switching frequency. Continuous control strategies yield good steady-state performance whereas the switching frequency limits transient performance.

Direct or finite control-set MPC (FCS-MPC) on the other hand directly manipulates the switching states, omitting the need of a modulator which results in general in a variable switching frequency. The switching sequence from a finite control-set that minimizes a cost function is applied by using the receding horizon principle. FCS-MPC achieves very high dynamic performance compared to modulator-based approaches [17] while avoiding unnecessarily high switching frequencies that would increase switching losses. However, the steady-state performance is limited by time resolution that results from sampling

Die approbierte gedruckte Originalversion dieser Diplomarbeit ist an der TU Wien Bibliothek verfügbar.
The approved original version of this thesis is available in print at TU Wien Bibliothek.

Die approbierte gedruckte Originalversion dieser Diplomarbeit ist an der TU Wien Bibliothek verfügbar.
The approved original version of this thesis is available in print at TU Wien Bibliothek.

rate and prediction horizon. This is due to the exponentially growing computational burden with the number of input switches and prediction horizon. Therefore FCS-MPC may not be suitable for applications where high tracking accuracy is required [3]. Another drawback of the FSC-MPC method is that the steady-state will be a limit cycle implying convergence of state variables to a bounded invariant set which leads to the formulation of practical asymptotical stability instead of asymptotic stability [18]. The authors of [19] suggested an improved sphere decoding algorithm (SDA) firstly introduced for a three-phase voltage source inverter (VSI) in [20] to reduce the computational cost of the underlying integer optimization problem. Implementation of the SDA is discussed in chapter 4 and the FCS-MPC will serve as a reference for later comparisons in chapter 5. A different approach to achieve longer prediction horizons is to approximate the tail cost using approximate dynamic programming as proposed in [21].

In order to unify high steady-state and transient performance, model predictive pulse pattern control for a three-phase VSI was proposed in [22] and validated experimentally for a five-phase VSI in [23]. A computational efficient field programmable gate array (FPGA) implementation using the fast gradient method (FGM) is presented in [24]. The approach modifies switching instants of optimal pulse patterns to achieve reference stator flux vector tracking. A two loop structure using a linear quadratic regulator (LQR) to provide a reference state flux for the model predictive pulse pattern control method was proposed in [25]. A similar predictive optimal switching strategy for an AC-DC converter using active and reactive power references suggested in [26] and [27] is restricted to unconstrained problems.

A review of applications of MPC in power electronics is given in [28] and a summary of recent developments can be found in [3]. A continuous MPC formulation for battery impedance control was presented in [1].

3.1.2 Backstepping Control

The Backstepping (BS) method [29, 30] is a nonlinear Lyapunov-based control framework that can be used for systems in so called strict-feedback form, also known as lower triangular form

$$\begin{aligned}
\dot{\boldsymbol{x}}_1 &= \boldsymbol{f}_1(\boldsymbol{x}_1) && + \boldsymbol{g}_1(\boldsymbol{x}_1)x_2 \\
\dot{x}_2 &= f_2(\boldsymbol{x}_1, x_2) && + g_2(\boldsymbol{x}_1, x_2)x_3 \\
&\vdots \\
\dot{x}_n &= f_n(\boldsymbol{x}_1, x_2, ..., x_n) && + g_n(\boldsymbol{x}_1, x_2, ..., x_n)u.
\end{aligned} \tag{3.1}$$

It is a systematical approach to derive a control law in a recursive manner that asymptotically stabilizes the closed loop. Due to its underlying structure it is also refered to as integrator backstepping. BS is a similar approach to feedback linearization [30, 31] without the drawback of cancelling useful nonlinearities, giving additional flexibility. The idea is to construct a Lyapunov function for a subsystem and a virtual control input that stabilizes it. This procedure is repeated and the initial Lyapunov function extended until a control law for the real input is found that yields asymptotic stability of the closed loop. In some cases the invariance principle of Krasovskii-LaSalle [30] is needed to prove not only stability but asymptotic stability. The integrator backstepping method was applied for impedance control of an electrohydraulic system in [32].

3.2 Cascade control

This thesis proposes a cascade control structure as depicted in fig. 3.2 that decouples the voltage tracking problem and disturbance rejection in the outer loop from coping with the switching dynamics in the inner loop. Due to different dynamics of voltage and current, the two loop strategy allows increasing time resolution in the inner loop related to current without necessity of very long prediction horizons for the outer loop voltage tracking problem, which is a similar motivation as in [33]. Fig. 3.3 illustrates the different time scales of the inner and outer loop with different prediction intervals. The finite control set is only considered in the inner loop. A Kalman Filter estimates the states $\hat{\boldsymbol{x}}$ and unknown load $\hat{i}_\mathrm{L}$ based on measureable state vector $\boldsymbol{w}$. Moreover, it is used to compensate the computational delay of one sampling period that occurs for computational demanding strategies based on MPC for instance. The Kalman Filter design is discussed in section 3.8.

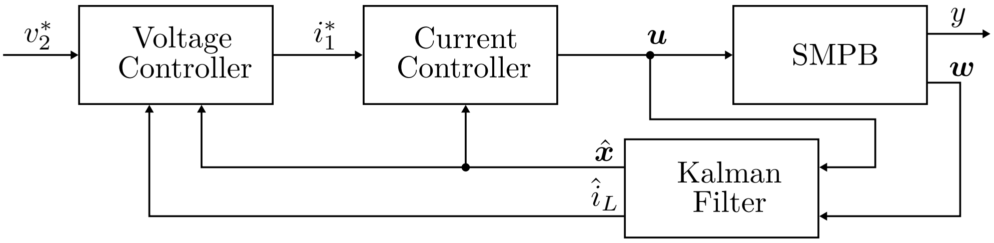

Figure 3.2: Cascade control structure with outer voltage control loop and inner current loop.

3.2.1 Outer loop - voltage control

The outer loop provides a continuous reference current i_1^* for the inner loop such that the output voltage is tracked accurately and load variations are compensated. While

Die approbierte gedruckte Originalversion dieser Diplomarbeit ist an der TU Wien Bibliothek verfügbar.
The approved original version of this thesis is available in print at TU Wien Bibliothek.

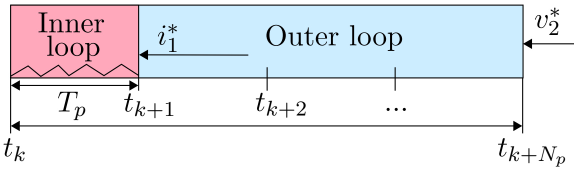

Figure 3.3: Different time scales of the inner and outer control loop.

the outer loop is not restricted to a specific control strategy, two variants are suggested in this thesis:

1. a continuous MPC that provides a reference current by minimizing the voltage tracking error over the prediction horizon and considering current limits on i_1,
2. a less computational demanding approach with drawbacks is to implement a Linear Quadratic Regulator (LQR) with anti-windup instead.

Both approaches will use the reduced order model with current as virtual control input from section 2.11 for the control design.

Constrained optimal voltage control

This subsection discusses a model predictive control problem with input constraints on virtual input i_1^* only. The discrete-time prediction model for the virtual input model (2.11) is given by

$$\boldsymbol{x}_{v,k+1} = \boldsymbol{\Phi}_v \boldsymbol{x}_{v,k} + \boldsymbol{\Gamma}_v u_k \tag{3.2a}$$

$$y_k = \boldsymbol{c}_v^{\mathrm{T}} \boldsymbol{x}_{v,k}. \tag{3.2b}$$

The optimal control sequence is found by minimizing the quadratic objective function

$$J_k = \sum_{i=1}^{N_p-1} q_i (y_{k+i}^* - y_{k+i})^2 + \sum_{i=0}^{N_c-1} r_i u_{v,k+i}^2, \tag{3.3}$$

with the reference value y_k^* and weighting factors q_i and r_i that penalize the control error and control effort. Tuning q_i and r_i results in a tradeoff between tracking convergence and control effort. The optimization problem can be formulated in dense form with input constraints only that can be solved highly efficiently using the fast gradient method. Details on the resulting optimization problem are discussed in chapter 4.

To achieve offset-free tracking due to model uncertainty or presence of constant disturbances, as well as to penalize only relative instead of absolute control effort, the

Die approbierte gedruckte Originalversion dieser Diplomarbeit ist an der TU Wien Bibliothek verfügbar.
The approved original version of this thesis is available in print at TU Wien Bibliothek.

prediction model can be extended with the absolute control input that represents a disturbance state and control move $\Delta u_k = u_{v,k} - u_{v,k-1}$ as control input [34], hence,

$$\begin{bmatrix} \boldsymbol{x}_{v,k+1} \\ u_{v,k} \end{bmatrix} = \begin{bmatrix} \boldsymbol{\Phi}_v & \boldsymbol{\Gamma}_v \\ \boldsymbol{0} & 1 \end{bmatrix} \begin{bmatrix} \boldsymbol{x}_{v,k} \\ u_{v,k-1} \end{bmatrix} + \begin{bmatrix} \boldsymbol{\Gamma}_v \\ 1 \end{bmatrix} \Delta u_k \tag{3.4a}$$

$$y_k = \begin{bmatrix} \boldsymbol{c}_v^{\mathrm{T}} & 0 \end{bmatrix} \begin{bmatrix} \boldsymbol{x}_{v,k} \\ u_{v,k-1} \end{bmatrix}. \tag{3.4b}$$

The objective function for the extended model is given by

$$J_k = \sum_{i=1}^{N_p-1} q_i (y^*_{k+i} - y_{k+i})^2 + \sum_{i=0}^{N_c-1} r_i (\Delta u_{k+i})^2. \tag{3.5}$$

Such a formulation comes with the drawback that the constraint on i_1 does not only imply an input constraint but a state constraint which complicates solving the associated optimization problem.

Unconstrained optimal voltage control

Although the formulation in the previous subsection is highly computationally efficient, another method with minimal computational cost as it can be calculated offline is presented in this subsection. To achieve zero steady-state error in presence of model mismatch or constant disturbances, the state vector $\boldsymbol{x}_{v,k}$ is extended with an error integral state $x_{I,k+1}$, i.e.,

$$\begin{bmatrix} \boldsymbol{x}_{v,k+1} \\ x_{I,k+1} \end{bmatrix} = \underbrace{\begin{bmatrix} \boldsymbol{\Phi}_v & \boldsymbol{0} \\ -\boldsymbol{c}_v^{\mathrm{T}} & 1 \end{bmatrix}}_{\boldsymbol{\Phi}_u} \begin{bmatrix} \boldsymbol{x}_{v,k} \\ x_{I,k} \end{bmatrix} + \underbrace{\begin{bmatrix} \boldsymbol{\Gamma}_v \\ 0 \end{bmatrix}}_{\boldsymbol{\Gamma}_u} u_{u,k} + \begin{bmatrix} \boldsymbol{0} \\ 1 \end{bmatrix} y^*_k \tag{3.6a}$$

$$y_k = \begin{bmatrix} \boldsymbol{c}_v^{\mathrm{T}} & 0 \end{bmatrix} \begin{bmatrix} \boldsymbol{x}_{v,k} \\ x_{I,k} \end{bmatrix}. \tag{3.6b}$$

This allows designing a discrete-time LQR [35] with state feedback law

$$u_{u,k} = \underbrace{\begin{bmatrix} \boldsymbol{k}_x^{\mathrm{T}} & k_I \end{bmatrix}}_{\boldsymbol{k}^{\mathrm{T}}} \underbrace{\begin{bmatrix} \boldsymbol{x}_{v,k} \\ x_{I,k} \end{bmatrix}}_{\boldsymbol{x}_{u,k+1}}. \tag{3.7}$$

Minimizing the infinite horizon objective function

$$J_\infty(\boldsymbol{x}_{v,0}) = \sum_{k=0}^{\infty} \boldsymbol{x}_{u,k}^{\mathrm{T}} \boldsymbol{Q}_u \boldsymbol{x}_{u,k} + u_{u,k} r_u u_{u,k} \tag{3.8}$$

Die approbierte gedruckte Originalversion dieser Diplomarbeit ist an der TU Wien Bibliothek verfügbar.
The approved original version of this thesis is available in print at TU Wien Bibliothek.
TU WIEN Bibliothek Your knowledge hub

yields the optimal feedback gain

$$\boldsymbol{k}^{\mathrm{T}} = -(r_u + \boldsymbol{\Gamma}_u^{\mathrm{T}} \boldsymbol{P}_u \boldsymbol{\Gamma}_u)^{-1} \boldsymbol{\Gamma}_u^{\mathrm{T}} \boldsymbol{P}_u \boldsymbol{\Phi}_u, \tag{3.9}$$

where $\boldsymbol{P}_u$ is the solution of the discrete-time algebraic Ricatti equation (DARE)

$$\boldsymbol{P}_u = \boldsymbol{\Phi}_u^{\mathrm{T}} \boldsymbol{P} \boldsymbol{\Phi}_u - \boldsymbol{\Phi}_u^{\mathrm{T}} \boldsymbol{P}_u \boldsymbol{\Gamma}_u (r_u + \boldsymbol{\Gamma}_u^{\mathrm{T}} \boldsymbol{P}_u \boldsymbol{\Gamma}_u)^{-1} \boldsymbol{\Gamma}_u^{\mathrm{T}} \boldsymbol{P}_u \boldsymbol{\Phi}_u + \boldsymbol{Q}_u. \tag{3.10}$$

The state weighting matrix has diagonal structure

$$\boldsymbol{Q}_u = \boldsymbol{q}_u \boldsymbol{I} \tag{3.11}$$

with

$$\boldsymbol{q}_u = \begin{bmatrix} q_{u,v_1} & q_{u,i_2} & q_{u,v_2} & q_{u,x_I} \end{bmatrix}^{\mathrm{T}} \tag{3.12}$$

and control weight

$$r_v. \tag{3.13}$$

Instead of explicitly considering constraints on the reference current that is treated as virtual control signal $u_{v,k} = i_1^*$, an anti-windup strategy is applied when virtual control saturation occurs. Hence, the actually applied control signal is

$$\tilde{u}_{u,k} = \begin{cases} i_{1,max} & \text{if } u_{u,k} > i_{1,max} \\ i_{1,min} & \text{if } u_{u,k} < i_{1,min} \\ u_{u,k} \quad (3.7) & \text{otherwise.} \end{cases} \tag{3.14}$$

Consequently, error integration is frozen when saturation occurs and error contribution would further increase the absolute value of the error integral state.

3.2.2 Inner loop - current control

The inner loop considers the switching system structure and has to achieve tight current tracking. The three different schemes

1. Finite Control-Set MPC (FCS-MPC),
2. Predictive Pulse Pattern Control (PPPC) and
3. Backstepping (BS) Control

are discussed in the next sections.

Die approbierte gedruckte Originalversion dieser Diplomarbeit ist an der TU Wien Bibliothek verfügbar.
The approved original version of this thesis is available in print at TU Wien Bibliothek.
TU WIEN Bibliothek Your knowledge hub

3.3 Finite Control-Set MPC

The full order model (2.6) of the SMPB has four binary inputs that result in $2^4 = 16$ possible switching combinations with the finite control set $\mathbb{U} = \mathscr{u} \times \mathscr{u} \times \mathscr{u} \times \mathscr{u}$ and $\mathscr{u} = \{0, 1\}$. When equal phases are assumed the reduced order model (2.10) with one input yielding in 5 switching combinations only can be used instead to reduce the computational cost. The associated finite control set is denoted as $\mathcal{U} = \{0, 1, 2, 3, 4\}$. This exploits the fact that each phase has an equal current contribution and the voltage dynamics of the first filter capacitance v_1 is determined only by the number of phases that are on (active) and off (inactive). As listed in table 3.1 the switching combinations grow exponentially with the prediction horzion N_p. For this reason the reduced order model is used to find the optimal number of active phases in a first step. The second step is to switch specific phases accordingly such that current is equally balanced. The former problem is referred to as total switching problem (TSP) and the latter as current balancing problem (CBP).

Table 3.1: The switching combinations grow exponentionally with the prediction horizon.

Prediction horizon	Switching combinations	
	Full order	Reduced order
1	16	5
2	256	25
3	4096	125
4	65536	625
5	1048576	3125
6	16777216	15625

The two step approach of subsequently solving the TSP and CBP is illustrated in fig. 3.4.

3.3.1 Total switching problem

The total switching problem (TSP) is to find the number of active switches needed to track the reference current. Therefore, an associated FCS-MPC problem is formulated in the following. The input sequence and state sequences over the control horizon N_c and prediction horizon N_p respectively are notated as

$$\boldsymbol{U}_k = \begin{bmatrix} u_k & u_{k+1} & \cdots & u_{N_c-1} \end{bmatrix}^{\mathrm{T}} \tag{3.15}$$

Die approbierte gedruckte Originalversion dieser Diplomarbeit ist an der TU Wien Bibliothek verfügbar.
The approved original version of this thesis is available in print at TU Wien Bibliothek.

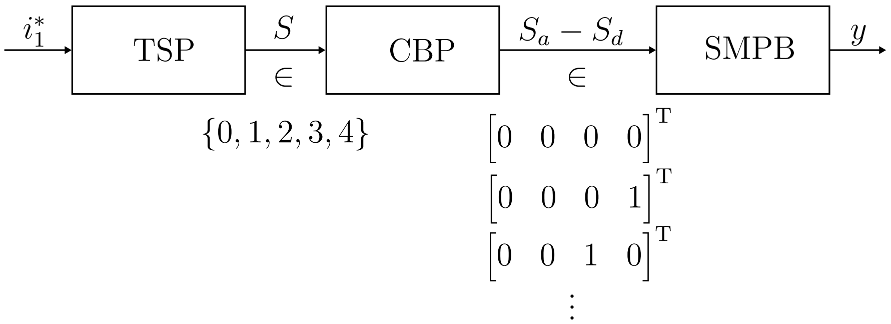
i_1^*
TSP
S
$\in$
$\{0,1,2,3,4\}$
CBP
$S_a - S_d$
$\in$
$\begin{bmatrix}0 & 0 & 0 & 0\end{bmatrix}^\mathrm{T}$
$\begin{bmatrix}0 & 0 & 0 & 1\end{bmatrix}^\mathrm{T}$
$\begin{bmatrix}0 & 0 & 1 & 0\end{bmatrix}^\mathrm{T}$
$\vdots$
SMPB
y

Figure 3.4: Two step current tracking approach.

$$\boldsymbol{X}_k = \begin{bmatrix}\boldsymbol{x}_{r,k+1}^\mathrm{T} & \boldsymbol{x}_{r,k+2}^\mathrm{T} & \cdots & \boldsymbol{x}_{r,N_p}^\mathrm{T}\end{bmatrix}^\mathrm{T}. \tag{3.16}$$

The state sequence can then be expressed as

$$\boldsymbol{X}_k = \mathcal{A}\boldsymbol{x}_{r,k} + \mathcal{B}\boldsymbol{U}_k, \tag{3.17}$$

where

$$\mathcal{A} = \begin{bmatrix}\boldsymbol{\Phi}_r \\ \boldsymbol{\Phi}_r^2 \\ \vdots \\ \boldsymbol{\Phi}_r^{N_p}\end{bmatrix}, \quad \mathcal{B} = \begin{bmatrix}\boldsymbol{\Gamma}_r & \boldsymbol{0} & \cdots & \boldsymbol{0} \\ \boldsymbol{\Phi}_r\boldsymbol{\Gamma}_r & \boldsymbol{\Gamma}_r & \boldsymbol{0} & \vdots \\ \vdots & \ddots & \ddots & \boldsymbol{0} \\ \boldsymbol{\Phi}_r^{N_p-1}\boldsymbol{\Gamma}_r & \cdots & \boldsymbol{\Phi}_r\boldsymbol{\Gamma}_r & \boldsymbol{\Gamma}_r\end{bmatrix}. \tag{3.18}$$

Consequently, the current output sequence

$$\boldsymbol{Y}_k = \begin{bmatrix}y_{i,k+1} & y_{i,k+2} & \cdots & y_{i,N_p}\end{bmatrix}^\mathrm{T} \tag{3.19}$$

is calculated as

$$\boldsymbol{Y}_k = \mathcal{C}(\mathcal{A}\boldsymbol{X}_k + \mathcal{B}\boldsymbol{U}_k) = \boldsymbol{F}\boldsymbol{X}_k + \boldsymbol{G}\boldsymbol{U}_k, \tag{3.20}$$

where

$$\mathcal{C} = \begin{bmatrix}\boldsymbol{c}_i^\mathrm{T} \\ \vdots \\ \boldsymbol{c}_i^\mathrm{T}\end{bmatrix}, \quad y_{i,k} = \underbrace{\begin{bmatrix}1 & 0 & 0 & 0\end{bmatrix}}_{\boldsymbol{c}_i^\mathrm{T}}\boldsymbol{x}_k. \tag{3.21}$$

Let the output reference trajectory at time step k be

$$\boldsymbol{Y}_k^* = \begin{bmatrix}i_1^* & i_1^* & \cdots & i_1^*\end{bmatrix}^\mathrm{T} \in \mathbb{R}^{N_p}, \tag{3.22}$$

λ_u denote a tuning factor that increases the switching cost, u_{k-1} refer to the previously applied input and $V_f(\boldsymbol{x}_{k+N_c})$ denote the terminal cost. The objective function is formulated as

$$J_k = \|\boldsymbol{Y}_k^* - \boldsymbol{Y}_k\|_{\boldsymbol{\Omega}}^2 + \lambda_u\|\boldsymbol{T}\boldsymbol{U}_k - \boldsymbol{E}u_{k-1}\|_{\boldsymbol{\Sigma}}^2 + V_f(\boldsymbol{x}_{k+N_c}), \tag{3.23}$$

Die approbierte gedruckte Originalversion dieser Diplomarbeit ist an der TU Wien Bibliothek verfügbar.
The approved original version of this thesis is available in print at TU Wien Bibliothek.

where

$$\boldsymbol{T} = \begin{bmatrix} \boldsymbol{I} & \mathbf{0} & \cdots & \cdots & \mathbf{0} \\ -\boldsymbol{I} & \boldsymbol{I} & \mathbf{0} & \cdots & \vdots \\ \mathbf{0} & -\boldsymbol{I} & \boldsymbol{I} & \mathbf{0} & \mathbf{0} \\ \vdots & \vdots & \ddots & \ddots & \vdots \\ \mathbf{0} & \cdots & \cdots & -\boldsymbol{I} & \boldsymbol{I} \end{bmatrix}, \quad \boldsymbol{E} = \begin{bmatrix} \boldsymbol{I} \\ \mathbf{0} \\ \vdots \\ \mathbf{0} \end{bmatrix} \tag{3.24}$$

and

$$\begin{aligned} V_f(\boldsymbol{x}_{r,k+N_c}) &= \|\boldsymbol{x}^*_{r,k+N_c} - \boldsymbol{x}_{r,k+N_c}\|^2_{\boldsymbol{P}} \\ &= (\boldsymbol{x}^*_{r,k+N_c} - \boldsymbol{x}_{r,k+N_c})^{\mathrm{T}} \boldsymbol{P} (\boldsymbol{x}^*_{r,k+N_c} - \boldsymbol{x}_{r,k+N_c}) \\ &= \boldsymbol{x}^{*\mathrm{T}}_{r,k+N_c} \boldsymbol{P} \boldsymbol{x}^*_{r,k+N_c} - 2\boldsymbol{x}^{*\mathrm{T}}_{r,k+N_c} \boldsymbol{P} \boldsymbol{x}_{r,k+N_c} + \boldsymbol{x}^{\mathrm{T}}_{r,k+N_c} \boldsymbol{P} \boldsymbol{x}_{r,k+N_c}. \end{aligned} \tag{3.25}$$

The objective function J_k has three goals:

1. output voltage tracking
2. minimizing switching effort
3. guarantee stability due to a terminal cost .

When the weighting matrices $\boldsymbol{\Omega}$ and $\boldsymbol{\Sigma}$ preserve diagonal structure, they allow to put emphasis on the tracking or switching goal for the corresponding prediction instance. The N_p-step-ahead state prediction at sample instance k is given by

$$\boldsymbol{x}_{r,k+N_p} = \boldsymbol{\Phi}_r^{N_p} \boldsymbol{x}_{r,k} + \mathcal{B}_{N_p} \boldsymbol{U}_k, \tag{3.26}$$

where $\mathcal{B}_{N_p}$ denotes the last row of $\mathcal{B}$.

State constraints

Due to the switching system structure the inputs are constrained to the finite control set $\mathcal{U}$. However, also the current i_1 needs to be constrained to $\pm i_{1,max}$ in order to ensure safe operating conditions. To this end, the state space is partitioned to determine the feasible input set $\mathcal{U}_f \subseteq \mathcal{U}$ that ensures the current constraint is not violated. This can be easily done by solving

$$\boldsymbol{U}_k = \mathcal{B}_i^{-1}(\boldsymbol{i}_{limit} - \mathcal{A}_i \boldsymbol{x}_r(j)), \tag{3.27}$$

where $\boldsymbol{i}_{limit}$ is a vector of length N_p with entries that refer to an active constraint, hence $i_1 = \pm i_{1,max}$ for the corresponding upper and lower switching constraint respectively. The matrices $\mathcal{A}_i$ and $\mathcal{B}_i$ refer to N_p state predictions projected to i_1 and $\boldsymbol{x}_r(j)$ is a

Die approbierte gedruckte Originalversion dieser Diplomarbeit ist an der TU Wien Bibliothek verfügbar.
The approved original version of this thesis is available in print at TU Wien Bibliothek.
TU WIEN Bibliothek Your knowledge hub

suitably fine resoluted slice j of the partitioned state space. The feasible set has to be reduced when the resulting entries for $\boldsymbol{U}_k$ are inside the maximum allowed control set $\mathcal{U}$. When online determing the optimal switching sequence, the current state is interpolated to the nearest slice of state partitions and the control set of consideration is adapted accordingly to the smallest finite control set that respects the current constraint. Besides this direct approach, the current can also be assumed to be constrained from the outer loop which would make this step obsolete.

Integer Quadratic Program

Expanding (3.23) yields

$$\begin{aligned}
J_k = {} & \|\boldsymbol{Y}_k^* - (\boldsymbol{F}\boldsymbol{x}_k + \boldsymbol{G}\boldsymbol{U}_k)\|_{\boldsymbol{\Omega}}^2 + \lambda_u \|\boldsymbol{T}\boldsymbol{U}_k - \boldsymbol{E}u_{k-1}\|_{\boldsymbol{\Sigma}}^2 \\
& + \boldsymbol{x}_{k+N_c}^{*\mathrm{T}} \boldsymbol{P} \boldsymbol{x}_{k+N_c}^* - 2\boldsymbol{x}_{k+N_c}^{*\mathrm{T}} \boldsymbol{P}(\boldsymbol{\Phi}_r^{N_p}\boldsymbol{x}_k + \mathcal{B}_{N_p}\boldsymbol{U}_k) \\
& + (\boldsymbol{\Phi}_r^{N_p}\boldsymbol{x}_k + \mathcal{B}_{N_p}\boldsymbol{U}_k)^{\mathrm{T}} \boldsymbol{P} (\boldsymbol{\Phi}_r^{N_p}\boldsymbol{x}_k + \mathcal{B}_{N_p}\boldsymbol{U}_k) \\
= {} & \|\boldsymbol{Y}_k^* - \boldsymbol{F}\boldsymbol{x}_k\|_{\boldsymbol{\Omega}}^2 - 2(\boldsymbol{Y}_k^* - \boldsymbol{F}\boldsymbol{x}_k)^{\mathrm{T}} \boldsymbol{\Omega}\boldsymbol{G}\boldsymbol{U}_k + \boldsymbol{U}_k^{\mathrm{T}}\boldsymbol{G}^{\mathrm{T}}\boldsymbol{\Omega}\boldsymbol{G}\boldsymbol{U}_k \\
& + \lambda_u \boldsymbol{U}_k^{\mathrm{T}}\boldsymbol{T}^{\mathrm{T}}\boldsymbol{\Sigma}\boldsymbol{T}\boldsymbol{U}_k - 2\lambda_u(\boldsymbol{E}u_{k-1})^{\mathrm{T}}\boldsymbol{\Sigma}\boldsymbol{T}\boldsymbol{U}_k + \lambda_u\|\boldsymbol{E}u_{k-1}\|_{\boldsymbol{\Sigma}}^2 \\
& + \boldsymbol{x}_{k+N_c}^{*\mathrm{T}} \boldsymbol{P} \boldsymbol{x}_{k+N_c}^* - 2\boldsymbol{x}_{k+N_c}^{*\mathrm{T}} \boldsymbol{P}(\boldsymbol{\Phi}_r^{N_p}\boldsymbol{x}_k + \mathcal{B}_{N_p}\boldsymbol{U}_k) \\
& + (\boldsymbol{\Phi}_r^{N_p}\boldsymbol{x}_k)^{\mathrm{T}}\boldsymbol{P}\boldsymbol{\Phi}_r^{N_p}\boldsymbol{x}_k + 2(\boldsymbol{\Phi}_r^{N_p}\boldsymbol{x}_k)^{\mathrm{T}}\boldsymbol{P}\mathcal{B}_{N_p}\boldsymbol{U}_k + (\mathcal{B}_{N_p}\boldsymbol{U}_k)^{\mathrm{T}}\boldsymbol{P}\mathcal{B}_{N_p}\boldsymbol{U}_k .
\end{aligned} \tag{3.28}$$

The control and prediction horizon shall have equal length, thus, $N = N_c = N_p$. The objective function (3.28) can then be written in compact form as a integer quadratic program (IQP)

$$J_k = \Lambda_k + 2\boldsymbol{\theta}_k^{\mathrm{T}}\boldsymbol{U}_k + \boldsymbol{U}_k^{\mathrm{T}}\boldsymbol{Q}\boldsymbol{U}_k, \tag{3.29}$$

with

$$\begin{aligned}
\Lambda_k = {} & \|\boldsymbol{Y}_k^* - \boldsymbol{F}\boldsymbol{x}_k\|_{\boldsymbol{\Omega}}^2 + \lambda_u\|\boldsymbol{E}u_{k-1}\|_{\boldsymbol{\Sigma}}^2 + \boldsymbol{x}_{k+N}^{*\mathrm{T}}\boldsymbol{P}\boldsymbol{x}_{k+N}^* \\
& - 2\boldsymbol{x}_{k+N}^{*\mathrm{T}}\boldsymbol{P}\boldsymbol{\Phi}_r^N\boldsymbol{x}_k + (\boldsymbol{\Phi}_r^N\boldsymbol{x}_k)^{\mathrm{T}}\boldsymbol{P}\boldsymbol{\Phi}_r^N\boldsymbol{x}_k
\end{aligned} \tag{3.30}$$

$$\boldsymbol{\theta}_k = ((\boldsymbol{F}\boldsymbol{x}_k - \boldsymbol{Y}_k^*)^{\mathrm{T}}\boldsymbol{\Omega}\boldsymbol{G} - \lambda_u(\boldsymbol{E}u_{k-1})^{\mathrm{T}}\boldsymbol{\Sigma}\boldsymbol{T} + (\boldsymbol{\Phi}_r^N\boldsymbol{x}_k - \boldsymbol{x}_{k+N}^{*\mathrm{T}})^{\mathrm{T}}\boldsymbol{P}\mathcal{B}_N)^{\mathrm{T}} \tag{3.31}$$

$$\boldsymbol{Q} = \boldsymbol{G}^{\mathrm{T}}\boldsymbol{\Omega}\boldsymbol{G} + \lambda_u\boldsymbol{S}^{\mathrm{T}}\boldsymbol{\Sigma}\boldsymbol{T} + \mathcal{B}_N^{\mathrm{T}}\boldsymbol{P}\mathcal{B}_N. \tag{3.32}$$

It can be seen that Λ_k is time varying but independent of the decision variable $\boldsymbol{U}_k$. Moreover, $\boldsymbol{Q}$ is a constant matrix, hence, only $\boldsymbol{\theta}_k$ needs to be calculated online. The terminal cost shall be zero for further analsyis, hence $V_f = 0$, or $\boldsymbol{P} = \boldsymbol{0}$.
The optimal switching sequence is obtained by solving

$$\begin{aligned}
\boldsymbol{U}_k^* = \underset{\boldsymbol{U}_k}{\operatorname{argmin}} \quad & J_k \\
\text{subject to} \quad & |i_1(t_{k+i})| \;\leq\; i_{1,max}, \quad i = 1, \dots, N \\
& \boldsymbol{U}_k \;\in\; \mathcal{U}_f \times \dots \times \mathcal{U}_f .
\end{aligned} \tag{3.33}$$

Die approbierte gedruckte Originalversion dieser Diplomarbeit ist an der TU Wien Bibliothek verfügbar.
The approved original version of this thesis is available in print at TU Wien Bibliothek.
TU WIEN Bibliothek Your knowledge hub

Integer Least Squares Problem

As shown in [36] minimizing the IQP (3.29) is equivalent as solving the associated integer least squares (ILS) problem with respect to the unconstrained optimum. For $\boldsymbol{Q} > 0$ the IQP (3.29) can be reformulated to the equivalent ILS problem, that is minimizing the euclidean distance

$$\|\boldsymbol{H}\boldsymbol{U}_k - \tilde{\boldsymbol{U}}_{unc,k}\|_2^2 \tag{3.34}$$

to the transformed unconstrained optimal solution

$$\tilde{\boldsymbol{U}}_{unc,k} = \boldsymbol{H}\boldsymbol{U}_{unc,k}. \tag{3.35}$$

The unconstrained optimal solution is given by

$$\boldsymbol{U}_{unc,k} = -\boldsymbol{Q}^{-1}\boldsymbol{\theta} \tag{3.36}$$

and the unique lower triangle matrix $\boldsymbol{H}$ can be found with the Cholesky decomposition

$$\boldsymbol{H}^{\mathrm{T}}\boldsymbol{H} = \boldsymbol{Q}. \tag{3.37}$$

An efficient algorithm to solve such an ILS problem is discussed in the following chapter in section 4.2.2.

3.3.2 Current balancing problem

The current balancing problem (CBP) is to distribute the current equally among the phases with the constraint given by S, the solution of the TSP that corresponds to the number of active phases per time step. As not only one element of the switching sequence $\boldsymbol{U} \in \mathcal{U}_f^N$ is applied but the whole sequence that corresponds to the considered prediction interval T_{P}, the state evolution has to be predicted consequently to determine individual switching states at intersampling time steps during T_{P}. The prediction model corresponds to the one used for the Kalman Filter design in section 3.8. The optimal individual switching sequence is obtained by minimizing the objective function

$$\begin{aligned} J^{\mathrm{CBP}} &= (\Delta i_{L_{14}})^2 + \lambda_{sw}(\Delta S)^2 \\ \text{subject to} \quad \boldsymbol{S} &\in \mathbb{U} : \textstyle\sum \boldsymbol{S} = S. \end{aligned} \tag{3.38}$$

for the entire control horizon. Thereby $\Delta i_{L_{14}}$ denotes the maximum individual phase current difference of the one-step phase current predictions and ΔS is the sum of switching actions when applying the candidate switching combination. The former ensures phase current do not diverge but remain in a tight band and the latter penalizes switching actions with the weight λ_{sw}. The objective function has to be evaluated only for entries $S > 0$ and $S < 4$, as $S = 0$ and $S = 4$ imply $\boldsymbol{S} = \begin{bmatrix}0 & 0 & 0 & 0\end{bmatrix}^{\mathrm{T}}$ and $\boldsymbol{S} = \begin{bmatrix}1 & 1 & 1 & 1\end{bmatrix}^{\mathrm{T}}$ respectively.

Die approbierte gedruckte Originalversion dieser Diplomarbeit ist an der TU Wien Bibliothek verfügbar.
The approved original version of this thesis is available in print at TU Wien Bibliothek.
TU WIEN Bibliothek Your knowledge hub

Die approbierte gedruckte Originalversion dieser Diplomarbeit ist an der TU Wien Bibliothek verfügbar.
The approved original version of this thesis is available in print at TU Wien Bibliothek.
TU Bibliothek Your knowledge hub WIEN

3.4 Predictive Pulse Pattern Control

The control strategy for the SMPB described in this section is inspired by the model predictive pulse pattern control method for an induction motor suggested in [22]. The proposed PPPC scheme allows two switching actions[1] per phase within the prediction interval T_p that is typically chosen to be equal the sampling period T_s. Therefore, a set of four optimal pulse patterns (OPP) which differ in simultaneously active phases is defined to cover each operating point. As summarized in table 3.2, pattern A allows 0 or 1 simultaneously active phases, pattern B allows 1 or 2, etc.

Table 3.2: Switching sequences for the set of pulse patterns.

Period	Pattern A				Pattern B				Pattern C				Pattern D			
	S_a	S_b	S_c	S_d	S_a	S_b	S_c	S_d	S_a	S_b	S_c	S_d	S_a	S_b	S_c	S_d
$t_0 \leq t < t_1$	1	0	0	0	1	0	0	0	1	1	0	0	1	1	1	0
$t_1 \leq t < t_2$	0	0	0	0	1	1	0	0	1	1	1	0	1	1	1	1
$t_2 \leq t < t_3$	0	1	0	0	0	1	0	0	0	1	1	0	0	1	1	1
$t_3 \leq t < t_4$	0	0	0	0	0	1	1	0	0	1	1	1	1	1	1	1
$t_4 \leq t < t_5$	0	0	1	0	0	0	1	0	0	0	1	1	1	0	1	1
$t_5 \leq t < t_6$	0	0	0	0	0	0	1	1	1	0	1	1	1	1	1	1
$t_6 \leq t < t_7$	0	0	0	1	0	0	0	1	1	0	0	1	1	1	0	1
$t_7 \leq t < t_8$	0	0	0	0	1	0	0	1	1	1	0	1	1	1	1	1

Using these pulse patterns implies reducing the number of possible control sequences and therefore degrades control performance in general as it affects reachability [37]. A detailed analysis in the context of principle control moves is given in [38]. The pulse patterns are optimal in the sense of minimal switching effort as only one switching state is changed at each switching instant $t_1 - t_7$, yielding in a fixed switching frequency. An example of a switching sequence for pulse pattern A is depicted in fig. 3.5.
The objective function

$$J_k = \sum_{i=1}^{8} \left((i_k^* - i_1(t_i))^2 + \sum_{j \in \mathcal{P}} \psi_j \left(\frac{1}{4} i_k^* - i_{L_{1_j}}(t_i) \right)^2 \right), \quad \mathcal{P} = \{a, b, c, d\} \tag{3.39}$$

---

[1] In fact, each pulse pattern contains one phase that switches only one time as the patterns are defined such that the corresponding second switching coincides with the end of the prediction interval. This way one decision variable can be eliminated while the possible switching sequence remains unchanged.

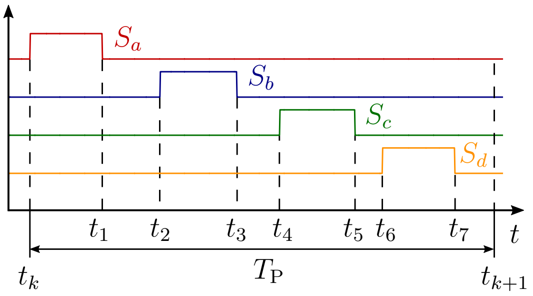

Figure 3.5: Example of a switching scheme for pulse pattern A.

comprises the sum current tracking error as well as the phase current tracking error at each switching instant and at the end of the prediction interval t_{k+1} with weighting factors ψ_j. The former will result in minimal sum current ripple and the latter is required to establish equal current balancing. By using the small ripple approximation [16] and approximating the voltage drop on phase resistances with the average phase current $i_{L_{1_j}}^{avg}$, the current predictions used in (3.39) can be expressed for each pulse pattern (sequence of switching states S_j depends on the OPP) recursively as

$$\begin{aligned} i_{L_{1_j}}(t_{i+1}) &= i_{L_{1_j}}(t_i) + \left(S_j(t_i)V_0 - v_1(t_0) - R_{1_j} i_{L_{1_j}}^{avg}\right) \frac{(t_{i+1}-t_i)}{L_{1_j}}, \\ &\text{with} \quad j \in \mathcal{P}, \quad i = 0, \dots, 7. \end{aligned} \tag{3.40}$$

Schematic current predictions for the set of pulse patterns are depicted in fig 3.6. The optimal vector of switching instants $\boldsymbol{t}^* = \begin{bmatrix} t_1 & t_2 & t_3 & t_4 & t_5 & t_6 & t_7 \end{bmatrix}^\mathrm{T}$ is obtained by solving the boundary control problem and $t_8 = t_{k+1}$

$$\begin{aligned} \boldsymbol{t}^* = \underset{\boldsymbol{t}}{\operatorname{argmin}} \quad & J_k \\ \text{subject to} \quad & t_i \ \leq \ t_{i+1}, \quad i = 0, \dots, 7, \end{aligned} \tag{3.41}$$

with $t_0 = t_k$. It shall be noted that the current constraint is assumed to be handled by the outer loop while the inner PPPC loop only accomplishes current tracking. Therefore, the switching ripple of the current has to be considered in the current limit. However, the state-space could easily be partitioned to find maximal on-times that can be added to the constraints of problem (3.41).

In contrast to a conventional FCS-MPC formulation as in section 3.3, the current predictions are based on the continuous-time dynamics which decouples time resolution from sampling rate and therefore yields in high accuracy as predictions include intersampling instants.

Die approbierte gedruckte Originalversion dieser Diplomarbeit ist an der TU Wien Bibliothek verfügbar.
The approved original version of this thesis is available in print at TU Wien Bibliothek.
TU WIEN Bibliothek Your knowledge hub

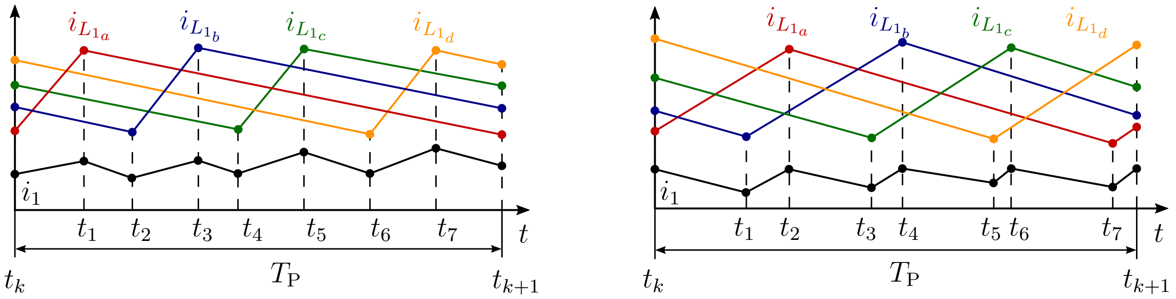

(a) Pattern A: 0 or 1 active phases.

(b) Pattern B: 1 or 2 active phases.

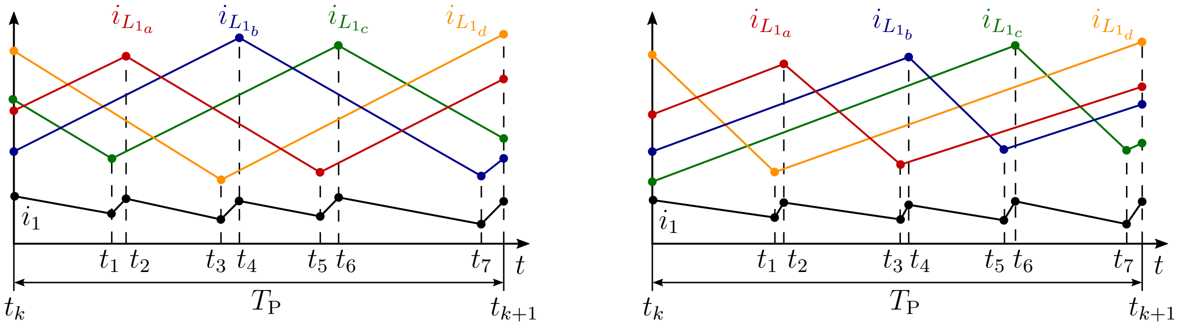

(c) Pattern C: 2 or 3 active phases.

(d) Pattern D: 3 or 4 active phases.

Figure 3.6: Current prediction at time instant k based on decision variables $t_1 - t_7$ for different pulse pattern switching sequences that differ in number of simultaneously active phases.

The objective function (3.39) is a function of the pulse pattern p and can be rewritten as

$$J_k(p) = \|\boldsymbol{i}_k^* - (\boldsymbol{F}(p)\boldsymbol{x}_{r,k} + \boldsymbol{G}_k(p)\boldsymbol{t}_k) + \boldsymbol{K}(p)\|_{\boldsymbol{\Psi}}^2, \quad p \in \{A, B, C, D\}, \tag{3.42}$$

where $\boldsymbol{x}_{r,k} = \begin{bmatrix} i_{L_{1_a},k} & i_{L_{1_b},k} & i_{L_{1_c},k} & i_{L_{1_d},k} & v_{1,k} \end{bmatrix}^\mathrm{T}$. The first eight elements of $\boldsymbol{i}^*$ are the sum current reference values i_1^* and the last four elements are the phase current reference values, hence $\frac{1}{4}i_1^*$. The decision variables that are the entries of $\boldsymbol{t}_k$ are normalized by $T_n = T_\mathrm{P}$ in order to improve the condition of the problem. The matrices $\boldsymbol{F}(A) - \boldsymbol{F}(D)$, $\boldsymbol{G}_k(A) - \boldsymbol{G}_k(D)$, $\boldsymbol{K}(A) - \boldsymbol{K}(D)$ and $\boldsymbol{\Psi}$ are defined in the appendix A.
Eventually $\boldsymbol{t}^*$ can be obtained by solving the standard quadratic problem

$$\begin{array}{rl} \min & \frac{1}{2}\boldsymbol{t}_k^\mathrm{T}\boldsymbol{H}_k\boldsymbol{t}_k + \boldsymbol{f}_k^\mathrm{T}\boldsymbol{t}_k \\ \text{subject to} & t_i \quad \leq \quad t_{i+1}, \quad i = 0, \ldots, 7, \\ \boldsymbol{H}_k & = 2\boldsymbol{G}_k^\mathrm{T}\boldsymbol{\Psi}\boldsymbol{G}_k, \\ \boldsymbol{f}_k & = 2(\boldsymbol{F}\boldsymbol{x}_{r,k} + \boldsymbol{K} - \boldsymbol{i}_k^*)^\mathrm{T}\,\boldsymbol{\Psi}\boldsymbol{G}_k \end{array} \tag{3.43}$$

Die approbierte gedruckte Originalversion dieser Diplomarbeit ist an der TU Wien Bibliothek verfügbar.
The approved original version of this thesis is available in print at TU Wien Bibliothek.
TU WIEN Bibliothek Your knowledge hub

with a conventional quadratic solver as discussed in chapter 4. The computational complexity is comparable with the problem formulated in [1], where a real-time capable active-set algorithm was verified with experimental results.

Die approbierte gedruckte Originalversion dieser Diplomarbeit ist an der TU Wien Bibliothek verfügbar.
The approved original version of this thesis is available in print at TU Wien Bibliothek.
TU WIEN Bibliothek Your knowledge hub

3.5 Backstepping control

This section treats the systematic derivation of a backstepping control law for the system described chapter 2. Rewriting system dynamics (2.1) into strict-feedback form (3.1) with state vector $\boldsymbol{x} = \begin{bmatrix} v_2 & i_2 & v_1 & i_{L_{1_a}} & i_{L_{1_b}} & i_{L_{1_c}} & i_{L_{1_d}} \end{bmatrix}^{\mathrm{T}}$, input vector $\boldsymbol{u} = \begin{bmatrix} S_a & S_b & S_c & S_d \end{bmatrix}^{\mathrm{T}}$ and disturbance $d = i_{\mathrm{L}}$ gives

$$\begin{aligned} \dot{x}_1 &= f_1(x_1) && + g_1 x_2 - g_1 d \\ \dot{x}_2 &= f_2(x_1, x_2) && + g_2 x_3 \\ \dot{x}_3 &= f_3(x_1, x_2, x_3) && + g_3(x_4 + x_5 + x_6 + x_7) \\ \dot{x}_4 &= f_4(x_1, x_2, x_3, x_4) && + g_4 u_1 \\ \dot{x}_5 &= f_5(x_1, x_2, x_3, x_5) && + g_5 u_2 \\ \dot{x}_6 &= f_6(x_1, x_2, x_3, x_6) && + g_6 u_3 \\ \dot{x}_7 &= f_7(x_1, x_2, x_3, x_7) && + g_7 u_4, \end{aligned} \tag{3.44}$$

with

$$i_1 = x_4 + x_5 + x_6 + x_7 = i_{L_{1_a}} + i_{L_{1_b}} + i_{L_{1_c}} + i_{L_{1_d}} \tag{3.45}$$

and

$$\begin{aligned} f_1(x_1) &= 0, & g_1 &= \frac{1}{C_2}, \\ f_2(x_1, x_2) &= -\frac{R_2 i_2 + v_2}{L_2}, & g_2 &= \frac{1}{L_2}, \\ f_3(x_1, x_2, x_3) &= -\frac{i_2}{C_1}, & g_3 &= \frac{1}{C_1}, \\ f_4(x_1, x_2, x_3, x_4) &= -\frac{R_{1_a} i_{L_{1_a}} + v_1}{L_{1_a}}, & g_4 &= \frac{V_0}{L_{1_a}}, \\ f_5(x_1, x_2, x_3, x_5) &= -\frac{R_{1_b} i_{L_{1_b}} + v_1}{L_{1_b}}, & g_5 &= \frac{V_0}{L_{1_b}}, \\ f_6(x_1, x_2, x_3, x_6) &= -\frac{R_{1_c} i_{L_{1_c}} + v_1}{L_{1_c}}, & g_6 &= \frac{V_0}{L_{1_c}}, \\ f_7(x_1, x_2, x_3, x_7) &= -\frac{R_{1_d} i_{L_{1_d}} + v_1}{L_{1_d}}, & g_7 &= \frac{V_0}{L_{1_d}}. \end{aligned} \tag{3.46}$$

The dynamics of the integrated voltage error $e_{v_{2_I}}$ and voltage error e_{v_2} are given by

$$\dot{e}_{v_{2_I}} = e_{v_2} = v_2 - v_{2_d} \tag{3.47}$$

$$\dot{e}_{v_2} = \dot{v}_2 - \dot{v}_{2_d} = -\dot{v}_{2_d} + g_1 i_2 - g_1 d. \tag{3.48}$$

Die approbierte gedruckte Originalversion dieser Diplomarbeit ist an der TU Wien Bibliothek verfügbar.
The approved original version of this thesis is available in print at TU Wien Bibliothek.
TU WIEN Bibliothek Your knowledge hub

Die approbierte gedruckte Originalversion dieser Diplomarbeit ist an der TU Wien Bibliothek verfügbar.
The approved original version of this thesis is available in print at TU Wien Bibliothek.

Introducing the virtual input

$$i_2 = \alpha_1(\boldsymbol{e}, \dot{v}_{2_d}) = \frac{1}{g_1}(-\beta_I e_{v_{2_I}} - \beta_v e_{v_2} + \dot{v}_{2_d}) + d, \tag{3.49}$$

let the error dynamics $\dot{\boldsymbol{e}}$ become linear such that it can be written as

$$\underbrace{\begin{bmatrix} \dot{e}_{v_{2_I}} \\ \dot{e}_{v_2} \end{bmatrix}}_{\dot{\boldsymbol{e}}} = \underbrace{\begin{bmatrix} 0 & 1 \\ -\beta_I & -\beta_v \end{bmatrix}}_{\boldsymbol{A}_e} \underbrace{\begin{bmatrix} e_{v_{2_I}} \\ e_{v_2} \end{bmatrix}}_{\boldsymbol{e}}. \tag{3.50}$$

Let

$$V_1(\boldsymbol{e}) = \boldsymbol{e}^{\mathrm{T}} \boldsymbol{P}_e \boldsymbol{e}, \quad \boldsymbol{P}_e > 0, \quad \boldsymbol{P}_e^{\mathrm{T}} = \boldsymbol{P}_e \tag{3.51}$$

be a Lyapunov candidate function. Its time derivative along the trajectories of (3.44) is given by

$$\dot{V}_1(\boldsymbol{e}) = \boldsymbol{e}^{\mathrm{T}} \boldsymbol{A}_e^{\mathrm{T}} \boldsymbol{P}_e \boldsymbol{e} + \boldsymbol{e}^{\mathrm{T}} \boldsymbol{P}_e \boldsymbol{A}_e \boldsymbol{e}. \tag{3.52}$$

The Lyapunov equation

$$\boldsymbol{A}_e^{\mathrm{T}} \boldsymbol{P}_e + \boldsymbol{P}_e \boldsymbol{A}_e + \boldsymbol{Q} = \boldsymbol{0} \tag{3.53}$$

has for every $\boldsymbol{Q} > 0$ and a Hurwitz matrix $\boldsymbol{A}_e$ a unique solution, such that

$$\dot{V}_1(\boldsymbol{e}) = -e_{v_{2_I}}^2 - e_{v_2}^2 < 0, \tag{3.54}$$

which asymptotically stabilizes the equilibrium. The closed loop performance can be tuned with parameters β_I and β_v that can be determined by placing the eigenvalues of $\boldsymbol{A}_e$.

In a next step, V_1 is augmented by the quadratic deviation of i_2 from its ideal trajectory $z_1 = i_2 - \alpha_1(\boldsymbol{e})$, which results in

$$V_2(\boldsymbol{e}, i_2) = V_1(\boldsymbol{e}) + \frac{\gamma_1}{2}(i_2 - \alpha_1(\boldsymbol{e}))^2, \qquad \gamma_1 > 0 \tag{3.55}$$

and its time derivative along the trajectories of (3.44)

$$\begin{aligned} \dot{V}_2(\boldsymbol{e}, i_2, v_1) &= \frac{\partial V_1}{\partial e_{v_{2_I}}} e_{v_2} + \frac{\partial V_1}{\partial e_{v_2}}(-\dot{v}_{2_d} + g_1 i_2 - g_1 d) \\ &\quad + \gamma_1 z_1 \left(f_2 + g_2 v_1 - \dot{\alpha}_1(\boldsymbol{e})\right) \\ &= \frac{\partial V_1}{\partial e_{v_{2_I}}} e_{v_2} + \frac{\partial V_1}{\partial e_{v_2}}(-\dot{v}_{2_d} + g_1 \alpha_1 - g_1 d) \\ &\quad + \gamma_1 z_1 \left(f_2 + g_2 v_1 - \dot{\alpha}_1(\boldsymbol{e}) + \frac{g_1}{\gamma_1} \frac{\partial V_1}{\partial e_{v_2}}\right). \end{aligned} \tag{3.56}$$

Die approbierte gedruckte Originalversion dieser Diplomarbeit ist an der TU Wien Bibliothek verfügbar.
The approved original version of this thesis is available in print at TU Wien Bibliothek.

Considering v_1 as virtual input, the ideal trajectory is given by

$$v_1 = \alpha_2(\boldsymbol{e}, z_1) = \frac{1}{g_2}\left(-k_1 z_1 - f_2 + \dot{\alpha}_1(\boldsymbol{e}) - \frac{g_1}{\gamma_1}\frac{\partial V_1}{\partial e_{v_2}}\right), \tag{3.57}$$

which asymptotically stabilizes the closed loop, as

$$\begin{aligned} \dot{V}_2(\boldsymbol{e}, z_1) = {} & \frac{\partial V_1}{\partial e_{v_{2_I}}} e_{v_2} + \frac{\partial V_1}{\partial e_{v_2}}(-\dot{v}_{2_d} + g_1\alpha_1(\boldsymbol{e}) - g_1 d) \\ & - \gamma_1 k_1 z_1^2 < 0. \end{aligned} \tag{3.58}$$

Augmenting V_2 by the quadratic deviation of v_1 from the ideal trajectory results in

$$\begin{aligned} V_3(\boldsymbol{e}, i_2, v_1) = V_2(\boldsymbol{e}, i_2) + \frac{\gamma_2}{2}(v_1 - \alpha_2(\boldsymbol{e}, z_1))^2, \\ \gamma_2 > 0. \end{aligned} \tag{3.59}$$

Substituting $v_1 = z_2 + \alpha_2(\boldsymbol{e}, z_1)$ leads to

$$\begin{aligned} \dot{V}_3(\boldsymbol{e}, z_1, z_2) = {} & \frac{\partial V_1}{\partial e_{v_{2_I}}} e_{v_2} + \frac{\partial V_1}{\partial e_{v_2}}(-\dot{v}_{2_d} + g_1\alpha_1(\boldsymbol{e}) - g_1 d) \\ & - \gamma_1 k_1 z_1^2 + \gamma_1 g_2 z_1 z_2 \\ & + \gamma_2 z_2 (f_3 + g_3 i_1 - \dot{\alpha}_2(\boldsymbol{e}, z_1)). \end{aligned} \tag{3.60}$$

Recursively, i_1 is considered as virtual input and the ideal trajectory

$$i_1 = \alpha_3(\boldsymbol{e}, z_1, z_2) = \frac{1}{g_3}\left(-k_2 z_2 - \frac{\gamma_1}{\gamma_2} g_2 z_1 - f_3 + \dot{\alpha}_2(\boldsymbol{e}, z_1)\right) \tag{3.61}$$

asymptotically stabilizes the closed loop, as

$$\begin{aligned} \dot{V}_3(\boldsymbol{e}, z_1, z_2) = {} & \frac{\partial V_1}{\partial e_{v_{2_I}}} e_{v_2} + \frac{\partial V_1}{\partial e_{v_2}}(-\dot{v}_{2_d} + g_1\alpha_1(\boldsymbol{e}) - g_1 d) \\ & - \gamma_1 k_1 z_1^2 - \gamma_2 k_2 z_2^2 < 0. \end{aligned} \tag{3.62}$$

Taking into account that $i_1 = i_{L_{1_a}} + i_{L_{1_b}} + i_{L_{1_c}} + i_{L_{1_d}}$ and equal current distribution among the four half-bridges is desired, V_3 can be augmented as

$$\begin{aligned} & V_4(\boldsymbol{e}, i_2, v_1, i_{L_1}, i_{L_2}, i_{L_3}, i_{L_4}) = V_3(\boldsymbol{e}, i_2, v_1) \\ & + \frac{\gamma_3}{2}\left(i_{L_{1_a}} - \frac{\alpha_3(\boldsymbol{e}, z_1, z_2)}{4}\right)^2 + \frac{\gamma_3}{2}\left(i_{L_{1_b}} - \frac{\alpha_3(\boldsymbol{e}, z_1, z_2)}{4}\right)^2 \\ & + \frac{\gamma_3}{2}\left(i_{L_{1_c}} - \frac{\alpha_3(\boldsymbol{e}, z_1, z_2)}{4}\right)^2 + \frac{\gamma_3}{2}\left(i_{L_{1_d}} - \frac{\alpha_3(\boldsymbol{e}, z_1, z_2)}{4}\right)^2, \end{aligned} \tag{3.63}$$

with the error states

$$\begin{aligned} z_3 &= i_{L_{1_a}} - \frac{\alpha_3(\boldsymbol{e}, z_1, z_2)}{4} & z_4 &= i_{L_{1_b}} - \frac{\alpha_3(\boldsymbol{e}, z_1, z_2)}{4} \\ z_5 &= i_{L_{1_c}} - \frac{\alpha_3(\boldsymbol{e}, z_1, z_2)}{4} & z_6 &= i_{L_{1_d}} - \frac{\alpha_3(\boldsymbol{e}, z_1, z_2)}{4}. \end{aligned} \tag{3.64}$$

The time derivative of (3.63) along the solutions of (3.44) is given by

$$\begin{aligned} \dot{V}_4 = {} & \frac{\partial V_1}{\partial e_{v_{2_I}}} e_{v_2} + \frac{\partial V_1}{\partial e_{v_2}} (-\dot{v}_{2_d} + g_1 \alpha_1(\boldsymbol{e}) - g_1 d) \\ & - \gamma_1 k_1 z_1^2 - \gamma_2 k_2 z_2^2 + \gamma_2 g_3 z_2 (z_3 + z_4 + z_5 + z_6) \\ & + \gamma_3 z_3 \left(f_4 + g_4 u_1 - \frac{\dot{\alpha}_3(\boldsymbol{e}, z_1, z_2)}{4} \right) \\ & + \gamma_3 z_4 \left(f_5 + g_5 u_2 - \frac{\dot{\alpha}_3(\boldsymbol{e}, z_1, z_2)}{4} \right) \\ & + \gamma_3 z_5 \left(f_6 + g_6 u_3 - \frac{\dot{\alpha}_3(\boldsymbol{e}, z_1, z_2)}{4} \right) \\ & + \gamma_3 z_6 \left(f_7 + g_7 u_4 - \frac{\dot{\alpha}_3(\boldsymbol{e}, z_1, z_2)}{4} \right). \end{aligned} \tag{3.65}$$

Finally, a control law for each half-bridge that asymptotically stabilizes the closed loop trajectories of (3.44), thus $\dot{V}_4 < 0$, can be derived as

$$\begin{aligned} u_1 &= \frac{1}{g_4} \left(-k_3 z_3 - \frac{\gamma_2}{\gamma_3} g_3 z_2 - f_4 + \frac{\dot{\alpha}_3(\boldsymbol{e}, z_1, z_2)}{4} \right) \\ u_2 &= \frac{1}{g_5} \left(-k_4 z_4 - \frac{\gamma_2}{\gamma_3} g_3 z_2 - f_5 + \frac{\dot{\alpha}_3(\boldsymbol{e}, z_1, z_2)}{4} \right) \\ u_3 &= \frac{1}{g_6} \left(-k_5 z_5 - \frac{\gamma_2}{\gamma_3} g_3 z_2 - f_6 + \frac{\dot{\alpha}_3(\boldsymbol{e}, z_1, z_2)}{4} \right) \\ u_4 &= \frac{1}{g_7} \left(-k_6 z_6 - \frac{\gamma_2}{\gamma_3} g_3 z_2 - f_7 + \frac{\dot{\alpha}_3(\boldsymbol{e}, z_1, z_2)}{4} \right). \end{aligned} \tag{3.66}$$

The tuning parameters γ_1, γ_2 and γ_3 reduce the deviation from the desired behaviour given by α_1, α_2 and α_3 respectively, while the corresponding coupling-terms are necessary for stability in the Lyapunov function time derivative. As a rule of thumb, they should be chosen such that

$$\begin{aligned} g_1 &\ll \gamma_1 \\ \gamma_1 g_2 &\ll \gamma_2 \\ \gamma_2 g_3 &\ll \gamma_3. \end{aligned} \tag{3.67}$$

Die approbierte gedruckte Originalversion dieser Diplomarbeit ist an der TU Wien Bibliothek verfügbar.
The approved original version of this thesis is available in print at TU Wien Bibliothek.
TU WIEN Bibliothek Your knowledge hub

Instead of deriving a separate control law for each half-bridge, when equal phase configurations are assumed, such that

$$L_{1_a} = L_{1_b} = L_{1_c} = L_{1_d} \tag{3.68}$$

$$R_{1_a} = R_{1_b} = R_{1_c} = R_{1_d} \tag{3.69}$$

holds, one could also use the lumped model (2.10) and introduce the deviation term of the ideal i_1 trajectory

$$\underline{z}_3 = i_1 - \alpha_3(\boldsymbol{e}, z_1, z_2). \tag{3.70}$$

Let

$$\underline{g}_4 = \frac{V_0}{L_1} \tag{3.71}$$

$$\underline{f}_4 = -\frac{R_1 i_1 + v_1}{L_1}. \tag{3.72}$$

This gives by augmenting V_3 with the quadratic deviation of i_1 from the ideal trajectory the Lyapunov function candidate

$$V_{4_0}(\boldsymbol{e}, i_2, v_1, i_1) = V_3(\boldsymbol{e}, i_2, v_1) + \frac{\underline{\gamma}_3}{2}\left(i_1 - \alpha_3(\boldsymbol{e}, z_1, z_2)\right)^2, \quad \underline{\gamma}_3 > 0. \tag{3.73}$$

Its time derivative follows then as

$$\begin{aligned} \dot{V}_{4_0} = {} & \frac{\partial V_1}{\partial e_{v_{2_I}}} e_{v_2} + \frac{\partial V_1}{\partial e_{v_2}}(-\dot{v}_{2_d} + g_1\alpha_1(\boldsymbol{e}) - g_1 d) \\ & - \gamma_1 k_1 z_1^2 - \gamma_2 k_2 z_2^2 + \gamma_2 g_3 z_2 \underline{z}_3 \\ & + \underline{\gamma}_3 \underline{z}_3 \left(\underline{f}_4 + \underline{g}_4 u_0 - \dot{\alpha}_3(\boldsymbol{e}, z_1, z_2)\right). \end{aligned} \tag{3.74}$$

It can be seen that the closed loop trajectories of (3.44) can be asymptotically stabilized with the single control law

$$u_0 = \alpha_4(\boldsymbol{e}, z_1, z_2, \underline{z}_3) \frac{1}{\underline{g}_4}\left(-k_3 \underline{z}_3 - \frac{\gamma_2}{\underline{\gamma}_3} g_3 z_2 - \underline{f}_4 + \dot{\alpha}_3(\boldsymbol{e}, z_1, z_2)\right), \tag{3.75}$$

such that $\dot{V}_{4_0} < 0$. The corresponding control structure is depicted in Fig. 3.7.
The conventional backstepping method described in this section does not consider input nor state constraints. Furthermore, the computation of the virtual control laws α_1, α_2 and α_3 and its derivatives become more and more demanding as the system order increases. To overcome both of these issues, an extension that uses so called command filters is addressed in the next section.

Die approbierte gedruckte Originalversion dieser Diplomarbeit ist an der TU Wien Bibliothek verfügbar.
The approved original version of this thesis is available in print at TU Wien Bibliothek.
TU WIEN Bibliothek Your knowledge hub

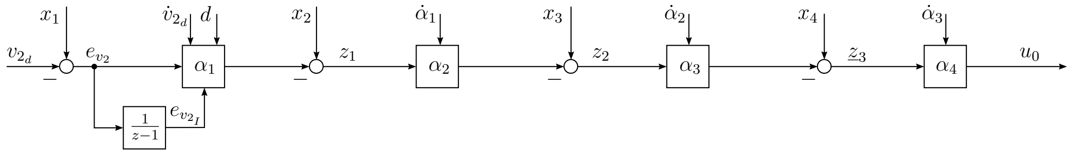

Figure 3.7: Backstepping control structure for the single control law case as defined in (3.75). The virtual control signals α_i and its time derivatives have to be calculated explicitly for the next stage.

3.6 Command Filtered Backstepping

Command Filtered Backstepping (CFBS) is a modification of the conventional backstepping method which brings two interesting advantages [4]. In contrast to the simple notation, analytical expressions of the time derivatives of the virtual command signals α_i with $i = \{1, \ldots, 4\}$ get more and more complicated for higher order systems. CFBS allows to derive them with a simple filtering approach. Secondly, input and state constraints can be considered while guaranteeing stability with Lyapunov arguments. Moreover, CFBS is not restricted to systems in strict-feedback form as the conventional approach. CFBS can also be extended to the adaptive case to deal with parameter uncertainties as shown in [39].
Define the tracking errors

$$\tilde{z}_i = x_i - x_{i_c} \tag{3.76}$$

and the compensated tracking errors

$$v_{c_i} = \tilde{z}_i - \xi_i, \tag{3.77}$$

with saturation signals ξ_i, $i = 1, ...4$. Thereby $\tilde{z}_1$ denotes the output voltage tracking error defined as

$$\tilde{z}_1 = x_1 - x_{1_c} = v_2 - v_{2_d}. \tag{3.78}$$

Consider the Lyapunov candidate function

$$\tilde{V}_1 = \frac{1}{2} v_{c_1}^2 \tag{3.79}$$

and its time derivative along trajectories of (3.44)

$$\begin{aligned}
\frac{\mathrm{d}}{\mathrm{d}t}\tilde{V}_1 &= v_{c_1}(f_1 + g_1 x_2 - g_1 d - \dot{x}_{1_c} - \dot{\xi}_1) \\
&= v_{c_1}(f_1 + g_1(\tilde{z}_2 + x_{2_c}) + g_1(\tilde{\alpha}_1 - \xi_2) - g_1(\tilde{\alpha}_1 - \xi_2) - g_1 d - \dot{x}_{1_c} - \dot{\xi}_1) \\
&= v_{c_1}(f_1 + g_1 \underbrace{(\tilde{z}_2 - \xi_2)}_{v_{c_2}} + g_1\tilde{\alpha}_1 + g_1(x_{2_c} - \tilde{\alpha}_1 + \xi_2) - g_1 d - \dot{x}_{1_c} - \dot{\xi}_1).
\end{aligned} \tag{3.80}$$

Die approbierte gedruckte Originalversion dieser Diplomarbeit ist an der TU Wien Bibliothek verfügbar.
The approved original version of this thesis is available in print at TU Wien Bibliothek.

Considering $\tilde{\alpha}_1$ as virtual input command

$$\tilde{\alpha}_1 = \frac{1}{g_1}(-k_1\tilde{z}_1 - f_1 + \dot{x}_{1_c}) + d \tag{3.81}$$

and choosing

$$\dot{\xi}_1 = g_1(x_{2_c} - \tilde{\alpha}_1 + \xi_2) - k_1\xi_1 \tag{3.82}$$

then (3.80) becomes

$$\begin{aligned}\frac{\mathrm{d}}{\mathrm{d}t}\tilde{V}_1 &= -k_1 v_{c_1}(\tilde{z}_1 - \xi_1) - g_1 v_{c_1} v_{c_2} \\ &= -k_1 v_{c_1}^2 - g_1 v_{c_1} v_{c_2}.\end{aligned} \tag{3.83}$$

Thus, the cross-coupling term $g_1 v_1 v_2$ needs to be compensated in the next step, to achieve asymptotic stability, hence $\dot{\tilde{V}}_1 < 0$. It can further be seen that ξ_1 has PT1-dynamics with plant parameter g_1 and control parameter k_1.
Augmenting (3.79) with the quadratic compensated tracking error $v_{c_2}^2$ gives the Lyapunov function candidate

$$\tilde{V}_2 = \tilde{V}_1 + \frac{\tilde{\gamma}_2}{2} v_{c_2}^2 \tag{3.84}$$

and its time derivative along the solutions of (3.44)

$$\begin{aligned}\frac{\mathrm{d}}{\mathrm{d}t}\tilde{V}_2 &= -k_1 v_{c_1}^2 - g_1 v_{1_c} v_{2_c} + \tilde{\gamma}_2 v_{c_2}(f_2 + g_2 x_3 - \dot{x}_{2_c} - \dot{\xi}_2) \\ &= -k_1 v_{c_1}^2 - g_1 v_{1_c} v_{2_c} \\ &+ \tilde{\gamma}_2 v_{c_2}(f_2 + g_2(\tilde{z}_3 + x_{3_c}) + g_2(\tilde{\alpha}_2 - \xi_3) - g_2(\tilde{\alpha}_2 - \xi_3) - \dot{x}_{2_c} - \dot{\xi}_2) = \\ &= -k_1 v_{c_1}^2 - g_1 v_{1_c} v_{2_c} \\ &+ \tilde{\gamma}_2 v_{c_2}(f_2 + g_2 \underbrace{(\tilde{z}_3 - \xi_3)}_{v_{c_3}} + g_2\tilde{\alpha}_2 + g_2(x_{3_c} - \tilde{\alpha}_2 + \xi_3) - \dot{x}_{2_c} - \dot{\xi}_2).\end{aligned} \tag{3.85}$$

The virtual input command $\tilde{\alpha}_2$ has to compensate the cross-coupling term which is achieved by

$$\tilde{\alpha}_2 = \frac{1}{g_2}(-k_2\tilde{z}_2 - f_2 + \dot{x}_{2_c} - \frac{g_1}{\tilde{\gamma}_2} v_{c_1}), \tag{3.86}$$

while $\dot{\xi}_2$ takes again PT1-dynamics

$$\dot{\xi}_2 = g_2(x_{3_c} - \tilde{\alpha}_2 + \xi_3) - k_2\xi_2, \tag{3.87}$$

which gives for (3.85)

$$\begin{aligned}\frac{\mathrm{d}}{\mathrm{d}t}\tilde{V}_2 &= -k_1 v_{c_1}^2 - \tilde{\gamma}_2 k_2 v_{c_2}(\tilde{z}_2 - \xi_2) - \tilde{\gamma}_2 g_2 v_{c_2} v_{c_3} = \\ &= -k_1 v_{c_1}^2 - \tilde{\gamma}_2 k_2 v_{c_2}^2 - \tilde{\gamma}_2 g_2 v_{c_2} v_{c_3}\end{aligned} \tag{3.88}$$

Die approbierte gedruckte Originalversion dieser Diplomarbeit ist an der TU Wien Bibliothek verfügbar.
The approved original version of this thesis is available in print at TU Wien Bibliothek.

and leaves another cross-coupling term that has to be canceled in the next step.
By augmenting (3.84) with the quadratic compensated tracking error $v_{c_3}^2$ another Lyapunov function candidate

$$\tilde{V}_3 = \tilde{V}_2 + \frac{\tilde{\gamma}_3}{2} v_{c3}^2 \tag{3.89}$$

can be found. Its time derivative along the solutions of (3.44) takes the form

$$\begin{aligned}
\frac{\mathrm{d}}{\mathrm{d}t}\tilde{V}_3 &= -k_1 v_{c_1}^2 - \tilde{\gamma}_2 k_2 v_{c_2}^2 - \tilde{\gamma}_2 g_2 v_{2_c} v_{3_c} + \tilde{\gamma}_3 v_{c_3}(f_3 + g_3 x_4 - \dot{x}_{3_c} - \dot{\xi}_3) \\
&= -k_1 v_{c_1}^2 - \tilde{\gamma}_2 k_2 v_{c_2}^2 - \tilde{\gamma}_2 g_2 v_{2_c} v_{3_c} \\
&+ \tilde{\gamma}_3 v_{c_3}(f_3 + g_3(\tilde{z}_4 + x_{4_c}) + g_3(\tilde{\alpha}_3 - \xi_4) - g_3(\tilde{\alpha}_3 - \xi_4) - \dot{x}_{3_c} - \dot{\xi}_3) = \\
&= -k_1 v_{c_1}^2 - \tilde{\gamma}_2 k_2 v_{c_2}^2 - \tilde{\gamma}_2 g_2 v_{2_c} v_{c_3} \\
&+ \tilde{\gamma}_3 v_{c_3}(f_3 + g_3 \underbrace{(\tilde{z}_4 - \xi_4)}_{v_{c_4}} + g_3\tilde{\alpha}_3 + g_3(x_{4_c} - \tilde{\alpha}_3 + \xi_4) - \dot{x}_{3_c} - \dot{\xi}_3).
\end{aligned} \tag{3.90}$$

The cross-coupling term can be compensated with the ideal virtual input command

$$\tilde{\alpha}_3 = \frac{1}{g_3}(-k_3\tilde{z}_3 - f_3 + \dot{x}_{3_c} - g_2\frac{\tilde{\gamma}_2}{\tilde{\gamma}_3} v_{c_2}), \tag{3.91}$$

while applying PT1-dynamics for $\dot{\xi}_3$ such that

$$\dot{\xi}_3 = g_3(x_{4_c} - \alpha_3 + \xi_4) - k_3\xi_3. \tag{3.92}$$

This results for (3.90) in

$$\begin{aligned}
\frac{\mathrm{d}}{\mathrm{d}t}\tilde{V}_3 &= -k_1 v_{c_1}^2 - \tilde{\gamma}_2 k_2 v_{c_2}^2 - \tilde{\gamma}_3 k_3 v_{c_3}(\tilde{z}_3 - \xi_3) - \gamma_3 g_3 v_{c_3} v_{c_4} = \\
&= -k_1 v_{c_1}^2 - \tilde{\gamma}_2 k_2 v_{c_2}^2 - \tilde{\gamma}_3 k_3 v_{c_3}^2 - \tilde{\gamma}_3 g_3 v_{c_3} v_{c_4},
\end{aligned} \tag{3.93}$$

which leaves another cross-coupling term that has to be canceled in the last step.
As in the section before, the approach can easily be applied to generate four different control laws for each half-bridge. Nevertheless, only the single control law using the lumped model (2.10) will be addressed here.
Consequently, (3.89) is augmented with the quadratic compensated tracking error $v_{c_4}^2$, which gives

$$\tilde{V}_4 = \tilde{V}_3 + \frac{\tilde{\gamma}_4}{2} v_{c4}^2 \tag{3.94}$$

and its time derivative along the solutions of (3.44)

$$\begin{aligned}
\frac{\mathrm{d}}{\mathrm{d}t}\tilde{V}_4 &= -k_1 v_{c_1}^2 - \tilde{\gamma}_2 k_2 v_{c_2}^2 - \tilde{\gamma}_3 k_3 v_{c_3}^2 - \tilde{\gamma}_3 g_3 v_{3_c} v_{4_c} + \tilde{\gamma}_4 v_{c_4}(f_4 + g_4 u_c - \dot{x}_{4_c} - \dot{\xi}_4) \\
&= -k_1 v_{c_1}^2 - \tilde{\gamma}_2 k_2 v_{c_2}^2 - \tilde{\gamma}_3 k_3 v_{c_3}^2 - \tilde{\gamma}_3 g_3 v_{3_c} v_{4_c} \\
&+ \tilde{\gamma}_4 v_{c_4}(f_4 + g_4(u_c - \tilde{\alpha}_4) + g_4\tilde{\alpha}_4 - \dot{x}_{4_c} - \dot{\xi}_4).
\end{aligned} \tag{3.95}$$

Die approbierte gedruckte Originalversion dieser Diplomarbeit ist an der TU Wien Bibliothek verfügbar.
The approved original version of this thesis is available in print at TU Wien Bibliothek.

The cross-coupling term can be compensated with the ideal, unconstrained input command

$$\tilde{\alpha}_4 = \frac{1}{g_4}(-k_4\tilde{z}_4 - f_4 + \dot{x}_{4_c} - g_3\frac{\tilde{\gamma}_3}{\tilde{\gamma}_4}v_{c3}), \tag{3.96}$$

with

$$\dot{\xi}_4 = g_4(u_c - \tilde{\alpha}_4) - k_4\xi_4. \tag{3.97}$$

This results for (3.95) in

$$\begin{aligned}\frac{\mathrm{d}}{\mathrm{d}t}\tilde{V}_4 &= -k_1v_{c_1}^2 - \tilde{\gamma}_2k_2v_{c_2}^2 - \tilde{\gamma}_3k_3v_{c_3}^2 - \tilde{\gamma}_4k_4v_{c_4}(\tilde{z}_4 - \xi_4)\\ &= -k_1v_{c_1}^2 - \tilde{\gamma}_2k_2v_{c_2}^2 - \tilde{\gamma}_3k_3v_{c_3}^2 - \tilde{\gamma}_4k_4v_{c_4}^2 < 0.\end{aligned} \tag{3.98}$$

The constrained input command u_c that is actually applied is the output of the last command filter CF4. The whole structure is depicted in Fig. 3.8.

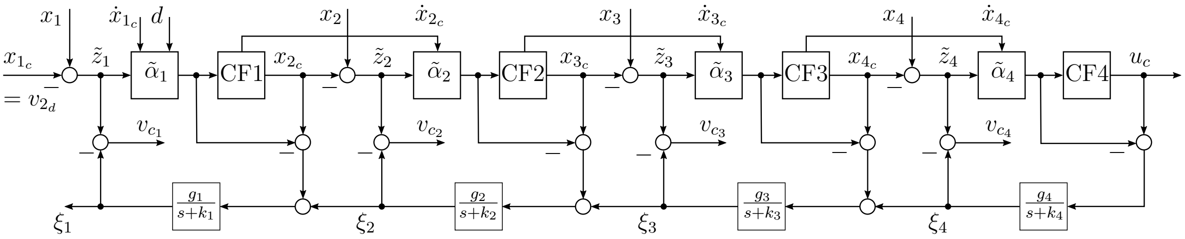

Figure 3.8: Command filtered backstepping structure. The virtual control signals $\tilde{\alpha}_i$ are computed as defined in (3.81), (3.86), (3.91) and (3.96) use the tracking errors $\tilde{z}_i$ and the time derivative of the filtered previous virtual control signal. The command filters (CF) allow imposing magnitude and rate constraints and provide the reference and its derivation for the next stage.

The command filter structure with natural frequency ω_n and damping coefficient ζ is illustrated in Fig. 3.9. As in this work magnitude saturation is sufficient, the continuous-time state-space representation can be written as

$$\begin{bmatrix}\dot{x}_{i_c}\\ \ddot{x}_{i_c}\end{bmatrix} = \begin{bmatrix}0 & 1\\ -\omega_n^2 & -2\zeta\omega_n\end{bmatrix}\begin{bmatrix}x_{i_c}\\ \dot{x}_{i_c}\end{bmatrix} + \begin{bmatrix}0\\ \omega_n^2\end{bmatrix}\mathrm{sat}\,(\tilde{\alpha}_{i-1}), \tag{3.99}$$

which has to be discretized for an implementation on a digital control unit. Thereby, care must be taken to respect the Nyquist-theorem regarding the choices of ω_n and the sample-rate. The authors in [4] suggest choosing $\omega_n > k_{i+1}$, such that x_{i+1_c} and $\dot{x}_{i+1_c}$ accurately track $\tilde{\alpha}_i$ and $\frac{\mathrm{d}}{\mathrm{d}t}\tilde{\alpha}_i$.

The great advantage of backstepping control is that it inherently stabilizes the closed loop in the sense of Lyapunov while $k_i > 0, i = 1, ..., 4$ and $\tilde{\gamma}_i > 0, i = 2, 3, 4$. However,

Die approbierte gedruckte Originalversion dieser Diplomarbeit ist an der TU Wien Bibliothek verfügbar.
The approved original version of this thesis is available in print at TU Wien Bibliothek.

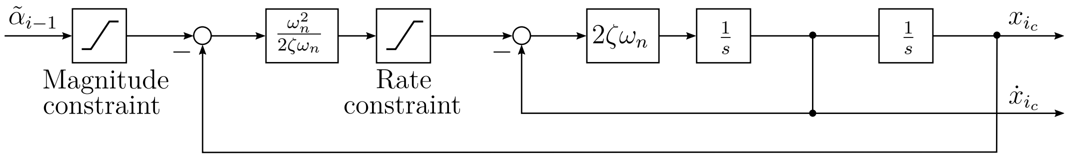

Figure 3.9: Command filter structure for $i = 2, 3, 4$. For an implementation on a digital control unit, the discrete-time state-space representation of (3.99) has to be used.

tuning these parameters becomes increasingly complex with higher system order as they all influence the closed loop performance. For this reason, the backstepping method can alternatively also be applied only in the inner loop, similarly as the aforementioned FCS-MPC and PPPC method using the two loop structure discussed in 3.2. This approach will be derived in the next section.

3.7 Inner Loop Command Filtered Backstepping

In the previous section, the backstepping method was used to systematically derive a stabilizing control law beginning from the output voltage v_2. In each stage, a virtual control signal was derived until the last stage, where the real control signal could be applied. Here instead, a desired reference for the sum phase current i_1^* , possibly from an outer loop, will be considered. The associated approach is referred to as Cascaded Backstepping (CBS). A similar approach of reference tracking of a LQR virtual control signal was suggested in [40] to control an active suspension system.
Denote the compensated tracking error as

$$v_c = \underbrace{i_1 - i_1^*}_{z} - \xi, \tag{3.100}$$

with the unconstrained and constrained reference current i_1 and i_1^* and tracking error z. Consider the following Lyapunov function candidate

$$V = \frac{1}{2} v_c^2 \tag{3.101}$$

and its time derivative along the solutions of (3.44)

$$\dot{V} = v_c(f_4 + g_4(u - u_c^0) + g_4 u_c^0 - \frac{\mathrm{d}}{\mathrm{d}t} i_1^* - \dot{\xi}). \tag{3.102}$$

Choosing the ideal, filtered and constrained input command as

$$u_c^0 = \alpha = \frac{1}{g_4}(-k\tilde{z} - f_4 + \frac{\mathrm{d}}{\mathrm{d}t} i_1^*), \tag{3.103}$$

Die approbierte gedruckte Originalversion dieser Diplomarbeit ist an der TU Wien Bibliothek verfügbar.
The approved original version of this thesis is available in print at TU Wien Bibliothek.
TU Bibliothek WIEN Your knowledge hub

with

$$\dot{\xi} = g_4(u - u_c^0) - k\xi, \tag{3.104}$$

results for (3.102) in

$$\begin{aligned} \dot{V} &= kv_c(-z + \xi) \\ &= -kv_c^2 < 0. \end{aligned} \tag{3.105}$$

Due to the flexible structure of the backstepping framework, the CFBS method presented in section 3.6 can also be used in the outer loop described in section 3.2 instead.

Die approbierte gedruckte Originalversion dieser Diplomarbeit ist an der TU Wien Bibliothek verfügbar.
The approved original version of this thesis is available in print at TU Wien Bibliothek.
TU WIEN Bibliothek Your knowledge hub

3.8 Observer Design

This chapter discusses the design of a stationary Kalman Filter to provide state estimations for the controller as described in chapter 3. This allows to

- reconstruct unmeasurable states
- improve quality of measured states
- compensate the computational delay
- increase robustness by estimating unknown disturbances .

The observer model is derived from model (2.1) and extending the state vector with the disturbance i_L, hence $\boldsymbol{x}_o = \begin{bmatrix} i_{L_{1_a}} & i_{L_{1_b}} & i_{L_{1_c}} & i_{L_{1_d}} & v_1 & i_2 & v_2 & i_\mathrm{L} \end{bmatrix}^\mathrm{T}$. Let the equivalent resistance be $r_0 \to \infty$ and consider the disturbance as constant but unknown

$$\frac{\mathrm{d}}{\mathrm{d}t} i_\mathrm{L} = 0. \tag{3.106}$$

The disturbance input vector

$$\boldsymbol{b}_d = \begin{bmatrix} 0 & 0 & 0 & 0 & 0 & 0 & -\frac{1}{C_2} \end{bmatrix}^\mathrm{T} \tag{3.107}$$

is discretized with

$$\boldsymbol{h} = \int_0^{T_s} \exp\left(\boldsymbol{A}\tau\right) \mathrm{d}\tau \boldsymbol{b}_d. \tag{3.108}$$

The discrete-time observer model is given by

$$\begin{bmatrix} \boldsymbol{x}_{k+1} \\ i_{\mathrm{L},k+1} \end{bmatrix} = \underbrace{\begin{bmatrix} \boldsymbol{\Phi} & \boldsymbol{h} \\ \boldsymbol{0} & 1 \end{bmatrix}}_{\boldsymbol{\Phi}_o} \underbrace{\begin{bmatrix} \boldsymbol{x}_k \\ i_{\mathrm{L},k} \end{bmatrix}}_{\boldsymbol{x}_{o,k}} + \underbrace{\begin{bmatrix} \boldsymbol{\Gamma} \\ 0 \end{bmatrix}}_{\boldsymbol{\Gamma}_o} \boldsymbol{u}_{o,k}, \tag{3.109a}$$

$$\boldsymbol{w}_m = \underbrace{\begin{bmatrix} \boldsymbol{C}_m & \boldsymbol{0} \end{bmatrix}}_{\boldsymbol{C}_o} \begin{bmatrix} \boldsymbol{x}_{o,k} \\ i_{\mathrm{L},k} \end{bmatrix}. \tag{3.109b}$$

with the vector of measurable states $\boldsymbol{w}_k = \boldsymbol{C}_m \boldsymbol{x}_k$. In this work it is assumed that each state but the unknown disturbance is measurable, hence $\boldsymbol{C}_m = \boldsymbol{I}$. The observer has Luenberger structure with the update law

$$\hat{\boldsymbol{x}}_{o,k+1} = \boldsymbol{\Phi}_o \hat{\boldsymbol{x}}_{o,k} + \boldsymbol{\Gamma}_o \boldsymbol{u}_{o,k} - \boldsymbol{L}(\boldsymbol{w}_k - \boldsymbol{C}_m \hat{\boldsymbol{x}}_{o,k}) \tag{3.110a}$$

$$= (\boldsymbol{\Phi}_o - \boldsymbol{L}\boldsymbol{C}_m)\hat{\boldsymbol{x}}_{o,k} + \boldsymbol{\Gamma}_o \boldsymbol{u}_{o,k} + \boldsymbol{L}\boldsymbol{C}_m \boldsymbol{x}_k. \tag{3.110b}$$

Die approbierte gedruckte Originalversion dieser Diplomarbeit ist an der TU Wien Bibliothek verfügbar.
The approved original version of this thesis is available in print at TU Wien Bibliothek.

The stationary Kalman gain $\boldsymbol{L}$ is given by

$$\boldsymbol{L} = \boldsymbol{\Phi}_o \boldsymbol{P}_o \boldsymbol{C}_o^{\mathrm{T}} (\boldsymbol{R}_o + \boldsymbol{C}_o \boldsymbol{P}_o \boldsymbol{C}_o^{\mathrm{T}})^{-1}, \tag{3.111}$$

where $\boldsymbol{P}_o$ is the stationary solution ($\boldsymbol{P}_o = \boldsymbol{P}_{o,k} = \boldsymbol{P}_{o,k+1}$) of the DARE

$$\boldsymbol{P}_o = \boldsymbol{\Phi}_o \boldsymbol{P}_o \boldsymbol{\Phi}_o^{\mathrm{T}} - \boldsymbol{\Phi}_o \boldsymbol{P}_o \boldsymbol{C}_o^{\mathrm{T}} (\boldsymbol{R}_o + \boldsymbol{C}_o \boldsymbol{P}_o \boldsymbol{C}_o^{\mathrm{T}})^{-1} \boldsymbol{C}_o \boldsymbol{P}_o \boldsymbol{\Phi}_o^{\mathrm{T}} + \boldsymbol{Q}_o. \tag{3.112}$$

An important distinction to the control methods that consider the quantized input structure is that the observer considers the average input $\boldsymbol{u}_{o,k} \in [0,4]$ over one sampling period T_s. This can be done without performance degradation as the control signal is updated exactly with the sampling period[2]. The weighting matrices $\boldsymbol{Q}_o > 0$ and $\boldsymbol{R}_o > 0$ refer to the covariance of process and noise measurement noise respectively, assuming uncorrelated white noise. They have diagonal structure

$$\boldsymbol{Q}_o = \boldsymbol{q}_o \boldsymbol{I} \tag{3.113}$$

$$\boldsymbol{R}_o = \boldsymbol{r}_o \boldsymbol{I}, \tag{3.114}$$

with

$$\boldsymbol{q}_0 = \begin{bmatrix} q_{0,i_{L_{1_a}}} & q_{0,i_{L_{1_b}}} & q_{0,i_{L_{1_c}}} & q_{0,i_{L_{1_d}}} & q_{0,v_1} & q_{0,i_2} & q_{0,v_2} \end{bmatrix}^{\mathrm{T}} \tag{3.115}$$

$$\boldsymbol{r}_0 = \begin{bmatrix} r_{0,i_{L_{1_a}}} & r_{0,i_{L_{1_b}}} & r_{0,i_{L_{1_c}}} & r_{0,i_{L_{1_d}}} & r_{0,v_1} & r_{0,i_2} & r_{0,v_2} \end{bmatrix}^{\mathrm{T}}. \tag{3.116}$$

By increasing q-values the convergence rate of the corresponding state estimation is raised. Increasing r-values on the other hand puts less confidence on the corresponding measurement which reduces sensitivity on measurement noise.

---

[2] Obviously the actuators can switch (using a direct pulse generator as in the case of PPPC or FCS-MPC or a pulse width modulator in the case of a backstepping-based approach) several times within T_s, however they run in open loop and the control signal is only updated at multiples of T_s.

Die approbierte gedruckte Originalversion dieser Diplomarbeit ist an der TU Wien Bibliothek verfügbar.
The approved original version of this thesis is available in print at TU Wien Bibliothek.

Die approbierte gedruckte Originalversion dieser Diplomarbeit ist an der TU Wien Bibliothek verfügbar.
The approved original version of this thesis is available in print at TU Wien Bibliothek.

Chapter 4

Optimization Techniques

In spite of considerable recent advances in semiconductor technology, the main concern when using MPC in power electronics is solving the resulting optimal control problem in real-time, hence, within one sampling interval, on embedded platforms with limited computational resources [2]. This chapter discusses effective optimization techniques to solve the constrained quadratic programs (QP) formulated in chapter 3.3 and 3.4. These cases require solving a QP with integer and continuous decision variables respectively.

4.1 Overview

QP-solvers can be classified in online- and offline-solvers. Solving offline-QPs in the context of MPC by means of multiparametric programming is also known as explicit MPC (eMPC) and enables real-time implementations as the online effort reduces to finding the optimal solution in look-up-tables after partitioning the state space into polyhedral regions and using piecewise affine (PWA)-models, [41, 42, 43]. However, the drawbacks are high memory requirements especially for larger problems, a lack of flexibility when it is favorable to change parameters online as well as limitation to constant reference setpoints within the prediction horizon [44]. Therefore, this work focuses on online solution approaches. QPs can be further distinct by condensed or sparse formulation. The condensed form eliminates states as a function of the initial state and decision variables as opposed to a sparse formulation where the future inputs and states are considered as decision variables. The condensed form therefore allows input constraints only whereas the sparse form addresses state constraints as well. However, some state constraints, such as absolute constraints, can be easily transformed to input constraints such that condensed form is preserved.

4.2 Integer quadratic programming

This section discusses methods to solve the integer quadratic program (IQP) of the form (3.29).

4.2.1 Exhaustive search

Exhaustive search algorithm (ESA) is the simplest approach to solve the IQP (3.29) and accomplishes this by evaluating the underlying objective function J for each possible input combination and choosing the input sequence with minimal cost. The one prediction horizon ESA is listed in alg. 1. As the prediction horizon is one, the TSP and CBP are combined and solved directly using the optimal value of the finite control set $\mathbb{U}$. However, the associated computational burden grows exponentially with the number of (binary) input switches m and prediction horizon N. For the SMPB described in chapter 2, this gives $m = 4$ and therefore $2^{4 \cdot N}$ possible switching sequences. For this reason this approach is only feasible for short prediction horizons not longer than 2 [14, 45, 17] and is not further considered.

Algorithm 1 Exhaustive search algorithm

```
function $\boldsymbol{u}^*(k) = \mathrm{ESA}(\boldsymbol{x}(k), \boldsymbol{u}(k-1))$
    $J^* \leftarrow \infty$; $\boldsymbol{u}^*(k) = \boldsymbol{u}(k-1)$
    for each $\boldsymbol{u} \in \mathbb{U}$ do
        $\boldsymbol{x}(k+1) \leftarrow \boldsymbol{A}\boldsymbol{x}(k) + \boldsymbol{B}\boldsymbol{u}$
        $\Delta u \leftarrow \sum \boldsymbol{u}(k) - \boldsymbol{u}(k-1)$
        if $J(\boldsymbol{x}(k+1), \Delta u) < J^*$ then
            $J^* \leftarrow J(\boldsymbol{x}(k+1), \Delta u)$
            $\boldsymbol{u}^*(k) \leftarrow \boldsymbol{u}$
        end if
    end for
end function
```

4.2.2 Sphere Decoding Algorithm

The Sphere Decoding Algorithm (SDA) is a branch-and-bound algorithm suggested in [20] to solve an IQP efficiently by reformulating it as an integer least squares (ILS) problem as in section 3.3. The idea is to discard input candidates that are outside of a sphere centered in the unconstrained solution and which radius is successively tightened. The algorithm is presented in a recursive manner in [20]. Despite the

Die approbierte gedruckte Originalversion dieser Diplomarbeit ist an der TU Wien Bibliothek verfügbar.
The approved original version of this thesis is available in print at TU Wien Bibliothek.

compact notation this difficults implementation on embedded platforms as recursions are often not supported by code generation tools. Therefore, a nonrecursive SDA is formulated and listed in alg. 2. The recursion is avoided by using a last in first out stack that allows pushing elements to the stack and popping elements from it. The algorithm takes the transformation matrix $\boldsymbol{H}$, the unconstrained solution $\boldsymbol{U}_u$ and the initial sphere radius ρ_0 as arguments and returns the optimal switching sequence $\boldsymbol{U}^*$. The initial sphere radius is crucial for the performance as it will determine how many candidate solutions can be discarded. As suggested in [20], the initial radius is set to

$$\rho_0 = \|\boldsymbol{U}_u - \boldsymbol{H}\boldsymbol{U}_s\|_2^2, \tag{4.1}$$

where the suboptimal solution $\boldsymbol{U}_s$ is set to the previous optimal switching sequence shifted by one time step. In the following $\boldsymbol{H}_{(i,1:i)}$ refers to the first i elements of the i-th row of $\boldsymbol{H}$ and $U_{u,i}$ denotes the i-th element of $\boldsymbol{U}_u$. The lower and upper constraints on the input are determined as discussed in section 3.3. The SDA also allows early termination when reaching the maximum number of iterations. In this case a suboptimal solution can be obtained by rounding the unconstrained solution and projecting each element of the switching sequence to the feasible set $\mathcal{U}_f$.

4.3 Quadratic programming with continuous variables

This section discusses methods to solve the quadratic program with continuous decision variables of the form (3.43) that occurs for the PPPC method in section 3.4.

The authors of [46] showed that although the sparse form increases the problem's dimension, the computational and memory demand grow linear with the horizon length as opposed to quadratic or cubic growth using the condensed form, which makes it favorable for long prediction horizons. Furthermore, the number of states and inputs is decisive to suitability of one of both forms. Most MPC algorithms are tailored to either the sparse or condensed form as they exploit the problem's structure and consequently favour one of them [47].

The most widely used iterative approaches for continuous quadratic MPC problems are the interior-point method, active-set method [48], both second order methods, and recently in this context, first-order methods such as the fast gradient method (FGM) [49, 50] or the alternating direction method of multipliers (ADMM) [51, 52]. Key criteria for a fast execution time of the FGM is a computational efficient projection on the constraint set, a so called simple set [53]. Tremendous effort has been evoked to provide state-of-the-art MPC code generation tools tailored for embedded platforms implementing interior-point solvers [54, 55, 56], the FGM [57, 58] and the active-set

Die approbierte gedruckte Originalversion dieser Diplomarbeit ist an der TU Wien Bibliothek verfügbar.
The approved original version of this thesis is available in print at TU Wien Bibliothek.
TU WIEN Bibliothek Your knowledge hub

Algorithm 2 Nonrecursive sphere decoding algorithm

```
function $\boldsymbol{U}^* = \mathrm{SDA}(\boldsymbol{H}, \boldsymbol{U}_u, \rho_0)$
    $i \leftarrow 1$
    $d^2 \leftarrow 0$
    $\rho \leftarrow \rho_0$
    doNextLevel $\leftarrow 1$
    while stackSize $> 0$ or doNextLevel $== 1$ do
        if doNextLevel $== 1$ then
            doNextLevel $\leftarrow 0$
            $u_{start} \leftarrow 0$
        else
            $\boldsymbol{U} \leftarrow$ pop
            $u_{start} \leftarrow$ pop
            $i \leftarrow$ pop
            $d^2 \leftarrow$ pop
        end if
        for each $u \in \mathcal{U}_f$ do
            if $u \geq \max(u_{start}, \mathrm{lowerConstraint}(i))$ and $u \leq \mathrm{upperConstraint}(i)$ then
                $U_i \leftarrow u$
                $d'^2 \leftarrow \|U_{u,i} - \boldsymbol{H}_{(i,1:i)}\boldsymbol{U}_{1:i}\|_2^2 + d^2$
                if $d'^2 \leq \rho^2$ then
                    if $i < N$ then
                        push $\leftarrow d^2$
                        push $\leftarrow i$
                        push $\leftarrow u + 1$
                        push $\leftarrow \boldsymbol{U}$
                        $u_{start} \leftarrow 0$
                        $i \leftarrow i + 1$
                        $d^2 \leftarrow d'^2$
                        doNextLevel $\leftarrow 1$
                        break
                    else
                        $\boldsymbol{U}^* \leftarrow \boldsymbol{U}$
                        $\rho^2 \leftarrow d'^2$
                    end if
                end if
            end if
        end for
    end while
end function
```

Die approbierte gedruckte Originalversion dieser Diplomarbeit ist an der TU Wien Bibliothek verfügbar.
The approved original version of this thesis is available in print at TU Wien Bibliothek.

method [59]. A performance benchmark is given in [60] and [61]. As this field has been extensively discussed in literature further details will be omitted.

4.4 Backstepping-based dynamic pruning

This section presents a Backstepping-based method to dynamically prune suboptimal switching sequences in order to reduce the search space related to a FCS-MPC problem. A similar approach using a Lyapunov candidate function to prune instable switching sequences was suggested in [62]. The SDA proposed in 4.2.2 allows to calculate long horizon FCS-MPC problems by discarding suboptimal candidates. However, the number of required iterations rises dramatically for transients, limiting feasible horizon lengths.

Instead of considering each entry in the finite control set, the cascaded backstepping (CBS) method is used to reduce the feasible set $\mathcal{U}_f$ in the SDA algorithm 2 to two for each time step. Thereby the continuous CBS output is considered and the adjacent lower and upper integer switching state reduce to the candidate switching states. As the procedure has to be done for each time step, a simple Kalman Filter like (pure simulator, without measurement apparently) prediction with the continuous CBS signal is made to prune the search space for the entire prediction horizon. Although this may lead to suboptimal solutions, simulation results in chapter 5 demonstrate that the performance is marginally affected while the solution space can be shrinked significantly.

Die approbierte gedruckte Originalversion dieser Diplomarbeit ist an der TU Wien Bibliothek verfügbar.
The approved original version of this thesis is available in print at TU Wien Bibliothek.

Die approbierte gedruckte Originalversion dieser Diplomarbeit ist an der TU Wien Bibliothek verfügbar.
The approved original version of this thesis is available in print at TU Wien Bibliothek.
TU WIEN Bibliothek Your knowledge hub

Chapter 5

Results

This chapter presents the simulation and measurement results as well as an analysis of the underlying computational demand of the proposed control algorithms. They were implemented in MATLAB/SIMULINK in discrete-time with a sampling rate of $f_s = 16\,\text{kHz}$ and single precision.

5.1 Simulation results

This section analyses and compares the transient and steady-state performance of the control strategies.

5.1.1 Steady-state performance

The figures 5.1a-5.1d illustrate the steady-state maximum ripple of output voltage v_2, sum phase current i_1 and average phase current $\frac{1}{4}(i_{L_{1_a}} + i_{L_{1_b}} + i_{L_{1_c}} + i_{L_{1_d}})$ as well as the resulting total switching frequency f_S for varying prediction horizon lengths N using the SDA to find the optimal switching sequence for the FCS-MPC problem in the inner loop. Morevover, the PPPC and CBS performance is depicted as a comparison - their corresponding horizontal positions are irrelevant. Both outperform the FCS-MPC even when using long prediction horizons. It can clearly be seen that the performance saturates and the benefit of further increasing the prediction horizon decreases while the computational demand rises exponentially. The switching frequency of the FCS-MPC increases linearly with the prediction which reduces voltage and current ripple. PPPC and CBS on the other hand achieve a constant switching frequency of 64 kHz with lower ripples.

Die approbierte gedruckte Originalversion dieser Diplomarbeit ist an der TU Wien Bibliothek verfügbar.
The approved original version of this thesis is available in print at TU Wien Bibliothek.

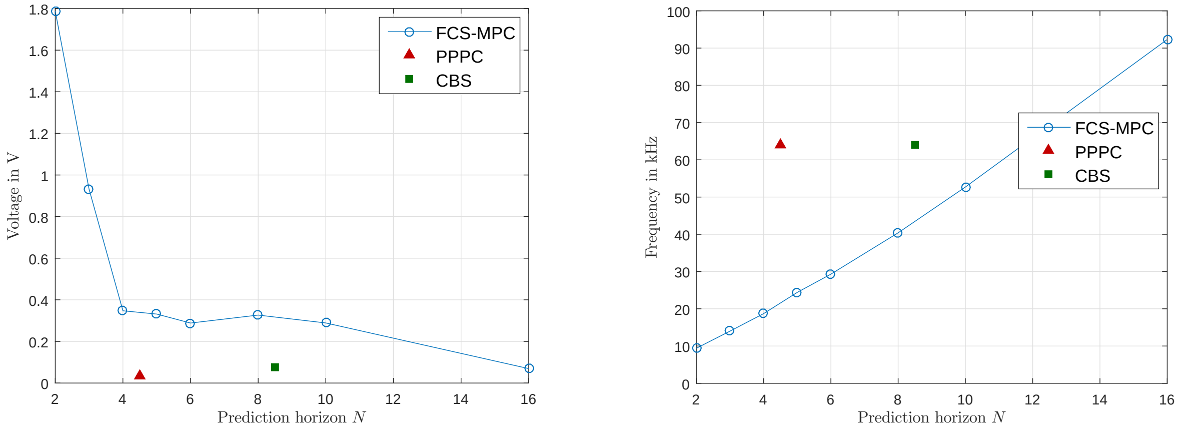

(a) Maximum output voltage ripple.

(b) Sum current switching frequency.

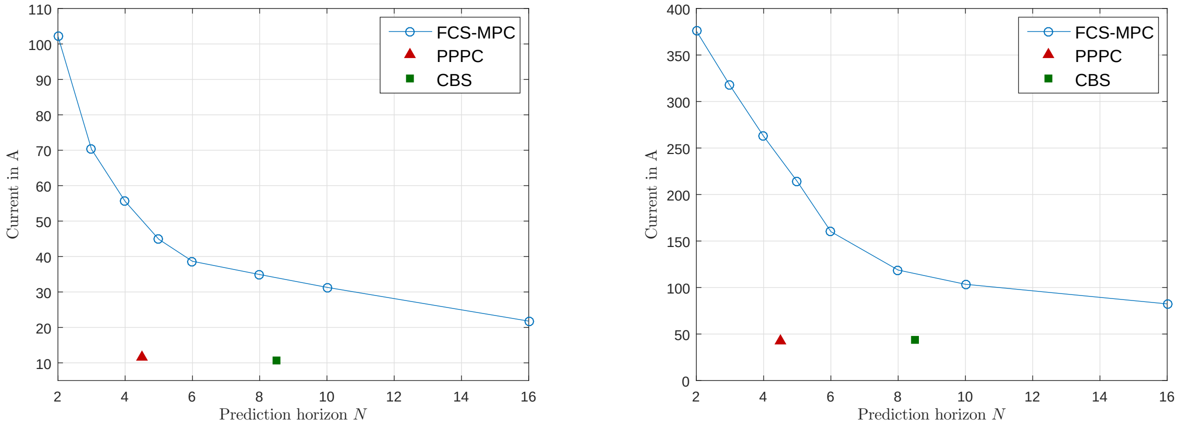

(c) Maximum sum current ripple.

(d) Maximum phase current ripple.

Figure 5.1: FCS-MPC steady-state performance for varying prediction horizon lengths N.

5.1.2 Comparing FCS-MPC with PPPC

The PPPC-strategy is compared with FCS-MPC using a prediction horizon of $N = 8$, both using the same prediction interval. Therefore, both controllers can apply N different switching states within one sampling period. Fig. 5.2a-5.2d show phase currents and switching states for a setpoint step from 0 V to 350 V with the current limit set to 150 A per phase. The corresponding output voltage and sum phase currents are depicted in fig. 5.3a and 5.3c. The PPPC achieves tighter current tracking while both controllers accomplish a transition time of 2.5 ms and suffer from a computational delay of one sampling period. Load step performance is depicted in fig. 5.3b and 5.3d. As expected, both controllers achieve good disturbance rejection below 2 ms for a constant power load with 125 kW without significant differences. Steady-state performance without load is depicted in fig. 5.4a-5.4d. Due to limited time resolution, FCS-MPC clearly performs worse than PPPC in steady-state. The former achieves an average phase and sum peak-to-peak current ripple of 55.8 A and 25 A, and an average phase and sum switching frequency of 14.9 kHz and 41.2 kHz. PPPC on the other hand accomplishes an average phase and sum peak-to-peak current ripple of 41.9 A and 9.9 A, and a phase and sum switching frequency of 16 kHz and 64 kHz. The peak-to-peak output voltage ripple is 391 mV for the FCS-MPC versus 42.2 mV for the PPPC.

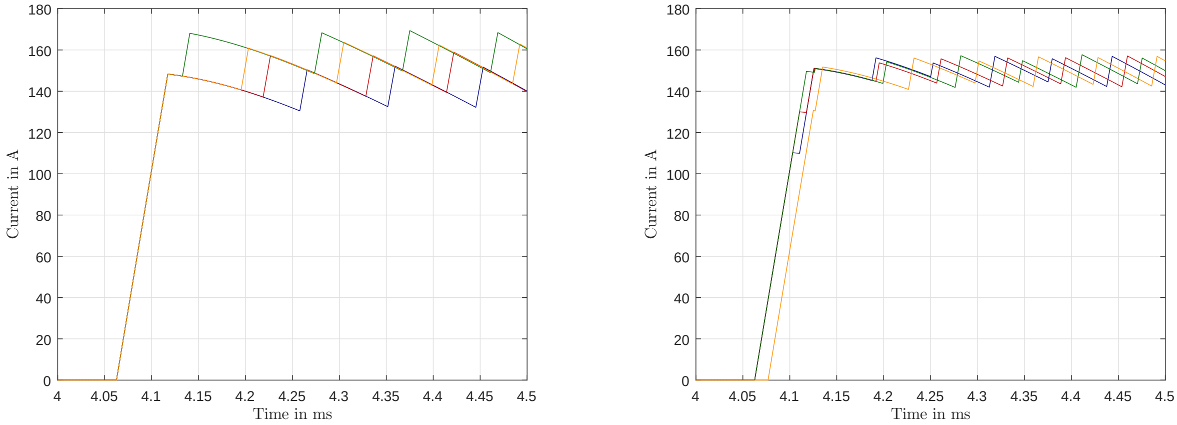

(a) Phase currents for FCS-MPC.

(b) Phase currents for PPPC.

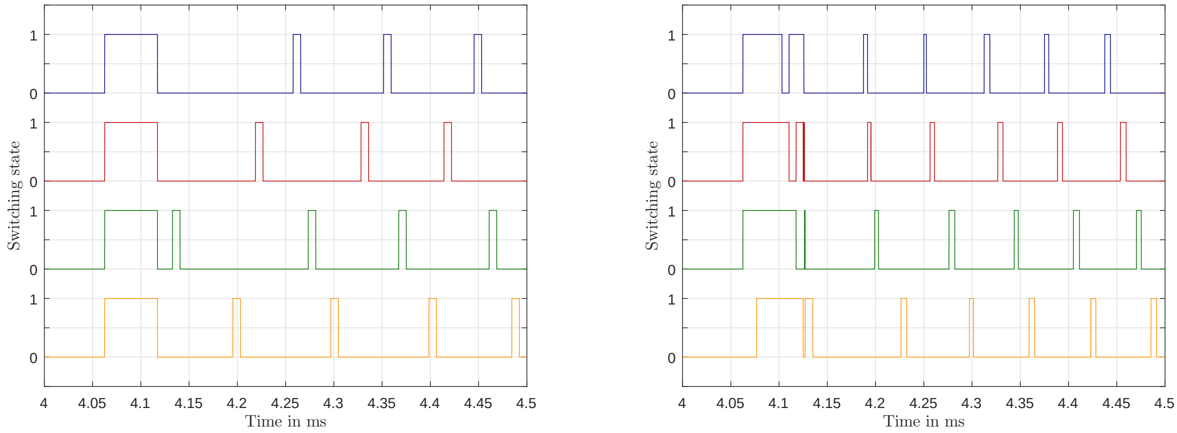

(c) Switching states for FCS-MPC.

(d) Switching states for PPPC.

Figure 5.2: Setpoint step from $v_2 = 0\,\mathrm{V}$ to $v_2 = 350\,\mathrm{V}$.

Die approbierte gedruckte Originalversion dieser Diplomarbeit ist an der TU Wien Bibliothek verfügbar.
The approved original version of this thesis is available in print at TU Wien Bibliothek.

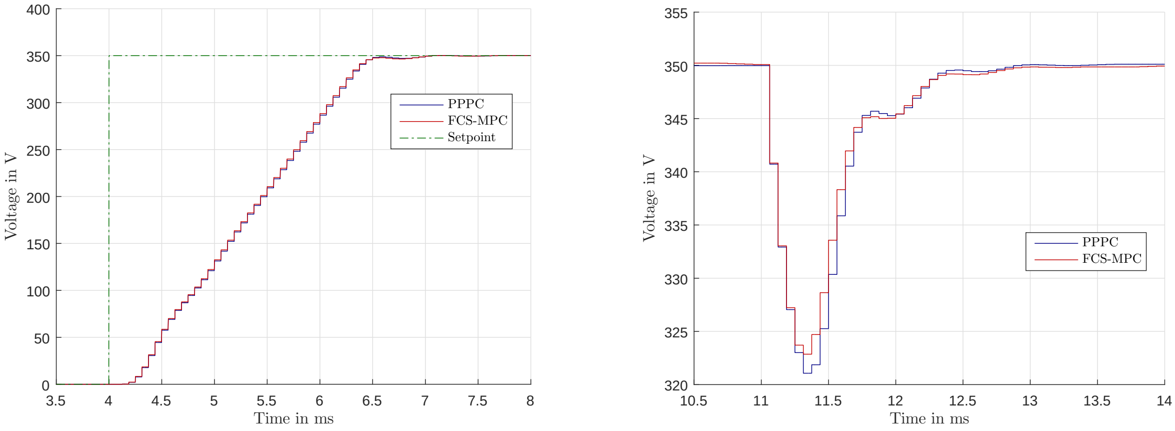

(a) Comparison of output voltage.

(b) Comparison of output voltage.

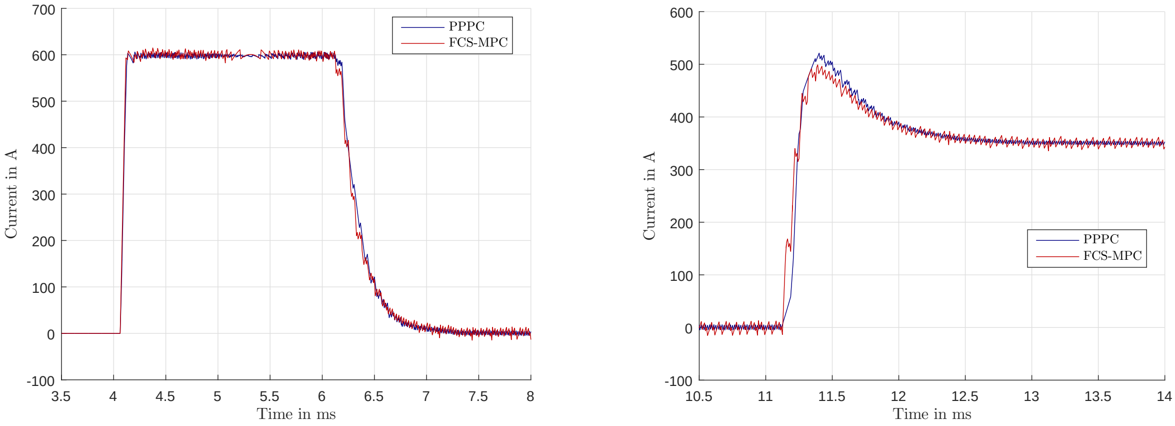

(c) Comparison of sum phase current.

(d) Comparison of sum phase current.

Figure 5.3: (a) and (c): Setpoint step from $v_2 = 0\,\mathrm{V}$ to $v_2 = 350\,\mathrm{V}$. (b) and (d): Load disturbance rejection when enabling a constant power load with 125 kW.

Die approbierte gedruckte Originalversion dieser Diplomarbeit ist an der TU Wien Bibliothek verfügbar.
The approved original version of this thesis is available in print at TU Wien Bibliothek.

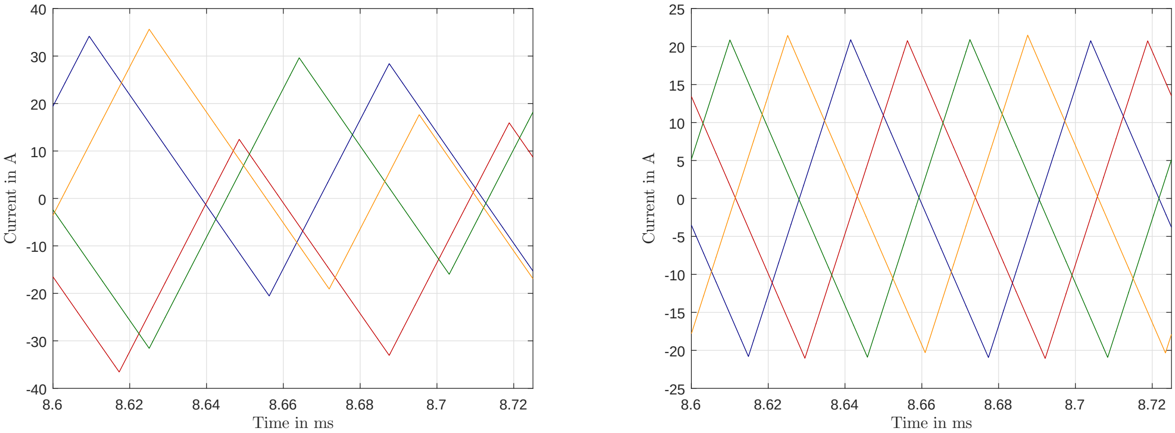

(a) Phase currents for FCS-MPC. (b) Phase currents for PPPC.

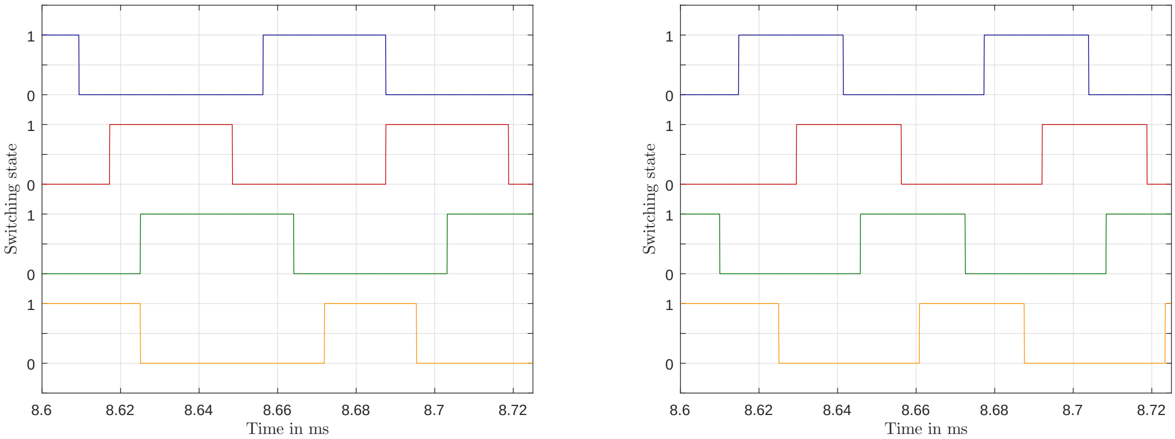

(c) Switching states for FCS-MPC. (d) Switching states for PPPC.

Figure 5.4: Steady-state performance at $v_2 = 350\,\mathrm{V}$ without load.

Die approbierte gedruckte Originalversion dieser Diplomarbeit ist an der TU Wien Bibliothek verfügbar.
The approved original version of this thesis is available in print at TU Wien Bibliothek.

5.1.3 Comparing CBS with PPPC

In this section the cascaded backstepping (CBS) method is compared with the PPPC while both use the same MPC in the outer loop. The CBS provides a continuous duty cycle for an underlying pulse width modulator. Fig. 5.5a and 5.5c compare the output voltage v_2 and sum phase current i_1 for a setpoint step from 0 V to 350 V. Both controllers respect the current limit of 600 A balanced among the phases as illustrated in fig. 5.6c and 5.6d. For a setpoint change there is no significant difference and both controllers settle in 2.5 ms. Fig. 5.5b and 5.5d show disturbance rejection when a 125 kW CPL is enabled. In this case the PPPC outperforms the CBS approach with faster recovery time. Steady-state performance is illustrated in fig. 5.6a for the CBS and in fig. 5.6b for the PPPC. As expected, both perform well with an average phase and sum peak-to-peak current ripple of 42.15 A and 10.3 A for the former and 41.9 A and 9.9 A for the latter. Both achieve an average phase and sum switching frequency of 16 kHz and 64 kHz. The peak-to-peak output voltage ripple is 50 mV for the CBS versus 42.2 mV for the PPPC. The phase currents for a step from $v_2 = 0$ V to $v_2 = 350$ V are depicted in 5.6c for the CBS and in 5.6d for the PPPC. The latter achieves tighter current control around the setpoint which outlines the overall superior performance of the PPPC.

Die approbierte gedruckte Originalversion dieser Diplomarbeit ist an der TU Wien Bibliothek verfügbar.
The approved original version of this thesis is available in print at TU Wien Bibliothek.
TU WIEN Bibliothek Your knowledge hub

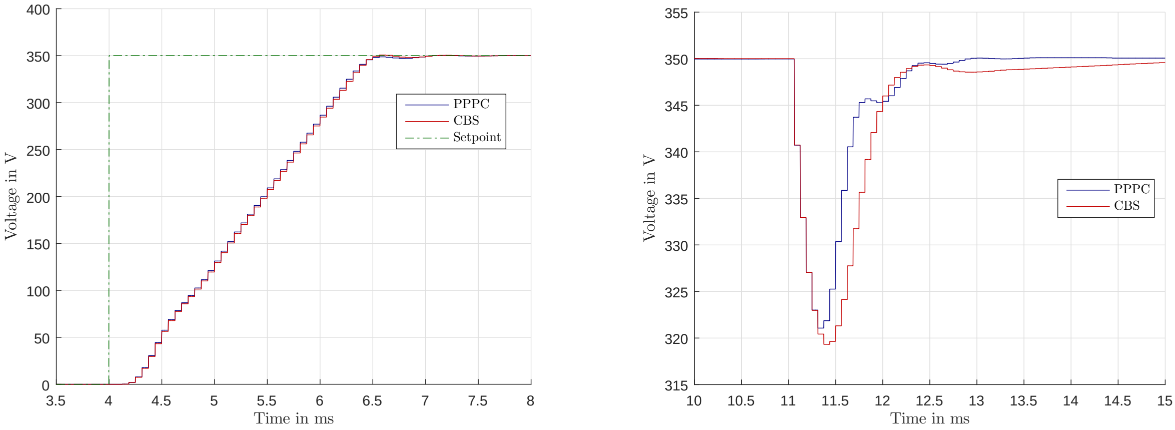

(a) Comparison of output voltage.

(b) Comparison of output voltage.

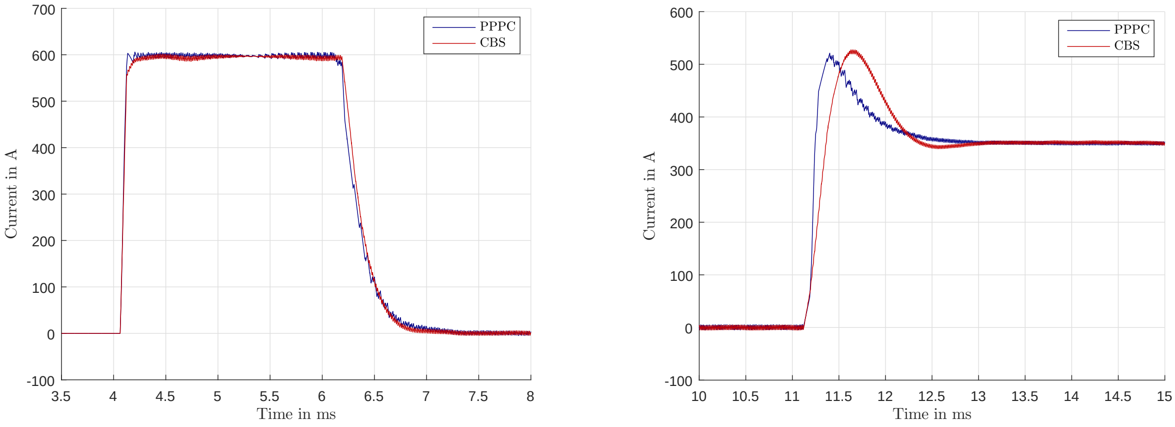

(c) Comparison of sum phase current.

(d) Comparison of sum phase current.

Figure 5.5: (a) and (c): Setpoint step from $v_2 = 0\,\mathrm{V}$ to $v_2 = 350\,\mathrm{V}$. (b) and (d): Load disturbance rejection when enabling a constant power load with 125 kW.

Die approbierte gedruckte Originalversion dieser Diplomarbeit ist an der TU Wien Bibliothek verfügbar.
The approved original version of this thesis is available in print at TU Wien Bibliothek.

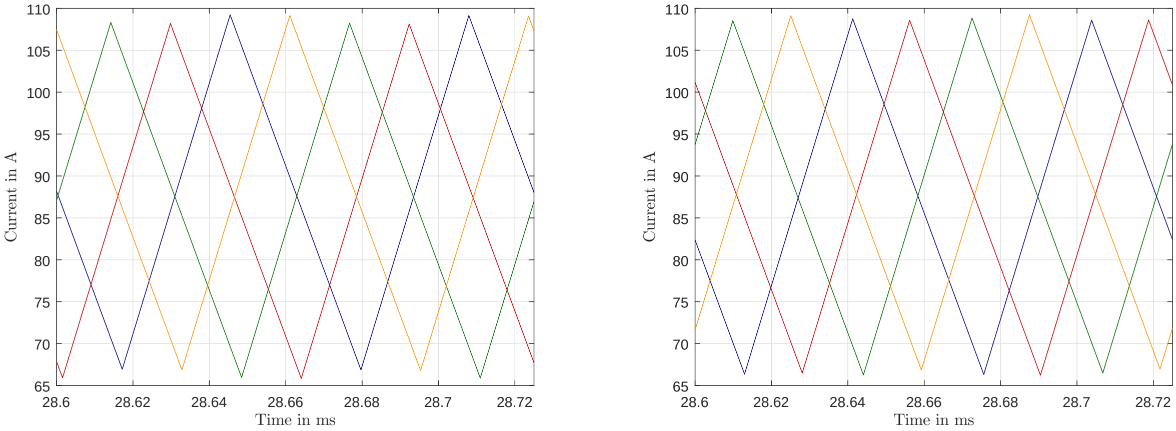

(a) Steady-state phase currents for CBS.

(b) Steady-state phase currents for PPPC.

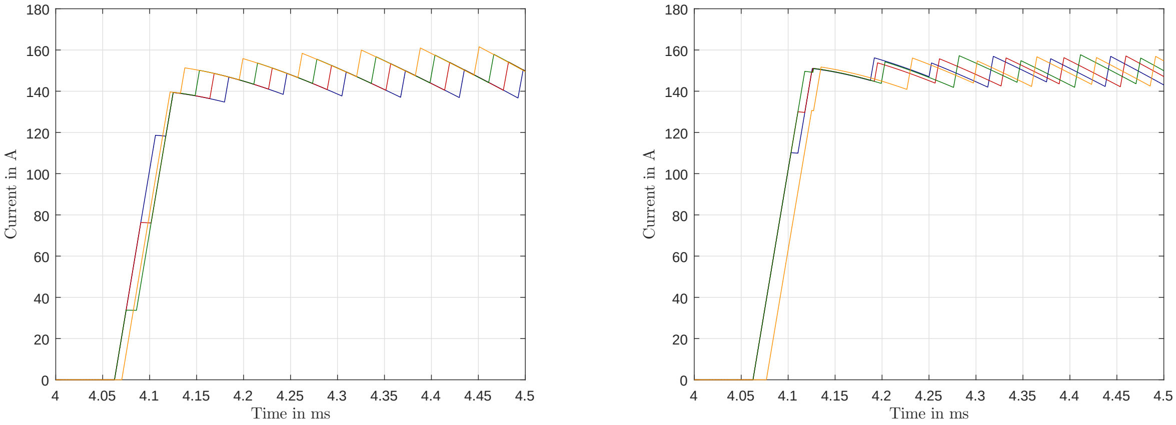

(c) Transient phase currents for CBS.

(d) Transient phase currents for PPPC.

Figure 5.6: Steady-state performance at $v_2 = 350\,\mathrm{V}$ with load $i_\mathrm{L} = 350\,\mathrm{A}$ and transient performance for a setpoint step from $v_2 = 0\,\mathrm{V}$ to $v_2 = 350\,\mathrm{V}$.

Die approbierte gedruckte Originalversion dieser Diplomarbeit ist an der TU Wien Bibliothek verfügbar.
The approved original version of this thesis is available in print at TU Wien Bibliothek.

Die approbierte gedruckte Originalversion dieser Diplomarbeit ist an der TU Wien Bibliothek verfügbar.
The approved original version of this thesis is available in print at TU Wien Bibliothek.

5.1.4 Comparing CBS with CFBS

As already mentioned the CBS applies the backstepping procedure only in the last step which simplifies the tuning in comparison with the full order CFBS. Fig. 5.7a-5.7d show a comparison of the output voltage and sum phase current. Furthermore, the CBS comprises a shorter pipeline than the CFBS which applies a filter in each step of the cascade that results in an increased delay. For this reason, the CBS achieves a superior transient performance while there is no noticeable difference in steady-state performance depicted in fig. 5.8a and 5.8b, as it is determined by the underlying pulse width modulation.

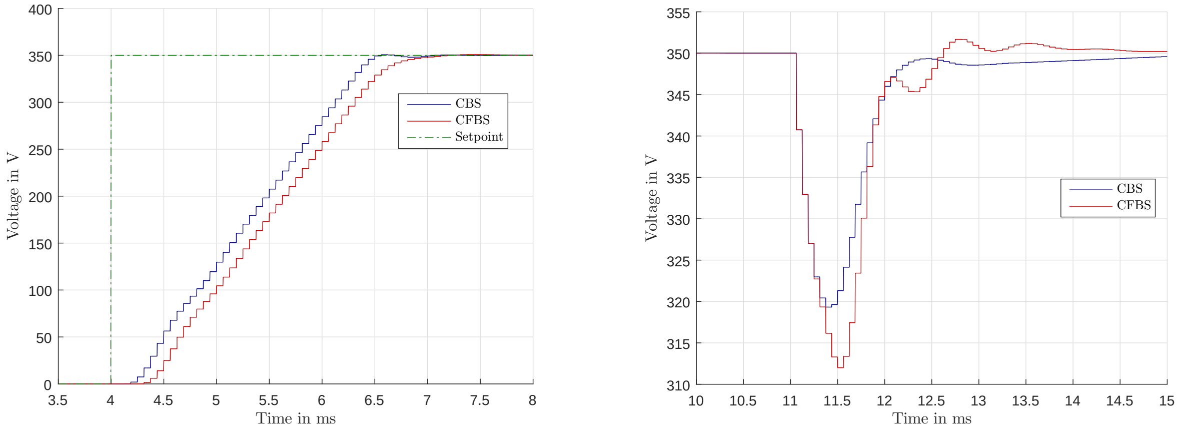

(a) Comparison of output voltage.

(b) Comparison of output voltage.

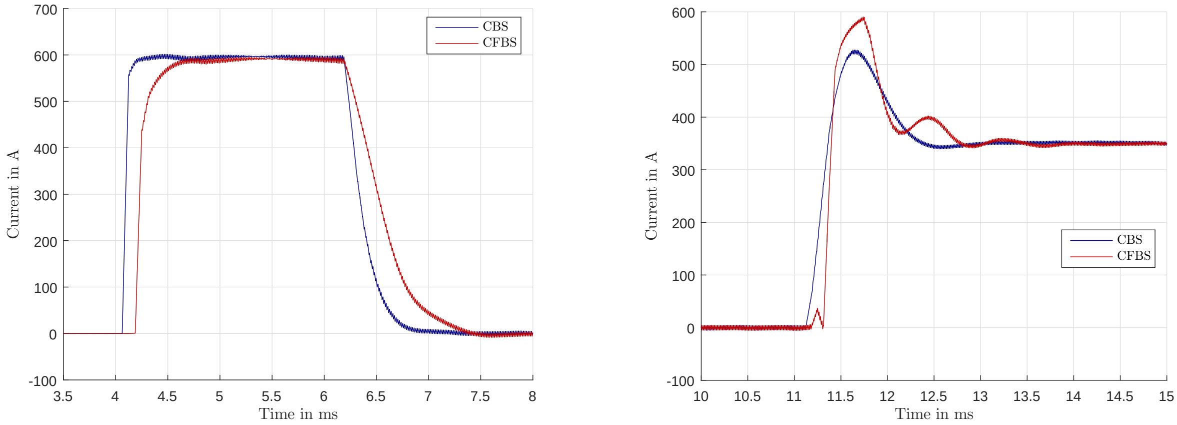

(c) Comparison of sum phase current.

(d) Comparison of sum phase current.

Figure 5.7: Comparison of CBS and CFBS. (a) and (c): Setpoint step from $v_2 = 0\,\mathrm{V}$ to $v_2 = 350\,\mathrm{V}$. (b) and (d): Load disturbance rejection when enabling a constant power load with 125 kW.

Die approbierte gedruckte Originalversion dieser Diplomarbeit ist an der TU Wien Bibliothek verfügbar.
The approved original version of this thesis is available in print at TU Wien Bibliothek.

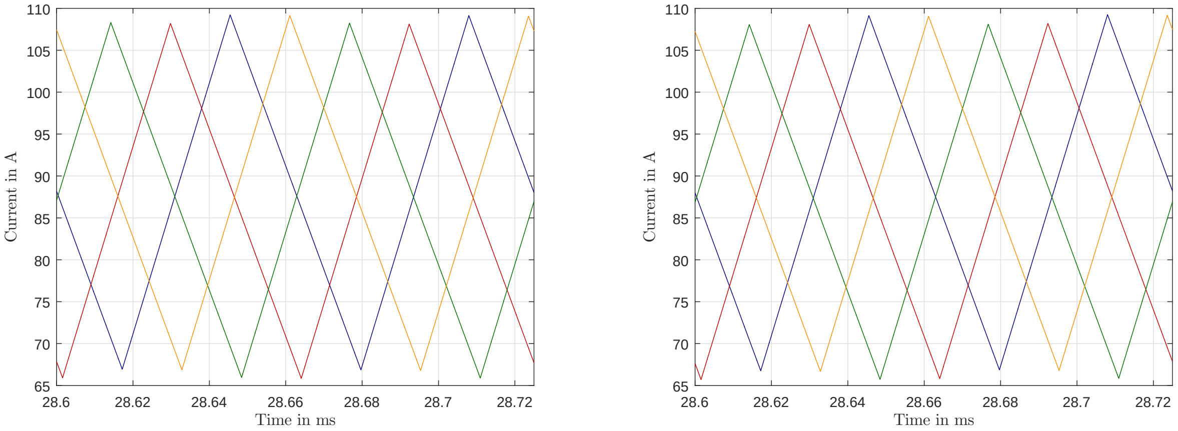

(a) Phase currents for CBS. (b) Phase currents for PPPC.

Figure 5.8: Steady-state performance at $v_2 = 350\,\text{V}$ with load $i_\text{L} = 350\,\text{A}$.

5.1.5 Outer Loop Variants

So far the MPC suggested in section 3.2 was used in the outer loop. As discussed, a LQR or the CFBS method can be used instead to provide a virtual reference current i_1^* for the inner loop. In that case, the CFBS scheme is only used to provide i_1^* while the current tracking itself is delegated to the inner loop. The output tracking is depicted using in fig. 5.9c, 5.9b and 5.9c for the MPC, LQR and CFBS in the outer loop respectively. Each controller employs the PPPC in the inner loop. It can be seen that the MPC achieves the best performance and the anti-windup strategy of the LQR yields poor performance when current saturation occurs. CFBS performs only slightly worse than the MPC but suffers from a current limit violation in the transient. This could be avoided with further tuning on the expense of dynamic response.

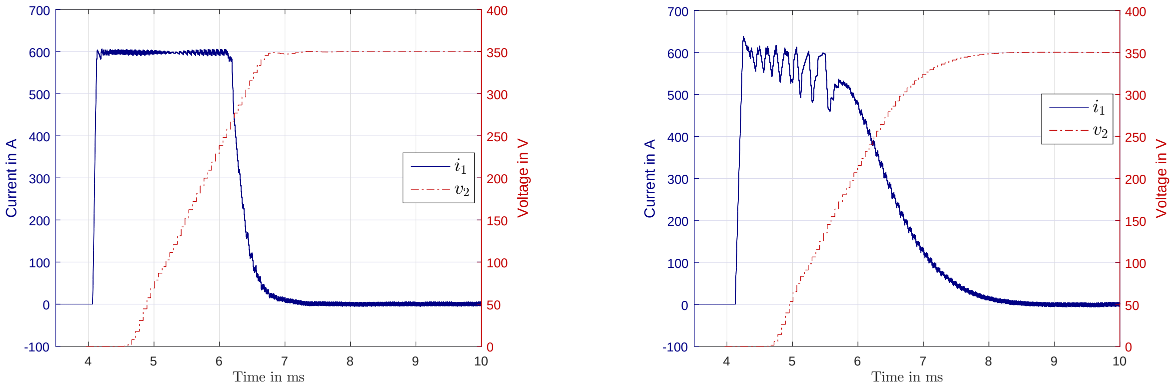

(a) MPC.

(b) LQR.

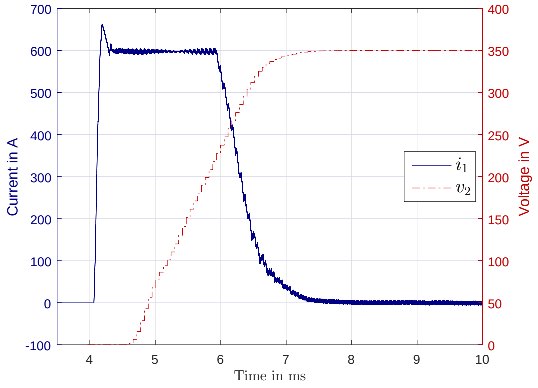

(c) CFBS.

Figure 5.9: Outer loop variants with PPPC in the inner loop. (a): MPC, (b): LQR, (c): CFBS.

Die approbierte gedruckte Originalversion dieser Diplomarbeit ist an der TU Wien Bibliothek verfügbar.
The approved original version of this thesis is available in print at TU Wien Bibliothek.

5.1.6 Load estimation

The Kalman Filter does not only provide state estimations for the feedback but also an estimation of the unknown load current i_L. Fig. 5.10a shows the disturbance rejection capabilities for a load step and the corresponding load estimation in fig 5.10b.

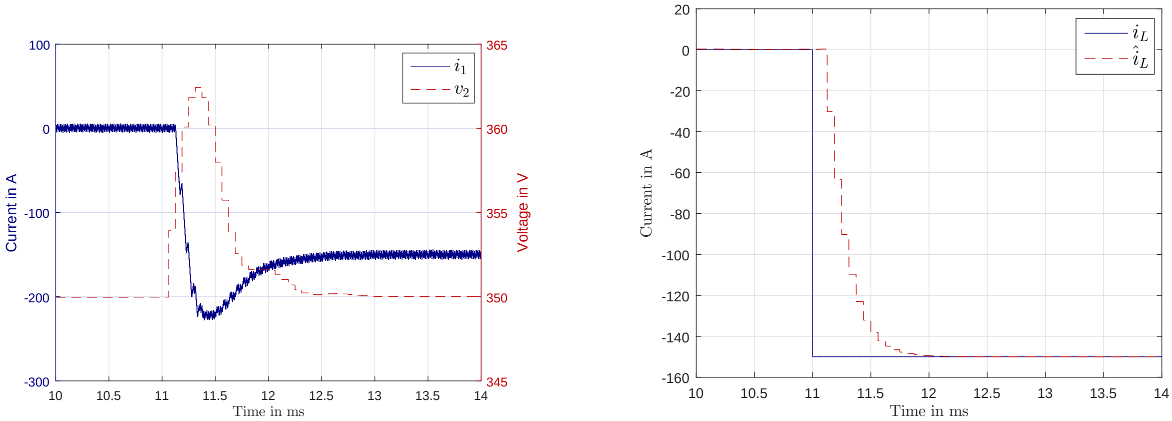

(a) Load step disturbance rejection.

(b) Load step estimation.

Figure 5.10: Output voltage v_2 and sum phase current i_1 load recovery with MPC in the outer and the PPPC in the inner loop and the corresponding load disturbance estimation for a constant disturbance.

5.2 Computational Effort

This section analyzes the computational effort of the proposed control strategies. To this end, the simulations were done on a dSpace MicroAutoBox real-time platform with a processor clock of 900 MHz. This embedded platform has a comparable computational power as the digital signal processor (DSP) employed in the test bed described in section 2.8. As the plant was also simulated on the MicroAutoBox, the associated integer input sequence was transformed to the corresponding duty cycle for one sampling period T_s. This was necessary as the full switching dynamics requires a significantly higher sampling rate which would be infeasible to simulate in real-time. However, the purpose of this measure was merely to evaluate the computational demand which does not necessitate the accurate dynamics. The turnaround time t_t is the time needed to complete the task that performs all necessary calculations. The real-time threshold is therefore a turnaround time of 62.5 µs. As the real-time criteria could not be met for each operating point and configuration, the simulations were not done with a hard real-

Die approbierte gedruckte Originalversion dieser Diplomarbeit ist an der TU Wien Bibliothek verfügbar.
The approved original version of this thesis is available in print at TU Wien Bibliothek.

time constraint that would stop the task from execution which still allows to measure the required computational time.

5.2.1 FCS-MPC

The FCS-MPC problem is solved using the SDA which requires only relatively few iterations to find the optimal solution in steady-state. However, as depicted in fig. 5.11, the number of required iterations rises dramatically during transient operating conditions such as setpoint changes or load steps. This is due to the warm start capabilities of the SDA and needs to be considered for a real-time implementation. Table 5.1 lists the required iterations for a setpoint change from $v_2 = 0\,\mathrm{V}$ to $0\,\mathrm{V}$ for the ES, SDA and SDA with dynamic pruning (SDA+DP) using different prediction horizon lengths. It shall be mentioned that these values are not absolute upper limits but correspond to the described scenario and might be higher for other cases. Although the SDA greatly reduces the required iterations in comparison with ES, they can be further decreased significantly using dynamic pruning. Fig. 5.12 depicts this relationship on a logarithmic scale.

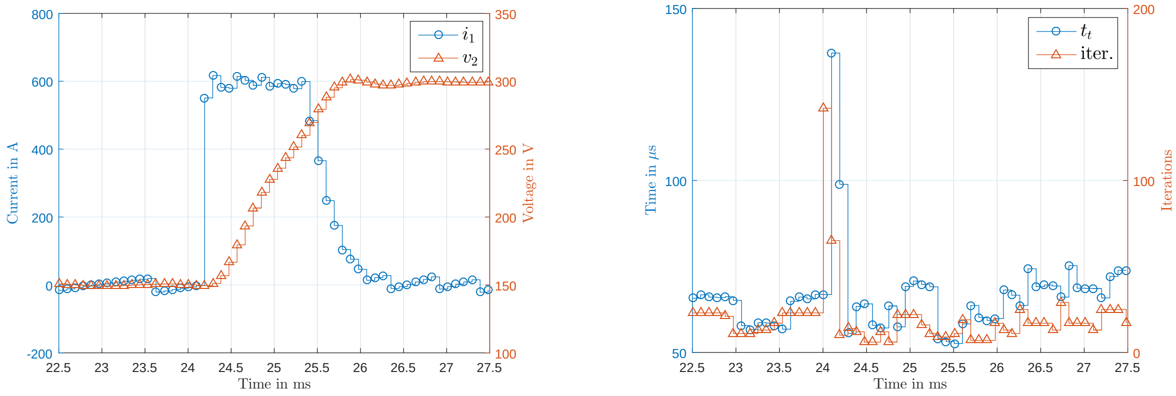

(a) Sum phase current and output voltage.

(b) Turnaround time and required iterations.

Figure 5.11: The SDA requires significantly more iterations to find the optimal solution during transients which increases the turnaround time t_t.

Fig. 5.13a, 5.13c illustrate the required iterations and associated turnaround time for $N = 4$ and $N = 8$ using the SDA. There is no limit imposed on the maximum iterations which yields therefore the optimal solution. This is in contrast to fig. 5.13b and 5.13d where the SDA+DP was used and no more than 15 and 110 iterations were allowed for $N = 4$ and $N = 8$ respectively. Such an early stop will yield a suboptimal solution. The iteration limits were therefore chosen properly such that the performance degradation

Die approbierte gedruckte Originalversion dieser Diplomarbeit ist an der TU Wien Bibliothek verfügbar.
The approved original version of this thesis is available in print at TU Wien Bibliothek.

Table 5.1: Required iterations for varying prediction horizon.

Prediction horizon	Iterations		
	ES	SDA	SDA+DP
2	25	10	4
3	125	39	9
4	625	120	18
5	3125	307	28
6	15625	683	57
8	390625	2979	112
10	9765625	11627	347
16	1.5259×10^{11}	486755	10561

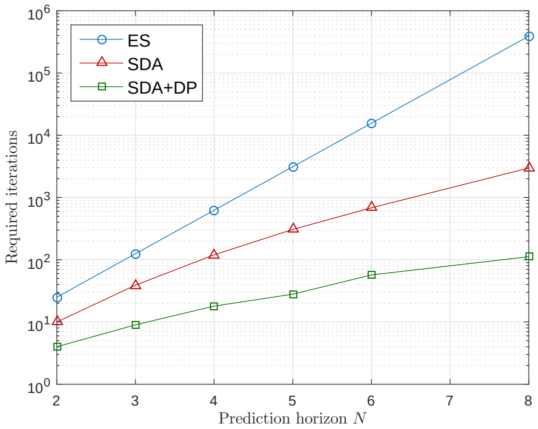

Figure 5.12: Maximum required iterations for transient operating condition on a logarithmic scale.

is negligible. Fig. 5.13e and 5.13f show the turnaround time using the SDA+DP with no limit on the iterations in the former and maximum 2000 iterations in the latter case.

Fig. 5.14a shows a comparison of the turnaround time of the SDA and the SDA+DP. Although the required iterations grow exponentially for both cases as shown in fig. 5.12, it can be seen that the cost per iteration can be reduced for higher prediction lengths using the SDA. SDA+DP on the other hand follows the opposite trend. This is due to the additional computational cost of running the backstepping algorithm in parallel for the dynamic pruning. Nevertheless, it can be seen, that the turnaround time is significantly reduced in comparison with the SDA. The turnaround time of the SDA+DP is illustrated in more detail in fig. 5.14b.

Die approbierte gedruckte Originalversion dieser Diplomarbeit ist an der TU Wien Bibliothek verfügbar.
The approved original version of this thesis is available in print at TU Wien Bibliothek.

Die approbierte gedruckte Originalversion dieser Diplomarbeit ist an der TU Wien Bibliothek verfügbar.
The approved original version of this thesis is available in print at TU Wien Bibliothek.
TU WIEN Bibliothek Your knowledge hub

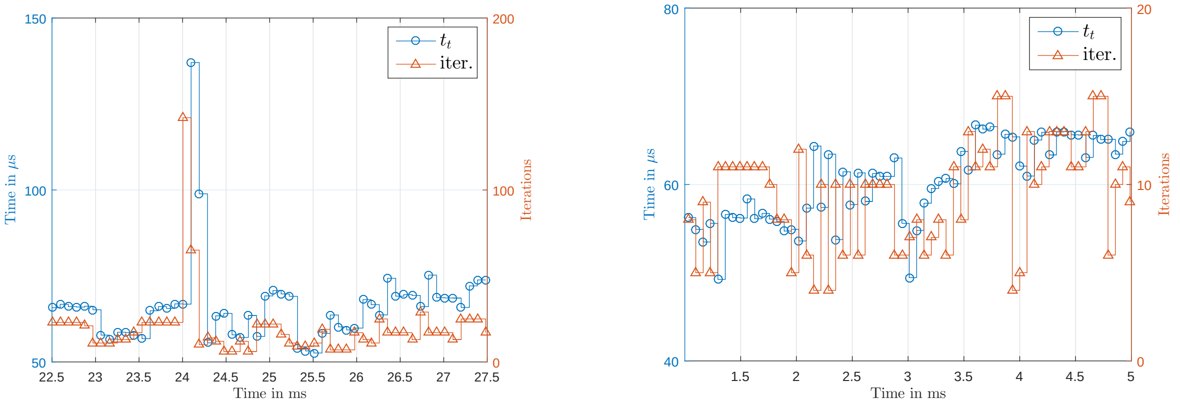

(a) $N = 4$. (b) $N = 4$ with DP and max. 15 iterations.

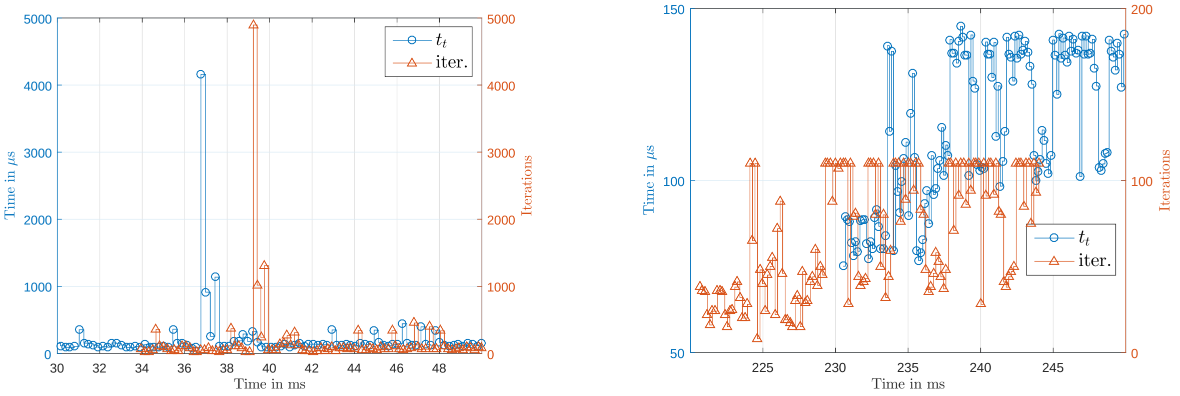

(c) $N = 8$. (d) $N = 8$ with DP and max. 110 iterations.

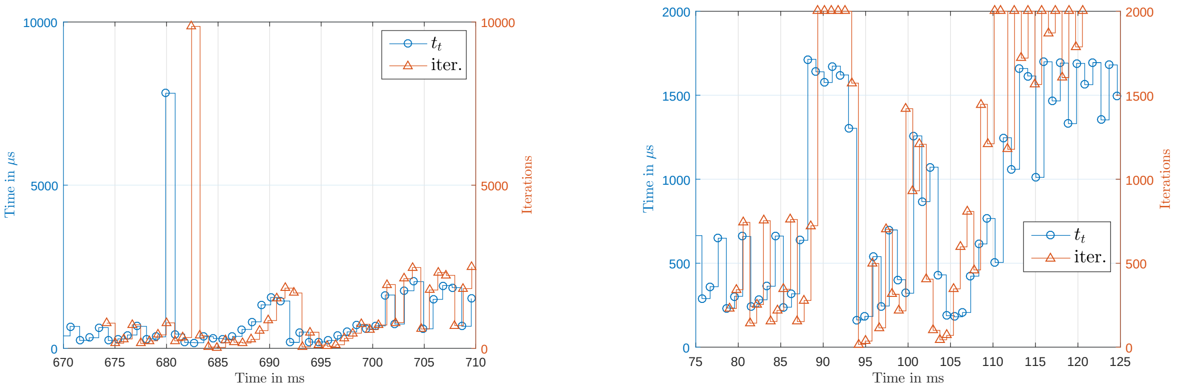

(e) $N = 16$ with DP. (f) $N = 16$ with DP and max. 2000 iterations.

Figure 5.13: FCS-MPC computational cost for varying prediction horizons N with and without dynamic pruning (DP).

Die approbierte gedruckte Originalversion dieser Diplomarbeit ist an der TU Wien Bibliothek verfügbar.
The approved original version of this thesis is available in print at TU Wien Bibliothek.

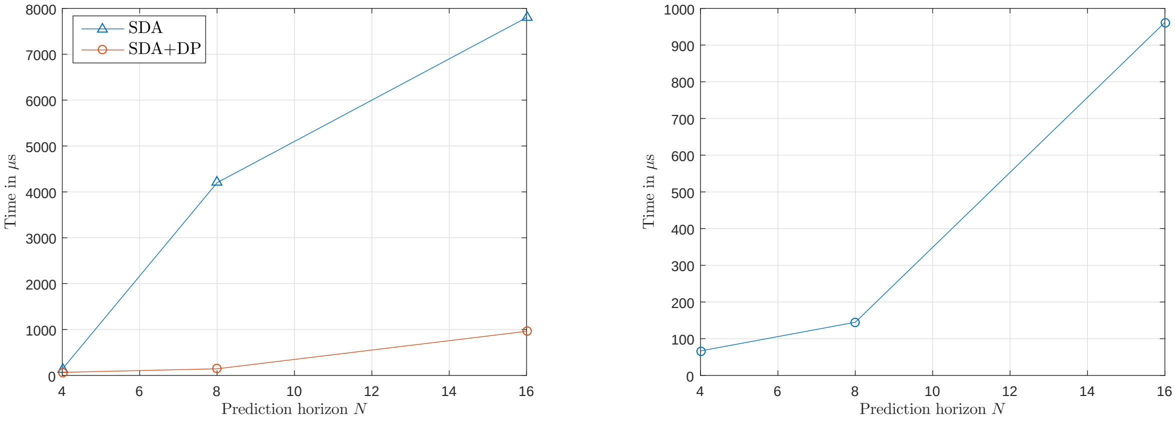

(a) Comparison of SDA and SDA+DP. (b) SDA+DP.

Figure 5.14: Turnaround time for FCS-MPC.

5.2.2 PPPC

The PPPC problem is solved using a FGM-implementation provided by the FiOrdOs toolbox [57]. The associated dual problem is solved with 1 outer iteration, outer accuracy tolerance $\varepsilon_o = 1$ and inner accuracy tolerance $\varepsilon_i = 10$. Either condition leads to an early termination. The required turnaround time for different maximum inner iteration limits is depicted in fig. 5.15a, 5.15b and 5.15c. It can be seen that, just like the SDA, the FGM algorithm also requires more iterations during transients as it also addresses a warm starting approach. Although the computational demand can be clearly reduced by limiting the allowed iterations, it is still above the required threshold of 65 µs. However, as already mentioned, a QP of comparable complexity could be solved in real-time with a tailored active set solver presented in [1]. For this reason, the PPPC strategy can be considered as real-time capable - nevertheless, the implementation would go beyond the scope of this thesis and will therefore be omitted.

5.2.3 Backstepping-based control

The required turnaround time for the CBS and CFBS method is depicted in fig. 5.16a and 5.16b. As expected, both can be calculated with little computational effort well below the real-time threshold. In contrast to the FCS-MPC and PPPC approach the turnaround time is almost constant regardless of the operating condition.

TU WIEN Bibliothek Your knowledge hub
Die approbierte gedruckte Originalversion dieser Diplomarbeit ist an der TU Wien Bibliothek verfügbar.
The approved original version of this thesis is available in print at TU Wien Bibliothek.

Die approbierte gedruckte Originalversion dieser Diplomarbeit ist an der TU Wien Bibliothek verfügbar.
The approved original version of this thesis is available in print at TU Wien Bibliothek.

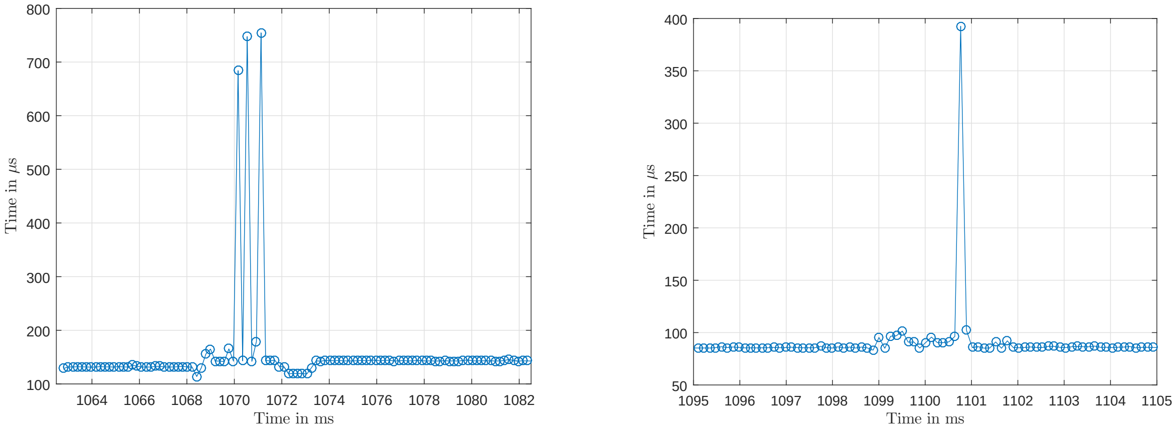

(a) Maximum 5 iterations for the inner problem.

(b) Maximum 2 iterations for the inner problem.

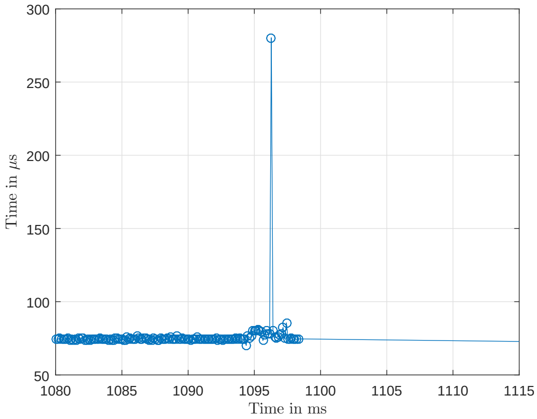

(c) Maximum 1 iteration for the inner problem.

Figure 5.15: Computational demand for PPPC.

Die approbierte gedruckte Originalversion dieser Diplomarbeit ist an der TU Wien Bibliothek verfügbar.
The approved original version of this thesis is available in print at TU Wien Bibliothek.

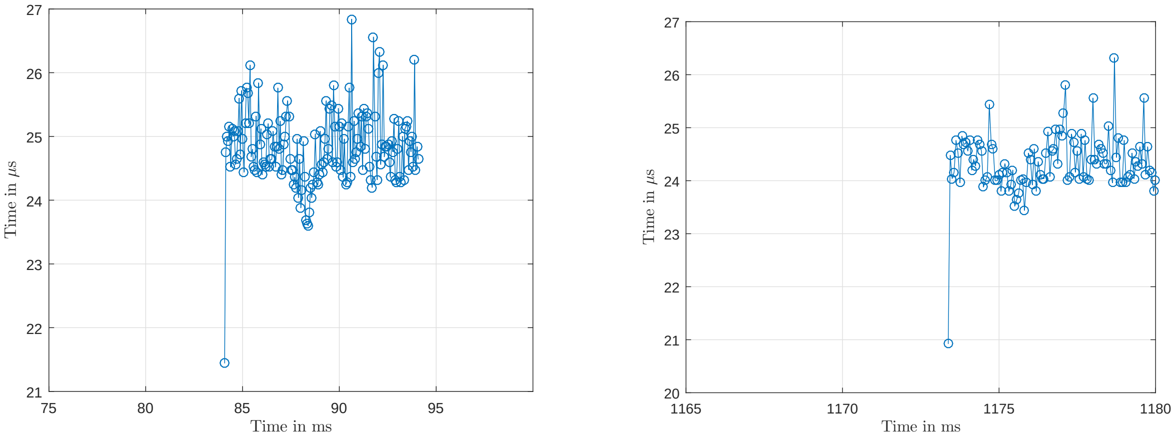

(a) CBS. (b) CFBS.

Figure 5.16: Computational demand for backstepping-based control.

5.3 Experimental results

The CFBS method with one common duty cycle could be tested in the test bed described in section 2.8 with system parameters listed in appendix B and controller parameters listed in appendix C. The MATLAB/SIMULINK code generation tool was used to for an implementation on an embedded DSP at a sampling rate of 16 kHz. The filtered measurements were directly fed to the control loop, omitting the use of an observer. Therefore, also the load current estimation was missing which lead to poor disturbance rejection. Moreover, the observer could not be used to compensate the computational delay. Instead, the states were extrapolated for one time step using the system dynamics. Fig. 5.17a and 5.17c show the output voltage for a setpoint step from $v_2 = 100\,\mathrm{V}$ to $v_2 = 350\,\mathrm{V}$ and the corresponding duty cycle. The poor performance was due to a model-plant-mismatch, as the controller assumed a DC-link of $V_0 = 820\,\mathrm{V}$ while the test bed was configured to $V_0 = 675\,\mathrm{V}$, which explains the different ratio of output voltage to duty cycle. Fig. 5.17b and 5.17d depict the output voltage and sum phase current when a constant load current of $i_\mathrm{L} = -100\,\mathrm{A}$ is injected. Due to the missing disturbance estimation the disturbance rejection fully relies on the error integration which was clearly not aggressive enough for a satisfying performance. The integral gain would need to be increased a lot which would also deteriorate transient performance for setpoint steps. Nevertheless, the basic functionality of the CFBS method could be validated. Further improvements as the inclusion of the observer and suitable coefficient tuning however could only be done in simulation but not verified on the test bed due to lack of time. These improved coefficients are also listed in appendix C.

Die approbierte gedruckte Originalversion dieser Diplomarbeit ist an der TU Wien Bibliothek verfügbar.
The approved original version of this thesis is available in print at TU Wien Bibliothek.

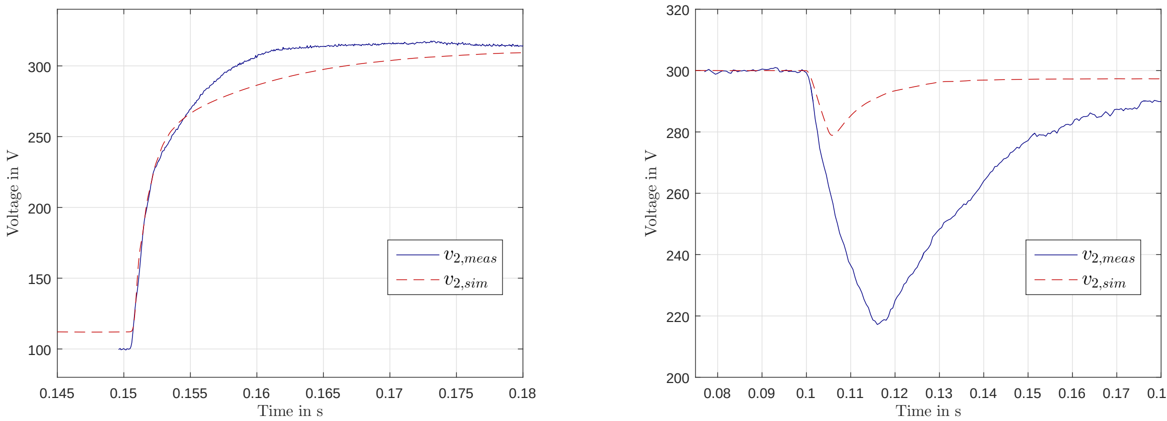

(a) Output voltage for setpoint step.

(b) Output voltage for load step.

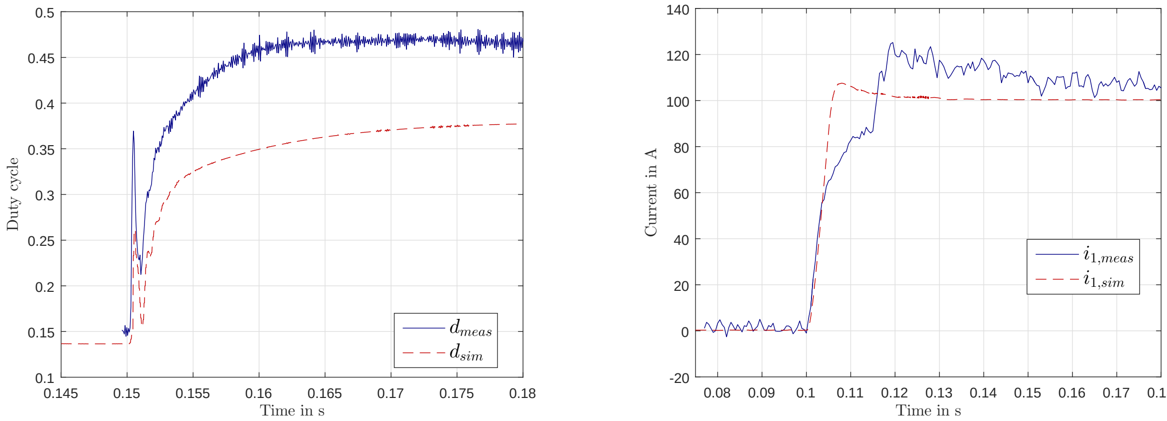

(c) Common duty cycle for setpoint step.

(d) Sum phase current for load step.

Figure 5.17: Setpoint change and load step on test bed.

Die approbierte gedruckte Originalversion dieser Diplomarbeit ist an der TU Wien Bibliothek verfügbar.
The approved original version of this thesis is available in print at TU Wien Bibliothek.

Chapter 6

Conclusion

This thesis proposed two control strategies to overcome the limitations of conventional FCS-MPC. The tailored PPPC approach allows fast tracking during transients as well as high performance in steady-state for a SMPB. While conventional PWM-based control strategies achieve good steady-state performance, their transient response is limited by the switching frequency. FCS-MPC on the other hand provides fast transient response but performs poorly in steady-state due to limited time resolution and resulting high computational effort when increasing the sampling rate. The PPPC strategy achieves both goals by solving a constrained quadratic program that can be solved efficiently with state-of-the-art methods.

The CFBS approach on the other hand is suggested as a PWM-based alternative with little computational cost. Its strength lies in flexibility, straight-forward implementation and inherently guaranteeing asymptotical closed loop stability in the sense of Lyapunov. Simulation results demonstrate the high performance of the PPPC strategy for transient and steady-state operating conditions that outperform the CFBS in dynamic response. Moreover, the CFBS approach could also be validated experimentally on the hardware test bed.

Finally, a Backstepping-based strategy to dynamically prune the search space of the integer quadratic program associated to the FCS-MPC is presented. The computational cost can be reduced significantly which enables longer prediction horizons.

6.1 Outlook

So far PPPC could only be validated with simulation results. The next goal is to prove the real-time capability of the method and validate it on a test bed. Moreover, the set of pulse patterns could be extended to pulse patterns that explicitly cover transient switching sequences to further improve the performance. Another interesting aspect is increasing the number of phases of the SMPB. A great advantage of the PPPC method

Die approbierte gedruckte Originalversion dieser Diplomarbeit ist an der TU Wien Bibliothek verfügbar.
The approved original version of this thesis is available in print at TU Wien Bibliothek.

is that the computational cost scales linearly with the number of switches in contrast to FCS-MPC, which grows exponentially.

Die approbierte gedruckte Originalversion dieser Diplomarbeit ist an der TU Wien Bibliothek verfügbar.
The approved original version of this thesis is available in print at TU Wien Bibliothek.
TU WIEN Bibliothek Your knowledge hub

Appendix A

Pulse Pattern Prediction Matrices

The objective function (3.42) for patterns $p \in \{A, B, C, D\}$ is given by

$$J_k(p) = \|\boldsymbol{i}_k^* - (\boldsymbol{F}(p)\boldsymbol{x}_{r,k} + \boldsymbol{G}_k(p)\boldsymbol{t}_k) + \boldsymbol{K}(p)\|_{\boldsymbol{\Psi}}^2, \tag{A.1}$$

with $\boldsymbol{G}_k(p) = \boldsymbol{G}^0(p) + \boldsymbol{G}_k^1(p)$. As already mentioned in section 3.4, the decision variables are normalized with $T_n = T_P$ to improve the condition of the problem. The associated prediction matrices are defined as

$$\boldsymbol{F}(A) = \begin{bmatrix} 1 & 1 & 1 & 1 & 0 \\ 1 & 1 & 1 & 1 & 0 \\ 1 & 1 & 1 & 1 & 0 \\ 1 & 1 & 1 & 1 & 0 \\ 1 & 1 & 1 & 1 & 0 \\ 1 & 1 & 1 & 1 & 0 \\ 1 & 1 & 1 & 1 & 0 \\ 1 - R_{1_a}a & 1 - R_{1_b}b & 1 - R_{1_c}c & 1 - R_{1_d}d & -abcd \\ 1 & 0 & 0 & 0 & 0 \\ 0 & 1 & 0 & 0 & 0 \\ 0 & 0 & 1 & 0 & 0 \\ 0 & 0 & 0 & 1 & 0 \end{bmatrix}, \tag{A.2}$$

Die approbierte gedruckte Originalversion dieser Diplomarbeit ist an der TU Wien Bibliothek verfügbar.
The approved original version of this thesis is available in print at TU Wien Bibliothek.
TU WIEN Bibliothek Your knowledge hub

$$\boldsymbol{F}(B) = \begin{bmatrix} 1 & 1 & 1 & 1 & 0 \\ 1 & 1 & 1 & 1 & 0 \\ 1 & 1 & 1 & 1 & 0 \\ 1 & 1 & 1 & 1 & 0 \\ 1 & 1 & 1 & 1 & 0 \\ 1 & 1 & 1 & 1 & 0 \\ 1 & 1 & 1 & 1 & 0 \\ 1 - R_{1_a} a & 1 - R_{1_b} b & 1 - R_{1_c} c & 1 - R_{1_d} d & -abcd \\ 1 & 0 & 0 & 0 & 0 \\ 0 & 1 & 0 & 0 & 0 \\ 0 & 0 & 1 & 0 & 0 \\ 0 & 0 & 0 & 1 - R_{1_d} \frac{d}{2} & -\frac{d}{2} \end{bmatrix}, \tag{A.3}$$

$$\boldsymbol{F}(C) = \begin{bmatrix} 1 & 1 & 1 & 1 & 0 \\ 1 & 1 & 1 & 1 & 0 \\ 1 & 1 & 1 & 1 & 0 \\ 1 & 1 & 1 & 1 & 0 \\ 1 & 1 & 1 & 1 & 0 \\ 1 & 1 & 1 & 1 & 0 \\ 1 & 1 & 1 & 1 & 0 \\ 1 - R_{1_a} a & 1 - R_{1_b} b & 1 - R_{1_c} c & 1 - R_{1_d} d & -abcd \\ 1 - R_{1_a} \frac{a}{2} & 0 & 0 & 0 & -\frac{a}{2} \\ 0 & 1 & 0 & 0 & 0 \\ 0 & 0 & 1 - R_{1_c} \frac{c}{2} & 0 & -\frac{c}{2} \\ 0 & 0 & 0 & 1 - R_{1_d} \frac{d}{2} & -\frac{d}{2} \end{bmatrix}, \tag{A.4}$$

Die approbierte gedruckte Originalversion dieser Diplomarbeit ist an der TU Wien Bibliothek verfügbar.
The approved original version of this thesis is available in print at TU Wien Bibliothek.

$$\boldsymbol{F}(D) = \begin{bmatrix} 1 & 1 & 1 & 1 & 0 \\ 1 & 1 & 1 & 1 & 0 \\ 1 & 1 & 1 & 1 & 0 \\ 1 & 1 & 1 & 1 & 0 \\ 1 & 1 & 1 & 1 & 0 \\ 1 & 1 & 1 & 1 & 0 \\ 1 & 1 & 1 & 1 & 0 \\ 1 - R_{1_a} a & 1 - R_{1_b} b & 1 - R_{1_c} c & 1 - R_{1_d} d & -abcd \\ 1 - R_{1_a} \frac{a}{2} & 0 & 0 & 0 & -\frac{a}{2} \\ 0 & 1 & 0 & 0 & 0 \\ 0 & 0 & 1 & 0 & 0 \\ 0 & 0 & 0 & 1 - R_{1_d} \frac{d}{2} & -\frac{d}{2} \end{bmatrix}, \tag{A.5}$$

$$\boldsymbol{G}^0(A) = V_0 \begin{bmatrix} a & 0 & 0 & 0 & 0 & 0 & 0 \\ a & 0 & 0 & 0 & 0 & 0 & 0 \\ a & -b & b & 0 & 0 & 0 & 0 \\ a & -b & b & 0 & 0 & 0 & 0 \\ a & -b & b & -c & c & 0 & 0 \\ a & -b & b & -c & c & 0 & 0 \\ a & -b & b & -c & c & -d & d \\ a & -b & b & -c & c & -d & d \\ \frac{a}{2} & 0 & 0 & 0 & 0 & 0 & 0 \\ 0 & -\frac{b}{2} & \frac{b}{2} & 0 & 0 & 0 & 0 \\ 0 & 0 & 0 & -\frac{c}{2} & \frac{c}{2} & 0 & 0 \\ 0 & 0 & 0 & 0 & 0 & -\frac{d}{2} & \frac{d}{2} \end{bmatrix}, \tag{A.6}$$

Die approbierte gedruckte Originalversion dieser Diplomarbeit ist an der TU Wien Bibliothek verfügbar.
The approved original version of this thesis is available in print at TU Wien Bibliothek.
TU WIEN Bibliothek Your knowledge hub

$$\boldsymbol{G}^0(B) = V_0 \begin{bmatrix} a & 0 & 0 & 0 & 0 & 0 & 0 \\ -b & ab & 0 & 0 & 0 & 0 & 0 \\ -b & a & b & 0 & 0 & 0 & 0 \\ -b & a & -c & bc & 0 & 0 & 0 \\ -b & a & -c & b & c & 0 & 0 \\ -b & a & -c & b & -d & C & 0 \\ -b & a & -c & b & -d & c & d \\ -b & a & -c & b & -d & c & -a \\ 0 & a & 0 & 0 & 0 & 0 & 0 \\ -\frac{b}{2} & 0 & 0 & \frac{b}{2} & 0 & 0 & 0 \\ 0 & 0 & -\frac{c}{2} & 0 & 0 & \frac{c}{2} & 0 \\ 0 & 0 & 0 & 0 & -\frac{d}{2} & 0 & 0 \end{bmatrix}, \tag{A.7}$$

$$\boldsymbol{G}^0(C) = V_0 \begin{bmatrix} ab & 0 & 0 & 0 & 0 & 0 & 0 \\ -c & abc & 0 & 0 & 0 & 0 & 0 \\ -c & a & bc & 0 & 0 & 0 & 0 \\ -c & a & -d & bcd & 0 & 0 & 0 \\ -c & a & -d & b & cd & 0 & 0 \\ -c & a & -d & b & -a & acd & 0 \\ -c & a & -d & b & -a & c & ad \\ -c & a & -d & b & -a & c & -b \\ 0 & a & 0 & 0 & -\frac{a}{2} & 0 & 0 \\ 0 & 0 & 0 & b & 0 & 0 & 0 \\ -c & 0 & 0 & 0 & 0 & c & 0 \\ 0 & 0 & -\frac{d}{2} & 0 & 0 & 0 & 0 \end{bmatrix}, \tag{A.8}$$

Die approbierte gedruckte Originalversion dieser Diplomarbeit ist an der TU Wien Bibliothek verfügbar.
The approved original version of this thesis is available in print at TU Wien Bibliothek.

$$\boldsymbol{G}^0(D) = V_0 \begin{bmatrix} abc & 0 & 0 & 0 & 0 & 0 & 0 \\ -d & abcd & 0 & 0 & 0 & 0 & 0 \\ -d & a & bcd & 0 & 0 & 0 & 0 \\ -d & a & -a & abcd & 0 & 0 & 0 \\ -d & a & -a & b & acd & 0 & 0 \\ -d & a & -a & b & -b & abcd & 0 \\ -d & a & -a & b & -b & c & abd \\ -d & a & -a & b & -b & c & -c \\ 0 & \frac{a}{2} & 0 & 0 & 0 & 0 & 0 \\ 0 & 0 & 0 & b & 0 & 0 & 0 \\ 0 & 0 & 0 & 0 & 0 & c & 0 \\ -\frac{d}{2} & 0 & 0 & 0 & 0 & 0 & 0 \end{bmatrix}, \tag{A.9}$$

$$\boldsymbol{G}_k^1(A) = \begin{bmatrix} \Delta i_1^0 & 0 & 0 & 0 & 0 & 0 & 0 \\ 0 & \Delta i_1^0 & 0 & 0 & 0 & 0 & 0 \\ 0 & 0 & \Delta i_1^0 & 0 & 0 & 0 & 0 \\ 0 & 0 & 0 & \Delta i_1^0 & 0 & 0 & 0 \\ 0 & 0 & 0 & 0 & \Delta i_1^0 & 0 & 0 \\ 0 & 0 & 0 & 0 & 0 & \Delta i_1^0 & 0 \\ 0 & 0 & 0 & 0 & 0 & 0 & \Delta i_1^0 \\ 0 & 0 & 0 & 0 & 0 & 0 & 0 \\ \frac{\Delta i_{L_{1_a}}^0}{2} & 0 & 0 & 0 & 0 & 0 & 0 \\ 0 & \frac{\Delta i_{L_{1_b}}^0}{2} & \frac{\Delta i_{L_{1_b}}^0}{2} & 0 & 0 & 0 & 0 \\ 0 & 0 & 0 & \frac{\Delta i_{L_{1_c}}^0}{2} & \frac{\Delta i_{L_{1_c}}^0}{2} & 0 & 0 \\ 0 & 0 & 0 & 0 & 0 & \frac{\Delta i_{L_{1_d}}^0}{2} & \frac{\Delta i_{L_{1_d}}^0}{2} \end{bmatrix}, \tag{A.10}$$

Die approbierte gedruckte Originalversion dieser Diplomarbeit ist an der TU Wien Bibliothek verfügbar.
The approved original version of this thesis is available in print at TU Wien Bibliothek.

$$\boldsymbol{G}_k^1(B) = \begin{bmatrix} \Delta i_1^0 & 0 & 0 & 0 & 0 & 0 & 0 \\ 0 & \Delta i_1^0 & 0 & 0 & 0 & 0 & 0 \\ 0 & 0 & \Delta i_1^0 & 0 & 0 & 0 & 0 \\ 0 & 0 & 0 & \Delta i_1^0 & 0 & 0 & 0 \\ 0 & 0 & 0 & 0 & \Delta i_1^0 & 0 & 0 \\ 0 & 0 & 0 & 0 & 0 & \Delta i_1^0 & 0 \\ 0 & 0 & 0 & 0 & 0 & 0 & \Delta i_1^0 \\ 0 & 0 & 0 & 0 & 0 & 0 & 0 \\ 0 & \dfrac{\Delta i_{L_{1_a}}^0}{2} & 0 & 0 & 0 & 0 & \dfrac{\Delta i_{L_{1_a}}^0}{2} \\ \dfrac{\Delta i_{L_{1_b}}^0}{2} & 0 & 0 & \dfrac{\Delta i_{L_{1_b}}^0}{2} & 0 & 0 & 0 \\ 0 & 0 & \dfrac{\Delta i_{L_{1_c}}^0}{2} & 0 & 0 & \dfrac{\Delta i_{L_{1_c}}^0}{2} & 0 \\ 0 & 0 & 0 & 0 & \dfrac{\Delta i_{L_{1_d}}^0}{2} & 0 & 0 \end{bmatrix}, \qquad \text{(A.11)}$$

Die approbierte gedruckte Originalversion dieser Diplomarbeit ist an der TU Wien Bibliothek verfügbar.
The approved original version of this thesis is available in print at TU Wien Bibliothek.

$$
\boldsymbol{G}_k^1(C) = \begin{bmatrix}
\Delta i_1^0 & 0 & 0 & 0 & 0 & 0 & 0 \\
0 & \Delta i_1^0 & 0 & 0 & 0 & 0 & 0 \\
0 & 0 & \Delta i_1^0 & 0 & 0 & 0 & 0 \\
0 & 0 & 0 & \Delta i_1^0 & 0 & 0 & 0 \\
0 & 0 & 0 & 0 & \Delta i_1^0 & 0 & 0 \\
0 & 0 & 0 & 0 & 0 & \Delta i_1^0 & 0 \\
0 & 0 & 0 & 0 & 0 & 0 & \Delta i_1^0 \\
0 & 0 & 0 & 0 & 0 & 0 & 0 \\
0 & 0 & 0 & 0 & \dfrac{\Delta i_{L_{1_a}}^0}{2} & 0 & 0 \\
0 & 0 & 0 & \dfrac{\Delta i_{L_{1_b}}^0}{2} & 0 & 0 & \dfrac{\Delta i_{L_{1_b}}^0}{2} \\
\dfrac{\Delta i_{L_{1_c}}^0}{2} & 0 & 0 & 0 & 0 & \dfrac{\Delta i_{L_{1_c}}^0}{2} & 0 \\
0 & 0 & \dfrac{\Delta i_{L_{1_d}}^0}{2} & 0 & 0 & 0 & 0
\end{bmatrix}, \tag{A.12}
$$

TU Bibliothek, WIEN, Your knowledge hub
Die approbierte gedruckte Originalversion dieser Diplomarbeit ist an der TU Wien Bibliothek verfügbar.
The approved original version of this thesis is available in print at TU Wien Bibliothek.

$$\boldsymbol{G}_k^1(D) = \begin{bmatrix} \Delta i_1^0 & 0 & 0 & 0 & 0 & 0 & 0 \\ 0 & \Delta i_1^0 & 0 & 0 & 0 & 0 & 0 \\ 0 & 0 & \Delta i_1^0 & 0 & 0 & 0 & 0 \\ 0 & 0 & 0 & \Delta i_1^0 & 0 & 0 & 0 \\ 0 & 0 & 0 & 0 & \Delta i_1^0 & 0 & 0 \\ 0 & 0 & 0 & 0 & 0 & \Delta i_1^0 & 0 \\ 0 & 0 & 0 & 0 & 0 & 0 & \Delta i_1^0 \\ 0 & 0 & 0 & 0 & 0 & 0 & 0 \\ 0 & 0 & \frac{\Delta i_{L_{1_a}}^0}{2} & 0 & 0 & 0 & 0 \\ 0 & 0 & 0 & \frac{\Delta i_{L_{1_b}}^0}{2} & \frac{\Delta i_{L_{1_b}}^0}{2} & 0 & 0 \\ 0 & 0 & 0 & 0 & 0 & \frac{\Delta i_{L_{1_c}}^0}{2} & \frac{\Delta i_{L_{1_c}}^0}{2} \\ \frac{\Delta i_{L_{1_d}}^0}{2} & 0 & 0 & 0 & 0 & 0 & 0 \end{bmatrix}, \qquad \text{(A.13)}$$

$$\boldsymbol{K}(A) = \begin{bmatrix} 0 \\ 0 \\ 0 \\ 0 \\ 0 \\ 0 \\ 0 \\ 0 \\ 0 \\ 0 \\ 0 \\ 0 \end{bmatrix}, \quad \boldsymbol{K}(B) = \begin{bmatrix} 0 \\ 0 \\ 0 \\ 0 \\ 0 \\ 0 \\ 0 \\ 0 \\ ad \\ 0 \\ 0 \\ \frac{d}{2} \end{bmatrix}, \quad \boldsymbol{K}(C) = \begin{bmatrix} 0 \\ 0 \\ 0 \\ 0 \\ 0 \\ 0 \\ 0 \\ 0 \\ abd \\ \frac{a}{2} \\ 0 \\ \frac{d}{2} \end{bmatrix}, \quad \boldsymbol{K}(D) = \begin{bmatrix} 0 \\ 0 \\ 0 \\ 0 \\ 0 \\ 0 \\ 0 \\ 0 \\ 0 \\ abcd \\ \frac{a}{2} \\ \frac{d}{2} \end{bmatrix}, \qquad \text{(A.14)}$$

Die approbierte gedruckte Originalversion dieser Diplomarbeit ist an der TU Wien Bibliothek verfügbar.
The approved original version of this thesis is available in print at TU Wien Bibliothek.

with

$$a = \frac{1}{L_{1_a}} T_n, \qquad b = \frac{1}{L_{1_b}} T_n, \tag{A.15}$$

$$c = \frac{1}{L_{1_c}} T_n, \qquad d = \frac{1}{L_{1_d}} T_n, \tag{A.16}$$

$$ab = a + b, \qquad ac = a + c, \tag{A.17}$$

$$ad = a + d, \qquad bc = b + c, \tag{A.18}$$

$$cd = c + d, \qquad abc = a + b + c, \tag{A.19}$$

$$abcd = a + b + c + d, \qquad acd = a + c + d, \tag{A.20}$$

$$bcd = b + c + d, \qquad abd = a + b + d. \tag{A.21}$$

The autonomous phase current gradients (excluding impact of V_0) are given in accordance with (3.40) and normalized switching instants by

$$\Delta i^0_{L_{1_j}} = \left(-v_1(t_0) - R_{1_j} i^{avg}_{L_{1_j}} \right) j, \quad j \in \mathcal{P} = \{a, b, c, d\}, \tag{A.22}$$

and hence

$$\Delta i^0_1 = \sum_{j \in \mathcal{P}} \Delta i^0_{L_{1_j}}. \tag{A.23}$$

Note that the matrices $\boldsymbol{G}^0(A) - \boldsymbol{G}^0(D)$ can be calculated offline while $\boldsymbol{G}^1_k(A) - \boldsymbol{G}^1_k(D)$ depend on the current state and have to be evaluated online. The weighting matrix is defined as

$$\boldsymbol{\Psi} = \begin{bmatrix} 1 & 0 & 0 & 0 & 0 & 0 & 0 & 0 & 0 & 0 & 0 & 0 \\ 0 & 1 & 0 & 0 & 0 & 0 & 0 & 0 & 0 & 0 & 0 & 0 \\ 0 & 0 & 1 & 0 & 0 & 0 & 0 & 0 & 0 & 0 & 0 & 0 \\ 0 & 0 & 0 & 1 & 0 & 0 & 0 & 0 & 0 & 0 & 0 & 0 \\ 0 & 0 & 0 & 0 & 1 & 0 & 0 & 0 & 0 & 0 & 0 & 0 \\ 0 & 0 & 0 & 0 & 0 & 1 & 0 & 0 & 0 & 0 & 0 & 0 \\ 0 & 0 & 0 & 0 & 0 & 0 & 1 & 0 & 0 & 0 & 0 & 0 \\ 0 & 0 & 0 & 0 & 0 & 0 & 0 & 1 & 0 & 0 & 0 & 0 \\ 0 & 0 & 0 & 0 & 0 & 0 & 0 & 0 & \psi_a & 0 & 0 & 0 \\ 0 & 0 & 0 & 0 & 0 & 0 & 0 & 0 & 0 & \psi_b & 0 & 0 \\ 0 & 0 & 0 & 0 & 0 & 0 & 0 & 0 & 0 & 0 & \psi_c & 0 \\ 0 & 0 & 0 & 0 & 0 & 0 & 0 & 0 & 0 & 0 & 0 & \psi_d \end{bmatrix}. \tag{A.24}$$

Die approbierte gedruckte Originalversion dieser Diplomarbeit ist an der TU Wien Bibliothek verfügbar.
The approved original version of this thesis is available in print at TU Wien Bibliothek.

Appendix B

System Parameter

The system parameters are listed in table B.1.

Table B.1: Parameters of the BE.

Parameter		Nominal value
DC-link capacitance	C_0	∞
DC-link voltage	V_0	820 V
Lumped filter inductance	L_1	75 µH
Lumped inductor resistance	R_1	2.5 mΩ
Filter capacitance	C_1	1575 µF
Cable inductance	L_2	10 µH
Cable resistance	R_2	50 mΩ
Load input capacitance	C_2	2300 µF
Sampling rate	f_s	16 kHz
Maximum sum inductor current	$i_{1,max}$	±600 A
Load power (CPL)	P	up to 160 kW

Die approbierte gedruckte Originalversion dieser Diplomarbeit ist an der TU Wien Bibliothek verfügbar.
The approved original version of this thesis is available in print at TU Wien Bibliothek.

Appendix C

Controller Parameters

Table C.1: LQR with i_1 as virtual control input.

Parameter	Value
q_{u,v_1}	0
q_{u,i_2}	0
q_{u,v_2}	75
q_{u,x_I}	1
r_v	1
$k_{x,1}$	-5.7865
$k_{x,2}$	-0.0866
$k_{x,3}$	-8.5522
k_I	0.8848

Table C.2: FCS-MPC.

Parameter	Value
λ_u	1
λ_{sw}	1×10^6
$\boldsymbol{\Omega}$	$\boldsymbol{I}$
$\boldsymbol{\Sigma}$	$\boldsymbol{I}$

Die approbierte gedruckte Originalversion dieser Diplomarbeit ist an der TU Wien Bibliothek verfügbar.
The approved original version of this thesis is available in print at TU Wien Bibliothek.

Table C.3: PPPC.

Parameter	Value
ψ_a	19
ψ_b	19
ψ_c	19
ψ_d	19

Table C.4: CFBS (1 phase, simulation setup).

Parameter	Value
k_1	6×10^3
k_2	1.5×10^4
k_3	1×10^3
k_4	6×10^3
k_I	187.5
$\tilde{\gamma}_1$	1
$\tilde{\gamma}_2$	g_2
$\tilde{\gamma}_3$	$\gamma_2 g_3$
$\tilde{\gamma}_4$	$\gamma_3 g_4$
ω_u	$5.0265 \times 10^4\,\mathrm{rad\,s^{-1}}$
ω_{i_2}	$5.0265 \times 10^4\,\mathrm{rad\,s^{-1}}$
ω_{v_1}	$2 \times 10^4\,\mathrm{rad\,s^{-1}}$
ω_{i_1}	$9 \times 10^4\,\mathrm{rad\,s^{-1}}$
ζ_u	1
ζ_{i_2}	1
ζ_{v_1}	1
ζ_{i_1}	1

Die approbierte gedruckte Originalversion dieser Diplomarbeit ist an der TU Wien Bibliothek verfügbar.
The approved original version of this thesis is available in print at TU Wien Bibliothek.

Die approbierte gedruckte Originalversion dieser Diplomarbeit ist an der TU Wien Bibliothek verfügbar.
The approved original version of this thesis is available in print at TU Wien Bibliothek.
TU WIEN Bibliothek Your knowledge hub

Table C.5: CFBS (1 phase, experimental setup).

Parameter	Value
k_1	5×10^3
k_2	3×10^4
k_3	5×10^2
k_4	6×10^3
k_I	312.5
$\tilde{\gamma}_1$	1
$\tilde{\gamma}_2$	g_2
$\tilde{\gamma}_3$	$\gamma_2 g_3$
$\tilde{\gamma}_4$	$\gamma_3 g_4$
ω_u	$5.0265 \times 10^4\,\mathrm{rad\,s^{-1}}$
ω_{i_2}	$5.0265 \times 10^4\,\mathrm{rad\,s^{-1}}$
ω_{v_1}	$1 \times 10^4\,\mathrm{rad\,s^{-1}}$
ω_{i_1}	$5.0265 \times 10^4\,\mathrm{rad\,s^{-1}}$
ζ_u	1
ζ_{i_2}	1
ζ_{v_1}	1
ζ_{i_1}	1

Table C.6: Kalman Filter design (reduced order).

Parameter	Value
q_{o,i_1}	1000
q_{o,v_1}	1
q_{o,i_2}	1000
q_{o,v_2}	1
q_{o,i_L}	100
r_{o,i_1}	1
r_{o,v_1}	1
r_{o,i_2}	1
r_{o,v_2}	1

Table C.7: Kalman Filter design (full order).

Parameter	Value
$q_{o,i_{L_{1_a}}} - q_{o,i_{L_{1_d}}}$	100
q_{o,v_1}	1
q_{o,i_2}	100
q_{o,v_2}	1
q_{o,i_L}	200
$r_{o,i_{L_{1_a}}} - r_{o,i_{L_{1_d}}}$	1
r_{o,v_1}	1
r_{o,i_2}	1
r_{o,v_2}	1

Die approbierte gedruckte Originalversion dieser Diplomarbeit ist an der TU Wien Bibliothek verfügbar.
The approved original version of this thesis is available in print at TU Wien Bibliothek.
TU WIEN Bibliothek Your knowledge hub

Appendix D

Listing of MATLAB Setup

File	**Description**
start_here.m	Main file. Initializes simulation environment
init_LQR.m	Initialize Linear Quadratic Regulator
init_i1MPC	Initialize Outer loop MPC
init_PPC.m	Initialize (Predictive) Pulse Pattern Control
init_CBS.m	Initialize Cascade Backstepping
init_CFBS.m	Initialize Command Filtered Backstepping
init_FCSMPC.m	Initialize Finite Control Set-MPC
kalman_design.m	Reduced order Kalman Filter
kalman_design_full.m	Full order Kalman Filter

Die approbierte gedruckte Originalversion dieser Diplomarbeit ist an der TU Wien Bibliothek verfügbar.
The approved original version of this thesis is available in print at TU Wien Bibliothek.
TU WIEN Bibliothek Your knowledge hub

Bibliography

[1] Oliver König. *Battery impedance emulation for power-hardware-in-the-loop using model predictive control*. PhD thesis, Technische Universität Wien, 2013.

[2] Patricio Cortés, Marian P Kazmierkowski, Ralph M Kennel, Daniel E Quevedo, and José Rodríguez. Predictive control in power electronics and drives. *IEEE Transactions on industrial electronics*, 55(12):4312–4324, 2008.

[3] Sergio Vazquez, Jose Rodriguez, Marco Rivera, Leopoldo G Franquelo, and Margarita Norambuena. Model predictive control for power converters and drives: Advances and trends. *IEEE Transactions on Industrial Electronics*, 2016.

[4] Jay A Farrell, Marios Polycarpou, Manu Sharma, and Wenjie Dong. Command filtered backstepping. *IEEE Transactions on Automatic Control*, 54(6):1391–1395, 2009.

[5] Khiem Nguyen-Duy, Arnold Knott, and Michael AE Andersen. A review on the implementation of nonlinear source emulators. In *Power and Electrical Engineering of Riga Technical University (RTUCON), 2014 55th International Scientific Conference on*, pages 56–62. IEEE, 2014.

[6] Oliver König, Christoph Hametner, Günter Prochart, and Stefan Jakubek. Battery emulation for power-hil using local model networks and robust impedance control. *IEEE Transactions on Industrial Electronics*, 61(2):943–955, 2014.

[7] Christoph Hametner, Johannes Unger, and Stefan Jakubek. Local model network based dynamic battery cell model identification. In *Proceedings of the 11th WSEAS international conference on instrumentation, measurement, circuits and systems (S. 116–123). Rovaniemi: World Scientific and Engineering Academy and Society (WSEAS)*, 2012.

[8] Alexander Schirrer, Guilherme Aschauer, and Stefan Jakubek. Hardware-in-the-loop testing of high-speed pantographs using real-time catenary emulation. In *Dynamics and Control of Advanced Structures and Machines*, pages 75–83. Springer, 2017.

Die approbierte gedruckte Originalversion dieser Diplomarbeit ist an der TU Wien Bibliothek verfügbar.
The approved original version of this thesis is available in print at TU Wien Bibliothek.

[9] Vlad Grigore, Jari Hatonen, Jorma Kyyra, and Teuvo Suntio. Dynamics of a buck converter with a constant power load. In *Power Electronics Specialists Conference, 1998. PESC 98 Record. 29th Annual IEEE*, volume 1, pages 72–78. IEEE, 1998.

[10] Ali Emadi, Alireza Khaligh, Claudio H Rivetta, and Geoffrey A Williamson. Constant power loads and negative impedance instability in automotive systems: definition, modeling, stability, and control of power electronic converters and motor drives. *IEEE Transactions on Vehicular Technology*, 55(4):1112–1125, 2006.

[11] Oliver König, Gregor Gregorčič, and Stefan Jakubek. Model predictive control of a dc–dc converter for battery emulation. *Control Engineering Practice*, 21(4):428–440, 2013.

[12] S Mariethoz, AG Beccuti, and M Morari. Model predictive control of multiphase interleaved dc-dc converters with sensorless current limitation and power balance. In *Power Electronics Specialists Conference, 2008. PESC 2008. IEEE*, pages 1069–1074. IEEE, 2008.

[13] James Blake Rawlings and David Q Mayne. *Model predictive control: Theory and design*. Nob Hill Pub., 2009.

[14] Samir Kouro, Patricio Cortés, René Vargas, Ulrich Ammann, and José Rodríguez. Model predictive control—a simple and powerful method to control power converters. *IEEE Transactions on Industrial Electronics*, 56(6):1826–1838, 2009.

[15] Eduardo F Camacho and Carlos Bordons Alba. *Model predictive control*. Springer Science & Business Media, 2013.

[16] Robert W Erickson and Dragan Maksimovic. *Fundamentals of power electronics*. Springer Science & Business Media, 2007.

[17] Tobias Geyer and Daniel E Quevedo. Performance of multistep finite control set model predictive control for power electronics. *IEEE Transactions on Power Electronics*, 30(3):1633–1644, 2015.

[18] Ricardo P Aguilera and Daniel E Quevedo. Predictive control of power converters: Designs with guaranteed performance. *IEEE Transactions on Industrial Informatics*, 11(1):53–63, 2015.

[19] Roky Baidya, Ricardo P Aguilera, Pablo Acuna, Ramon Delgado, Tobias Geyer, Daniel Quevedo, and Toit Mouton. Fast multistep finite control set model predictive control for transient operation of power converters. In *Industrial Electron-*

Die approbierte gedruckte Originalversion dieser Diplomarbeit ist an der TU Wien Bibliothek verfügbar.
The approved original version of this thesis is available in print at TU Wien Bibliothek.
TU WIEN Bibliothek Your knowledge hub

ics Society, IECON 2016-42nd Annual Conference of the IEEE, pages 5039–5045. IEEE, 2016.

[20] Tobias Geyer and Daniel E Quevedo. Multistep finite control set model predictive control for power electronics. *IEEE Transactions on Power Electronics*, 29(12):6836–6846, 2014.

[21] Bartolomeo Stellato, Tobias Geyer, and Paul Goulart. High-speed finite control set model predictive control for power electronics. *IEEE Transactions on Power Electronics*, 2016.

[22] Tobias Geyer, Nikolaos Oikonomou, Georgios Papafotiou, and Frederick D Kieferndorf. Model predictive pulse pattern control. *IEEE Transactions on Industry Applications*, 48(2):663–676, 2012.

[23] Nikolaos Oikonomou, Christof Gutscher, Petros Karamanakos, Frederick D Kieferndorf, and Tobias Geyer. Model predictive pulse pattern control for the five-level active neutral-point-clamped inverter. *IEEE Transactions on Industry Applications*, 49(6):2583–2592, 2013.

[24] Helfried Peyrl, Junyi Liu, and Tobias Geyer. An fpga implementation of the fast gradient method for solving the model predictive pulse pattern control problem. In *Sensorless Control for Electrical Drives and Predictive Control of Electrical Drives and Power Electronics (SLED/PRECEDE), 2013 IEEE International Symposium on*, pages 1–6. IEEE, 2013.

[25] Peter Hokayem, Tobias Geyer, and Nikolaos Oikonomou. Active damping for model predictive pulse pattern control. In *Energy Conversion Congress and Exposition (ECCE), 2014 IEEE*, pages 1220–1227. IEEE, 2014.

[26] Sergio Vazquez, Abraham Marquez, Ricardo Aguilera, Daniel Quevedo, Jose I Leon, and Leopoldo G Franquelo. Predictive optimal switching sequence direct power control for grid-connected power converters. *IEEE Transactions on Industrial Electronics*, 62(4):2010–2020, 2015.

[27] Sergio Vazquez, Ricardo P Aguilera, Pablo Acuna, Josep Pou, Jose I Leon, Leopoldo G Franquelo, and Vassilios G Agelidis. Model predictive control for single-phase npc converters based on optimal switching sequences. *IEEE Transactions on Industrial Electronics*, 63(12):7533–7541, 2016.

Die approbierte gedruckte Originalversion dieser Diplomarbeit ist an der TU Wien Bibliothek verfügbar.
The approved original version of this thesis is available in print at TU Wien Bibliothek.
TU WIEN Bibliothek Your knowledge hub

[28] Sergio Vazquez, Jose I Leon, Leopoldo G Franquelo, Jose Rodriguez, Hector A Young, Abraham Marquez, and Pericle Zanchetta. Model predictive control: A review of its applications in power electronics. *IEEE Industrial Electronics Magazine*, 8(1):16–31, 2014.

[29] Miroslav Krstic, Ioannis Kanellakopoulos, and Peter V Kokotovic. *Nonlinear and adaptive control design*. Wiley, 1995.

[30] Hassan K Khalil. *Nonlinear Systems*. Prentice-Hall, New Jersey, 1996.

[31] Alberto Isidori. *Nonlinear control systems*. Springer Science & Business Media, 2013.

[32] W Kemmetmüller and A Kugi. Immersion and invariance-based impedance control for electrohydraulic systems. *International Journal of Robust and Nonlinear Control*, 20:725–744, 2010.

[33] Petros Karamanakos, Tobias Geyer, and Stefanos Manias. Direct model predictive current control strategy of dc–dc boost converters. *IEEE Journal of Emerging and Selected Topics in Power Electronics*, 1(4):337–346, 2013.

[34] Urban Maeder, Francesco Borrelli, and Manfred Morari. Linear offset-free model predictive control. *Automatica*, 45(10):2214–2222, 2009.

[35] Peter Dorato, Vito Cerone, and Chaouki Abdallah. *Linear-quadratic control: an introduction*. Simon & Schuster, 1994.

[36] Tobias Geyer and Daniel E Quevedo. Multistep direct model predictive control for power electronics—part 1: Algorithm. In *Energy Conversion Congress and Exposition (ECCE), 2013 IEEE*, pages 1154–1161. IEEE, 2013.

[37] Daniel E Quevedo, Ricardo P Aguilera, and Tobias Geyer. Predictive control in power electronics and drives: Basic concepts, theory, and methods. In *Advanced and Intelligent Control in Power Electronics and Drives*, pages 181–226. Springer, 2014.

[38] Johannes Unger, Martin Kozek, and Stefan Jakubek. Reduced order optimization for model predictive control using principal control moves. *Journal of Process Control*, 22(1):272–279, 2012.

[39] Wenjie Dong, Jay A Farrell, Marios M Polycarpou, Vladimir Djapic, and Manu Sharma. Command filtered adaptive backstepping. *IEEE Transactions on Control Systems Technology*, 20(3):566–580, 2012.

Die approbierte gedruckte Originalversion dieser Diplomarbeit ist an der TU Wien Bibliothek verfügbar.
The approved original version of this thesis is available in print at TU Wien Bibliothek.

[40] Zhen Liu, Cheng Luo, and Dewen Hu. Active suspension control design using a combination of lqr and backstepping. In *Control Conference, 2006. CCC 2006. Chinese*, pages 123–125. IEEE, 2006.

[41] Alberto Bemporad, Manfred Morari, Vivek Dua, and Efstratios N Pistikopoulos. The explicit linear quadratic regulator for constrained systems. *Automatica*, 38(1):3–20, 2002.

[42] Sébastien Mariéthoz and Manfred Morari. Explicit model-predictive control of a pwm inverter with an lcl filter. *IEEE Transactions on Industrial Electronics*, 56(2):389–399, 2009.

[43] Yeye Shen, Lei Xie, and Xiuliang Li. Explicit hybrid model predictive control of the forward dc-dc converter. In *Control and Decision Conference (CCDC), 2013 25th Chinese*, pages 638–642. IEEE, 2013.

[44] Petros Karamanakos, Tobias Geyer, and Ralph Kennel. A computationally efficient model predictive control strategy for linear systems with integer inputs. *IEEE Transactions on Control Systems Technology*, 24(4):1463–1471, 2016.

[45] Venkata Yaramasu, Marco Rivera, Mehdi Narimani, Bin Wu, and Jose Rodriguez. Finite state model-based predictive current control with two-step horizon for four-leg npc converters. *Journal of Power Electronics*, 14(6):1178–1188, 2014.

[46] Juan L Jerez, Eric C Kerrigan, and George A Constantinides. A condensed and sparse qp formulation for predictive control. In *Decision and Control and European Control Conference (CDC-ECC), 2011 50th IEEE Conference on*, pages 5217–5222. IEEE, 2011.

[47] D Kouzoupis, A Zanelli, Helfried Peyrl, and Hans Joachim Ferreau. Towards proper assessment of qp algorithms for embedded model predictive control. In *Control Conference (ECC), 2015 European*, pages 2609–2616. IEEE, 2015.

[48] Jorge Nocedal and Stephen J Wright. Numerical optimization 2nd, 2006.

[49] Yurii Nesterov. A method of solving a convex programming problem with convergence rate o (1/k2). In *Soviet Mathematics Doklady*, volume 27, pages 372–376, 1983.

[50] Stefan Richter, Colin N Jones, and Manfred Morari. Real-time input-constrained mpc using fast gradient methods. In *Decision and Control, 2009 held jointly with the 2009 28th Chinese Control Conference. CDC/CCC 2009. Proceedings of the 48th IEEE Conference on*, pages 7387–7393. IEEE, 2009.

Die approbierte gedruckte Originalversion dieser Diplomarbeit ist an der TU Wien Bibliothek verfügbar.
The approved original version of this thesis is available in print at TU Wien Bibliothek.

[51] Juan L Jerez, Paul J Goulart, Stefan Richter, George A Constantinides, Eric C Kerrigan, and Manfred Morari. Embedded online optimization for model predictive control at megahertz rates. *IEEE Transactions on Automatic Control*, 59(12):3238–3251, 2014.

[52] Thuy V Dang, Keck Voon Ling, and Jan M Maciejowski. Embedded admm-based qp solver for mpc with polytopic constraints. In *Control Conference (ECC), 2015 European*, pages 3446–3451. IEEE, 2015.

[53] Yurii Nesterov. *Introductory lectures on convex optimization: A basic course*, volume 87. Springer Science & Business Media, 2013.

[54] Jacob Mattingley, Yang Wang, and Stephen Boyd. Receding horizon control. *IEEE Control Systems*, 31(3):52–65, 2011.

[55] Alexander Domahidi, Aldo U Zgraggen, Melanie N Zeilinger, Manfred Morari, and Colin N Jones. Efficient interior point methods for multistage problems arising in receding horizon control. In *Decision and Control (CDC), 2012 IEEE 51st Annual Conference on*, pages 668–674. IEEE, 2012.

[56] Gianluca Frison, Henrik Brandenborg Sørensen, Bernd Dammann, and John Bagterp Jørgensen. High-performance small-scale solvers for linear model predictive control. In *Control Conference (ECC), 2014 European*, pages 128–133. IEEE, 2014.

[57] Fabian Ullmann. Fiordos: A matlab toolbox for c-code generation for first order methods. *MS thesis*, 2011.

[58] Pablo Zometa, Markus Kögel, and Rolf Findeisen. μao-mpc: a free code generation tool for embedded real-time linear model predictive control. In *American Control Conference (ACC), 2013*, pages 5320–5325. IEEE, 2013.

[59] Hans Joachim Ferreau, Christian Kirches, Andreas Potschka, Hans Georg Bock, and Moritz Diehl. qpoases: A parametric active-set algorithm for quadratic programming. *Mathematical Programming Computation*, 6(4):327–363, 2014.

[60] D Kwame Minde Kufoalor, BJT Binder, Hans Joachim Ferreau, Lars Imsland, Tor Arne Johansen, and Moritz Diehl. Automatic deployment of industrial embedded model predictive control using qpoases. In *Control Conference (ECC), 2015 European*, pages 2601–2608. IEEE, 2015.

Die approbierte gedruckte Originalversion dieser Diplomarbeit ist an der TU Wien Bibliothek verfügbar.
The approved original version of this thesis is available in print at TU Wien Bibliothek.
TU WIEN Bibliothek Your knowledge hub

[61] BJT Binder, D Kwame Minde Kufoalor, and Tor Arne Johansen. Scalability of qp solvers for embedded model predictive control applied to a subsea petroleum production system. In *Control Applications (CCA), 2015 IEEE Conference on*, pages 1173–1178. IEEE, 2015.

[62] Gideon Prior and Miroslav Krstic. A control lyapunov approach to finite control set model predictive control for permanent magnet synchronous motors. *Journal of Dynamic Systems, Measurement, and Control*, 137(1):011001, 2015.

TU WIEN Bibliothek Your knowledge hub
Die approbierte gedruckte Originalversion dieser Diplomarbeit ist an der TU Wien Bibliothek verfügbar.
The approved original version of this thesis is available in print at TU Wien Bibliothek.

Eidesstattliche Erklärung

Hiermit erkläre ich, dass die vorliegende Arbeit gemäß dem Code of Conduct – Regeln zur Sicherung guter wissenschaftlicher Praxis (in der aktuellen Fassung des jeweiligen Mitteilungsblattes der TU Wien), insbesondere ohne unzulässige Hilfe Dritter und ohne Benutzung anderer als der angegebenen Hilfsmittel, angefertigt wurde. Die aus anderen Quellen direkt oder indirekt übernommenen Daten und Konzepte sind unter Angabe der Quelle gekennzeichnet. Die Arbeit wurde bisher weder im In– noch im Ausland in gleicher oder in ähnlicher Form in anderen Prüfungsverfahren vorgelegt.

Wien, Juni, 2017

Wolfgang Falmbigl

TU WIEN Bibliothek Your knowledge hub
Die approbierte gedruckte Originalversion dieser Diplomarbeit ist an der TU Wien Bibliothek verfügbar.
The approved original version of this thesis is available in print at TU Wien Bibliothek.